1964

Skin Friction Drag and Shear Stress Distribution on Several Streamlined Bodies of Revolution With Varied Fineness Ratio.

Dunning, Cleveland L.

Monterey, California. Naval Postgraduate School

https://hdl.handle.net/10945/26252

SKIN FRICTION DRAG AND SHEAR STRESS DISTRIBUTION ON SEVERAL STREAMLINED BODIES OF REVOLUTION WITH VARIED FINENESS RATIO

CLEVELAND L. DUNNING
ROBERT F. OVERMYER
COLBEN K. SIME, JR.

[redacted]

SKIN FRICTION DRAG AND SHEAR STRESS DISTRIBUTION ON SEVERAL STREAMLINED BODIES OF REVOLUTION WITH VARIED FINENESS RATIO

*****

Cleveland L. Dunning

Robert F. Overmyer

and

Colben K. Sime, Jr.

[redacted]

[redacted]

[redacted]

SKIN FRICTION DRAG AND SHEAR STRESS DISTRIBUTION ON SEVERAL STREAMLINED BODIES OF REVOLUTION WITH VARIED FINENESS RATIO

by

Cleveland L. Dunning
Captain, United States Marine Corps

Robert F. Overmyer

Captain, United States Marine Corps

and

Colben K. Sime, Jr.

Captain, United States Marine Corps

Submitted in partial fulfillment of
the requirements for the degree of

MASTER OF SCIENCE

with major in Aeronautics

United States Naval Postgraduate School
Monterey, California

1964

SKIN FRICTION DRAG AND SHEAR STRESS DISTRIBUTION ON SEVERAL STREAMLINED BODIES OF REVOLUTION WITH VARIED FINENESS RATIO

by

Cleveland L. Dunning

Robert F. Overmyer

and

Colben K. Sime, Jr.

This thesis is accepted in partial fulfillment

for the degree of

MASTER OF SCIENCE

with major in Aeronautics

from the

United States Naval Postgraduate School

ACKNOWLEDGEMENT

The authors wish to express their sincere gratitude to Professor George J. Higgins for his great interest, help and encouragement in the completion of this work. Professor Higgins, in addition to his full schedule as a faculty member and on short notice, proposed this project and has graciously provided time and guidance toward the fulfillment of this objective. In addition, many stimulating discussions by Professor Higgins in previous courses in fluid mechanics and aerodynamics are acknowledged.

ABSTRACT

Experimental techniques were employed to determine the coefficient of skin friction drag and the distribution of local frictional intensity for several low drag bodies of revolution with mixed laminar and turbulent flow. The data were obtained as a function of fineness ratio and Reynolds number from experiments conducted in the U. S. Naval Postgraduate School subsonic wind tunnel under conditions equivalent to incompressible flow.

Skin friction drag coefficients were determined first by the indirect method of subtracting pressure drag from total drag. A second more direct method was the determination of local shear distributions and integration over the surface area to obtain total frictional drag. The possibility of inaccuracies introduced by assumptions and agreement between results of the two methods are discussed.

TABLE OF CONTENTS

LIST OF TABLES

LIST OF ILLUSTRATIONS

TABLE OF SYMBOLS

Symbol	Definition	Units
C_{D_f}	Skin friction drag coefficient based on wetted surface area	-
$C_{D_{wet}}$	Total drag coefficient based on wetted surface area	-
C_{D_p}	Pressure drag coefficient based on wetted surface area	-
C_{D_t}	Coefficient of total drag - includes support and buoyancy drag	-
$C_{D_{supp}}$	Coefficient of support drag	-
C_f	Flat plate drag coefficient	-
$C_{f_{lam}}$	Laminar flat plate drag coefficient	-
$C_{f_{turb}}$	Turbulent flat plate drag coefficient	-
$C_{f_{trans}}$	Flat plate drag coefficient at transition	-
ΔC_{D_B}	Coefficient of buoyancy drag	-
$\Delta C_{D_{S+B}}$	Coefficient of buoyancy plus support drag	-
D_f	Friction drag	lbs.
D_t	Total drag	lbs.
D	Diameter	ft.
L	Axial length	ft.
p	Local static pressure	lb./ft.^{2}
p_o	Stream static pressure	lb./ft.^{2}
Δp	Local static minus stream static pressure	lb./ft.^{2}
q_o	Free stream dynamic pressure	lb./ft.^{2}
r	Radius	ft.
R_L	Reynolds number based on axial length	-
R_s	Local Reynolds number based on developed length	-

Symbol	Definition	Units
s	Variable developed length	ft.
S	Developed length	ft.
S_o	Frontal area	ft.
S_w	Wetted surface area	ft.^{2}
V	Local velocity	ft./sec.
V_o	Free stream velocity	ft./sec.
X	Variable axial length	ft.
$\left(\frac{\partial v}{\partial y}\right)_o$	Velocity gradient at surface	$\frac{\text{ft./sec.}}{\text{ft.}}$
$\left(\frac{\partial \frac{V}{V_o}}{\partial y}\right)_o$	Slope of non-dimensional velocity profile	1/ft.
ρ	Density of air	$\frac{\text{lb.-sec.}^2}{\text{ft.}^4}$
θ	Angle between local tangent to surface and body axis	deg.
μ	Absolute viscosity	$\frac{\text{lb.-sec.}}{\text{ft.}^2}$
τ_o	Local shear stress at the surface	lb./ft.^{2}

1. Introduction.

The aerodynamic forces on a body immersed in an incompressible fluid flow consist of contributions from normal pressures and tangential shear stresses. The problem of determining the coefficient of skin friction drag and distribution of local frictional intensity for several bodies of revolution as a function of fineness ratio and Reynolds number was undertaken at the United States Naval Postgraduate School, Monterey, California. Data for this analysis were obtained from subsonic wind tunnel tests on six models with fineness ratios from one to six at zero angle of attack and through a Reynolds number range of 0.1 to 5.0 x 10^6. The model shapes were based upon the NACA 66(215)-0XX airfoil.

The skin friction drag based on wetted surface area was to be initially determined from the difference of the total drag and pressure drag. A second method involving the integration of the local shear stresses in the boundary layer over the developed length of the body was later utilized to determine the skin friction drag.

The expected agreement in results from the two methods was dependent upon an accurate determination of the drag components of the mutually perpendicular pressure and shearing forces acting normal and tangential to the model surface. It was hoped that these results could be correlated with and compared to other analytically and experimentally determined skin friction drag coefficients of a flat plate at zero incidence and other axially symmetric bodies.

2. Equipment and Procedures.

Six similarly shaped bodies of revolution with various length to diameter ratios were used as a basis for the experimental portion of this investigation. The models were constructed of mahogany with a highly polished lacquer finish.

The models all had a longitudinal distribution of diameter corresponding to the chordwise distribution of thickness for the NACA 66(215)-0XX airfoil. Their low drag profile ends with a cusped trailing edge. The point of maximum diameter is at 45 percent of the length for each model. Fig. 1 contains a photograph of the models. The length to diameter ratios were one, two, three, four, five, and six with the maximum diameter of each body being six inches. Tables I and II contain the diameter-length coordinates and other model characteristics such as surface and frontal areas. Each model has a pressure orifice on the nose and tail with ten other pressure orifices located along the surface. Orifice locations are at the same X/L distance aft of the nose for all models. Table III contains the orifice locations in percent of length. A small brass tube inserted and sealed in each orifice was flush with the surface of the body and terminated in a hollowed chamber inside. A removable portion of the body permitted access to the 12 pressure tubes and the streamlined support strut connection located inside the model.

The tests were conducted in an Aerolab 90 closed circuit single return subsonic wind tunnel manufactured by the Aerolab Development Company of Pasadena, California. A diagram of this tunnel is shown in Fig. 2. The 100 horsepower electric motor

which powers a 6'4" variable pitch propeller is capable of producing air flow velocities of zero to 185 knots in the 32" X 45" X 48" test section. The estimated turbulence factor for the test section is 1.16 and the percentage turbulence is 0.20 percent as previously determined using procedures discussed by Pope [1].

An Aerolab "543" three component wind tunnel beam balance manufactured by the Aerolab Development Company was used to obtain drag measurements. Fig. 3 shows a diagram of this balance. The balance is limited to a maximum of 50 pounds of drag with a sensitivity of 0.005 pounds. These limits are well within those required for this study.

A standard pitot-static system in conjunction with standard direct lift micromanometer apparatus employing silicone (sp. gr. 0.935) as the working fluid was used to maintain the wind tunnel at the desired dynamic pressures. A multiple tube manometer also employing silicone as the working fluid was used to obtain static pressure measurements at the 12 orifices on the bodies of revolution.

a. Total Drag Measurements.

Figs. 4a, 4b, and 4c contain photographs of the wind tunnel and equipment set up used to measure total drag. Prior to mounting in the tunnel all model irregularities were smoothed and repolished. All screw access holes were filled with modeling clay to insure smooth flow over the model and preclude premature transition from laminar to turbulent flow. The support strut was attached to the balance through a hole in

the floor of the test section. The strut was shielded from the air stream by a streamlined fairing. Each model was aligned parallel to the test section to insure symmetric flow about the body and to prevent the development of undesirable lifting forces or yawing moments.

To minimize expected lateral oscillations with the tunnel operating at higher dynamic pressures, a small triply supported ring was centered over the tail of the models having large fineness ratios. The ring was positioned such that a 1/8 inch concentric clearance was maintained between the model tail and the ring except during oscillation. The expected lateral oscillations of the models with larger L/D ratios did not materialize. All oscillations were observed to be less than the 1/8 inch ring clearance at all dynamic pressures.

Total drag measurements were made on each model for increments of dynamic pressure equivalent to one centimeter silicone from one centimeter to 45 centimeters.

b. Support Drag.

Support drag measurements for L/D ratios of four, five, and six were obtained from the set up as shown in Fig. 5. For these measurements the model with L/D ratio of five was mounted in the tunnel utilizing the same configuration as that used for total drag measurements except for the addition of a dummy support. The dummy support was mounted on top of the model and held by two 1/8 inch diameter pins which were inserted into the model. The free end of the dummy support

extended above the model into a fairing mounted from the top of the test section are shown in Fig. 5. Equal amounts of the actual and dummy struts were exposed to the drag forces of the wind stream. The difference between the drag with a single strut and two struts was considered the increment of drag caused by the support.

Identical procedures were used to obtain support drag measurements for fineness ratios of one, two, and three. For the three shorter bodies the model with fineness ratio of two was used as a basis for the measurements.

c. Local Pressure Distribution Measurements.

Fig. 6 contains a photograph of the test section set up used to obtain local pressure distribution measurements on each of the models. Primary support of the models was achieved through the use of the streamlined support strut attached to the balance through the floor of the test section.

Small plastic pressure tubes were connected and cemented to twelve brass pressure tubes in the hollowed chamber of the model. The pressure tubes were of sufficient length to exit through a hole in the lower aft portion of the model and extend through the test section floor. The pressure tube extending from the model was formed into a small bundle and faired behind a secondary support. This technique prevented model oscillation and decreased flow interference around the orifice at the tail that would have been present with the ring support system as previously utilized for the drag measurements.

The first system pressure leakage or integrity test was made prior to the attachment of the pressure tubes from the model to the multiple tube manometer. Upon assurance that there were no leaks in this portion of the system the pressure tubes from the model were connected and cemented to the larger diameter pressure tubes leading into the multiple tube manometer. After this connection was made, an integrity check of each tube of the system from the orifice to the manometer was performed. This check consisted of introducing a pressure differential into the system through the orifice on the body. The magnitude of the pressure differential was greater than any pressures expected at any time during the tests. After the pressure differential was introduced the orifice was covered. Any system pressure leaks indicated by a rise or fall of the silicone level in the manometer were investigated and corrected.

Pressure distribution measurements were taken on each model at tunnel dynamic pressures equivalent to 2, 5, 12, 25 and 38 centimeters of silicone.

d. Boundary Layer Probe.

The velocity distribution within the boundary layer on the models having L/D ratios of three, four, five and six was determined by using a capillary pitot tube. The distance from the edge of the pitot tube to the center of the opening in the flattened tube was 0.009 inches. The pitot tube was ground flat on the bottom to permit a velocity survey as close to the body as possible.

The bodies were mounted in the tunnel using the same techniques as those for the total drag measurements. The test section was modified by mounting a plexiglass window in the top of the tunnel and a plexiglass panel equipped with small holes to permit access to the model with the small pitot tube through one side of the test section.

The tunnel was operated at dynamic pressures equivalent to 2, 5, and 12 centimeters of silicone. The survey pitot tube was connected through pressure tubing to a direct lift micromanometer. To insure that total pressure recovery was being realized with this apparatus frequent cross checks of free stream pressures were compared with the test section pitot-static system.

A twelve power telescope sight mounted on top of the wind tunnel in a position to view the test section was utilized to insure tangential alignment of the survey pitot tube on the body. The pitot tube was controlled in the horizontal plane through the access hole in the tunnel test section to insure pick up of the actual tangential component of the velocity in the boundary layer.

Models with L/D ratios of one, two, three and four were tested in the tunnel with fine threads of wool attached to the after portion of the body with cellophane tape. The bodies were mounted in the tunnel in the same manner as that used for the total drag measurements. The tufts of wool were mounted every quarter of an inch aft of the maximum diameter location in a helical pattern so as not to interfere with each other. The tunnel was run at various speeds with close

observation of the action of the tufts. The motion of the wool tufts gave a good indication of the degree of flow separation and the shift in separation point with increasing velocity. Severe separation was apparent only for fineness ratios of one and two. A small degree of separation was indicated on the extreme aft portion of the body L/D of three at very low velocities.

3. Presentation of Results.

The results of the tests to determine the coefficient of skin friction drag from the difference of $C_{D_{wet}}$ and C_{D_p} are tabulated in Table IV through Table IX. They are further graphically portrayed in Fig. 7 through Fig. 10.

Table X through Table XV contain the processed data and the results of the determination of C_{D_f} obtained from the difference of total and pressure drag. Tables XVI through XX contain data used for plotting local frictional intensity and the integrated friction drag. The intermediate and final results are shown graphically in Fig. 11 through Fig. 20.

A graphical comparison of the coefficients of skin friction drag obtained by two separate methods is shown in Figs. 21 and 22 as a function of Reynolds number and fineness ratio.

4. Skin Friction Drag Determined From Total Drag Minus Pressure Drag.

a. Total Drag.

The total drag on an arbitrary body can be considered as the summation of skin friction drag, form or pressure

drag, induced drag and interference drag. Since the tests utilized for this analysis were conducted at zero angles of attack on bodies of revolution with no appendages the effects of induced drag and interference drag were absent.

Wind tunnel measurements of the total drag on the six models of fineness ratio one, two, three, four, five and six were made at test section velocities in the range of 55 ft./sec. to 280 ft./sec. These velocities correspond to a range in Reynolds numbers of 0.1 to 5 X 10^6. These results which include the effects of test section horizontal buoyancy and support drag were reduced to coefficient form based on wetted surface area using the following relation:

$$C_{D_t} = \frac{D}{\frac{1}{2}\rho V^2 S_w}$$

The support drag was determined using a modification of the mirror or "image" methods discussed by Pope [1]. This technique required the determination of a drag coefficient from an additional test run on each of the models of fineness ratio two and five with the dummy support installed on the model. The subtraction of C_{D_t} for L/D ratios of two and five from the coefficient determined with the dummy support installed yielded two values of $C_{D_{supp}}$. The $C_{D_{supp}}$ determined from the test on fineness ratio two was applied to the models of L/D ratio one, two and three. The support drag coefficient determined from fineness ratio five was applied to the models of L/D ratio four, five and six.

Horizontal buoyancy drag and support drag in coefficient form were subtracted from C_{D_t} to obtain $C_{D_{wet}}$ for each body. The results of this determination of $C_{D_{wet}}$ for each of the six fineness ratios are graphically presented along with previously determined flat plate results as a function of R_L in Fig. 7.

Curves representing the skin friction coefficient of a flat plate, C_f, as a function of R_L are shown in this figure. The curve shown as laminar is representative of $C_{f_{lam}}$ based on the assumption of a pure laminar boundary layer. This curve was plotted from the following relation [2]:

$$C_{f_{lam}} = \frac{1.328}{R_L}$$

This equation is the result of an accurate solution to the Blasius equation made by L. Howarth. The following relationship developed from measured flat plate data [3] was used to obtain $C_{f_{turb}}$ as a function of R_L

$$C_{f_{turb}} = \frac{.445}{(\log_{10} R_L)^{2.58}}$$

As is shown in Fig. 7 the magnitude of the skin friction drag coefficient on a flat plate at a given R_L is dependent on the type of boundary layer flow. To determine the coefficient for a mixed flow condition; i.e., initial laminar flow with later transition to turbulent flow, the Reynolds number at which transition occurs ($R_{L_{crit}}$) must be determined. The critical Reynolds number for a smooth flat plate is a function

of test section turbulence. The flat plate critical Reynolds number of 2.142 X 10^6 for the tunnel has been estimated in previous academic studies using the "turbulence sphere" [1] and empirical data [4]. From these considerations the transition curve was constructed from the following equation which includes the term to compensate for mixed flow:

$$C_{f_{trans}} = \frac{.445}{(\log_{10} R_L)^{2.58}} - \frac{A}{R_L}$$

$$\text{where } A = R_{L_{crit}} (C_{f_{turb}} - C_{f_{lam}})$$

The graphic presentation in Fig. 7 of $C_{D_{wet}}$ versus R_L for the six models tested shows a smooth family of curves. The relatively large effects on $C_{D_{wet}}$ of varied fineness ratios within the family is evident with a comparison to flat plate values at given Reynolds number. The curves also show the effects of R_L on $C_{D_{wet}}$ for a given body.

The curves of L/D ratios of one and two plotted in Fig. 7 qualitatively show the same trend. With increasing R_L, $C_{D_{wet}}$ for fineness ratio of one remains relatively constant to a R_L near 4 X 10^5. At this point the previously laminar boundary layer, with its accompanying laminar separation, began a transition to turbulent flow prior to separation. As transition was completed to a point on the body forward of the relatively sharp decrease in radius aft of the point of maximum diameter, $C_{D_{wet}}$ dropped sharply. This situation occurs with smooth spheres in low turbulence flow [5] [6]. The mechanism accounting for this phenomenon is

the delayed separation caused by the turbulent boundary layer. The delayed separation greatly decreases pressure drag. The cause of the indicated decrease in C_{Dwet} for fineness ratio two is analogous to that of L/D ratio one. However, the increased length of this body is such that the rate of decrease in radius aft of maximum diameter at the 45 percent station is less than that for fineness ratio one. As a result the decrease in C_{Dwet} is more gradual. As fineness ratio is increased above two sudden decreases in C_{Dwet} are no longer evident. The curves more closely approximate the characteristic flat plate curves both in shape and in the magnitude of the drag coefficients. The curves at lower R_L are indicative of substantially laminar flow with relatively small pressure drag contributions. As the R_L is increased C_{Dwet} passes through a minimum. At this point the transition from laminar to turbulent flow moves steadily forward causing a rising trend in C_{Dwet}. These results furnish substantiation of the previously determined low wind tunnel turbulence factor which is a necessity for this type of a study.

Streamlining for the higher fineness ratios causes pressure drag to be less significant with the result that the drag coefficient curve in Fig. 7 for L/D ratios five and six closely approximate that for a flat plate. Streamlining reduces or eliminates boundary layer separation thus changes the relative contributions of pressure and frictional forces to the total drag. Total drag on a body of revolution at zero angle of attack can be resolved into contributions by

pressure forces acting normal to the surface and frictional effects acting tangent to the body surface. These mutually perpendicular forces are illustrated schematically in Fig. 8.

Shapiro [7] discusses several simple two dimensional experiments which illustrate the results of streamlining and its relative effect on friction and pressure drag contributions. In one experiment Shapiro compares the drag of a circular rod and an airfoil section of the same maximum thickness. The circular rod had approximately nine times the drag of the streamlined airfoil at the same test velocity. With a smaller area subjected to viscous forces total drag for the rod was dominated by pressure forces. Streamlining of the airfoil reduced total drag by nine fold thus illustrating the effect of streamlining on drag contributions. The same influence is experienced in streamlining the bodies of revolution from L/D ratio of one to the higher fineness ratios where pressure drag contributes a small portion of total drag.

b. Pressure Drag.

Pressure drag or form drag results from the distribution of normal pressure forces over the surface of the body. The components of these pressures acting in the lengthwise direction over a surface area equal to the frontal area of the body cause a drag force on the body. Certain areas of high pressure on the aft portion of a body may cause negative drag or thrust. Although, this may decrease total pressure drag it will not be great enough to cause an over-all negative or

zero drag. The net component of normal pressures perpendicular to the body axis would be lift. The models were symmetrical bodies of revolution tested at a zero angle of attack. Therefore, all pressure forces perpendicular to the axis were diametrically opposed by an equal pressure and cancelled, leaving only the drag component.

The surface pressure (Δp) at each orifice was obtained by subtracting the free stream static pressure of the test section from the local static pressure at each orifice. The values are listed in Tables X through XV. Values of $\Delta p/q_o$ were computed using the free stream dynamic pressure (q_o). Values of local static pressure at each orifice, stream static and total head pressures were obtained simultaneously with the aid of a multiple tube manometer. The free stream static pressure utilized for calculating Δp and the stream dynamic pressure were obtained from a pitot-static tube mounted in the test section ahead of the model.

The coefficient of pressure drag based on wetted surface area can be determined mathematically as follows:

$$C_{D_p} = \frac{2\pi}{S_w} \int \frac{\Delta p}{q_o} \sin\theta \, r \, dr$$

where S_w = wetted surface area of body

$\frac{\Delta p}{q_o}$ = nondimensional pressure difference at each point on the body

θ = angle between tangent to body surface and the body axis

r = radius to each point

Since each factor within the integral varies along the body it would be necessary to obtain the function defining each variable before this integral could be directly evaluated. Due to the limited number of orifices from which data was obtained it was impractical to determine an explicit function for each variable. Instead, the integral was evaluated using graphical methods.

The profile of each body was drawn to scale as shown in Figs. 9a through 9f. The value of $\frac{\Delta p}{q_0}$ for each orifice was multiplied by the local diameter and plotted perpendicular to the surface. The radius was replaced by diameter to double the scale of the graphical representation of pressure distribution. This increased the accuracy of the graphical integration of pressure drag forces. The horizontal component of this plot was then projected on a vertical reference line. With a curve faired through these points, they formed a closed curve representing the nondimensional pressure drag of the body. The area of this closed curve was graphically integrated and the value multiplied by π/S_W to obtain the coefficient of pressure drag. Figs. 9a and 9b illustrate representative graphical integration solutions conducted for L/D ratios of one and two. For the remaining models, only the distribution of normal pressure forces are plotted about the body (Figs. 9c through 9f) to illustrate the reduction in magnitude of the surface pressures with increasing fineness ratio. Reduced pressure forces agree with the results of low pressure drag for streamlined bodies.

The value of C_{D_p} was obtained by graphical integration of pressure forces at five different tunnel velocities for each body. Fig. 10 is a graph of the coefficient of pressure drag as a function of Reynolds number for each body with fineness ratios two through six. As was expected and outlined in various references, C_{D_p} was greatest for the body with the smallest L/D ratio due to separation of the flow over the aft portion of the body. The pressure drag is seen to decrease considerably as the L/D ratio increased.

From Fig. 10 it is seen that the value of C_{D_p} decreases with Reynolds number for the range of the test velocities for the bodies with an L/D of two and three. This decrease in drag is due to an aft shift of the separation point on the body associated with transition to turbulent flow with increasing velocity and Reynolds number.

Bodies with an L/D ratio of four, five, and six do not show this characteristic. The influence of separation does not appear to occur on the aft portion of the larger models under conditions of low Reynolds numbers. Separation characteristics were observed by the action of tufts of wool attached to the after body. With the tunnel operated through a wide range of dynamic pressures, no separation was observed for L/D ratios of four, five and six. Separation was apparent at low Reynolds numbers for L/D of one, two, and three. An aft shift in separation point was observed at higher Reynolds numbers for the three shorter models. The C_{D_p} of the bodies with an L/D ratio of four, five and six is seen to increase

with an increasing Reynolds number. This is probably due to an increase of turbulence in the wake as the transition point from laminar to turbulent flow moved forward on the body.

The local static pressures which were used to determine the pressure drag of the bodies was also utilized to obtain the super-velocity of the flow over the body. Pressures in an "incompressible" flow are transmitted without change through the boundary layer in directions normal to the surface [6]. Because of this characteristic of an incompressible fluid, an estimated velocity at the outer limit of the boundary layer may be computed using the static pressure obtained at the surface. Velocities encountered throughout the tests were of a magnitude such that compressibility effects are considered negligible and Bernoulli's Theorem for incompressible flow applies. Bernoulli's Theorem states:

$$p_o + \frac{\rho V_o^2}{2} = p + \frac{\rho V^2}{2}$$

where p_o = stream static pressure

V_o = stream velocity

p = static pressure at orifice

V = local velocity at orifice

ρ = density of air

The above equation can be solved for the local velocity as follows:

$$V = \sqrt{V_o^2 + \frac{2}{\rho}(P_o - P)}$$

When the ΔP obtained from the pressure tests is used in this formula the local super-velocity is obtained. The local increments of super-velocities are recorded in Tables X through XV in terms V/V_0 for later use in estimating the local tangential shearing stresses caused by the frictional effects of viscous flow along the body surfaces. Also, recorded in Tables X through XV are values of Reynolds number (R_s) based on the local super-velocities and the distance (s) aft of the nose as developed along the surface of the model.

c. Skin Friction Drag.

The bodies tested for this analysis were aligned for a zero angle of attack and zero sideslip angle which eliminated any induced drag created by lift in either plane. Velocities of the tests were sufficiently low that the effects of compressibility could be neglected and the flow considered to be incompressible. Therefore, skin friction and pressure drag form the total drag on the models.

The skin friction drag coefficient (C_{D_f}) was obtained by subtracting the pressure drag coefficients in Fig. 10 from the total drag coefficients ($C_{D_{wet}}$) of Fig. 7.

$$C_{D_f} = C_{D_{wet}} - C_{D_p}$$

The values of C_{D_f} as a function of Reynolds number for fineness ratios three, four, five and six are graphically presented in Fig. 11. Since the models with L/D ratios one and two possess drag characteristics similar to those of a

sphere and can be categorized as extreme cases of streamlined bodies, C_{D_f} curves for these two are not included in this figure.

The curves form a family which possesses characteristics comparable to those of $C_{D_{wet}}$ contained in Fig. 7. Initially, the curves show a decrease in C_{D_f} with increasing Reynolds number. Increasing Reynolds number above that where minimum drag is reached caused an increase in drag coefficient. This increase in drag is indicative of a forward movement of the transition point and an extension of the turbulent flow region.

The percentage of pressure drag and frictional drag contributions to the total drag of the models is shown in Fig. 12. The curve shows frictional drag over total drag (D_f/D_t) plotted against diameter over length (D/L) for the two Reynolds numbers of 1.0×10^6 and 1.5×10^6. Data points for the curves were taken from the graphs of total and frictional drag coefficients shown in Figs. 7 and 11 as a function of Reynolds number.

The curves in Fig. 12 show a high contribution by friction drag for the thinner bodies. For D/L of 0.167 frictional drag contributes 80 percent of total drag at $R_L = 1.0 \times 10^6$ and approximately 75 percent at $R_L = 1.5 \times 10^6$. For the very thin models the percentage of friction drag is seen to decrease along a smooth curve with increasing D/L. This decrease in the relative contributions of frictional drag is the result of reduced surface area over which the tangential shear stresses act. The curves are extended by dashed lines

to the point where D/L is zero and D_f/D_t is equal to one. This point would represent the case of a flat plate or an infinitely thin straight line where the total drag is composed entirely of frictional or viscous shearing forces.

A discontinuity occurs in the curves of Fig. 12 at different values of D/L for the two Reynolds numbers. The break in the curves shows an abrupt change in relative contributions of friction and pressure drag to the total drag forces. The large increase in the influences of pressure drag and reduction in frictional effects is the result of flow separation on the afterbody of the short models. For $R_L \doteq 1.0 \times 10^6$ the break in the curve occurs with a D/L value of approximately 0.40 to 0.50. At the higher Reynolds number of 1.5×10^6, with transition to turbulent flow and delayed separation, the discontinuity occurred at a D/L value greater than 0.5. An additional model with a fineness ratio between L/D of 1.0 and 2.0 would aid in more closely locating the discontinuity in data for Reynolds number of 1.5×10^6.

The shift in the point of flow separation, which would cause the discontinuity in the curves of D_f/D_t to be a function of Reynolds number as well as D/L, was observed during tests with tufts of wool attached to the aft portion of the models. Regions of separated flow were clearly indicated by random motion of the tufts in contrast to the smooth streaming of the tufts in regions of non-separated flow. The uniquely distinct behavior of the tufts in the two regions served to mark the point of separation and permitted

observations of the shift in transition point with changes in Reynolds number. From observing changes in separation point on the shorter models it is concluded that the influences of separation on pressure and friction drag caused the discontinuity in data.

5. Direct Determination of Local Skin Friction Intensity.

Most investigations concerning boundary layer distribution and local shearing stresses which result from viscosity and flow conditions in the boundary layer have been based primarily on extensions of flat plate theory or flow in straight pipes. Flat plate and pipe results have been well established theoretically or experimentally for both the laminar and turbulent flow regimes. More recent investigations have been made in the transition region by Miller [8] and others. It is evident that shear distributions in neither of the above cases corresponds to the case of flow about curvilinear contours in either two or three dimensions. The above cases cannot, in general, give sufficient emphasis to the effects of static pressure gradients, local super-velocities and other factors which significantly affect the boundary layer velocity profiles. Static pressure gradient, further, has a large influence in resolving such problems as the location of transition from laminar to turbulent flow and points of local flow separation.

The factors mentioned affect boundary layer profiles to such an extent that the practice of employing velocity distributions for specific cases, which are obtained either

experimentally or theoretically, for the purpose of extrapolating shear stress distributions for other shapes may yield unpredictable results.

The skin friction drag coefficients in Fig. 11, for the bodies of revolution with large fineness ratios, follow closely the general trend of the frictional drag curves for the flat plate. For thin bodies the drag curves fall between the flat plate data, indicating mixed flow between laminar and turbulent boundary layers. The trend toward transition at higher Reynolds numbers is also apparent. Even though the total skin friction drag on the thin models is not appreciably different from that for a flat plate at the same Reynolds number, it does not follow that the distribution of these drag forces as local shear stresses over the curvilinear surfaces will even resemble the distribution of frictional intensity on a flat plate.

Experiments have shown, in fact, that in a boundary layer with positive or negative pressure gradients, the velocity distribution differs considerably from that obtained on a flat plate with zero pressure gradient or in a straight pipe.

To emphasize this experimental observation the slopes of the velocity profiles $\left(\frac{\partial\left(\frac{V}{V_0}\right)}{\partial y}\right)_0$ in the laminar flow region of a flat plate are compared in Fig. 13 with the laminar region of two of the bodies of revolution studied in this analysis. The curve plotted for the flat plate was taken from the Blasius application of Prandtl's boundary layer theory to laminar flow on a flat plate. The Howarth solution of the

Blasius equation is tabulated in Schlichting [2]. Blasius considered a thin flat plate with zero angle of incidence and with zero static pressure gradient.

The slopes of the boundary layer velocity profiles for the bodies of revolution were obtained from a wind tunnel boundary layer probe to a point 0.009 inches from the body surface. The slopes of the velocity profiles at the surface were approximated by assuming a linear variation of velocity between the surface and the 0.009 inch point where the boundary layer probe was taken. This may appear to be a rough approximation; however, the results plotted in Fig. 13 serve to illustrate the influences of negative or favorable pressure gradients on the boundary layer and consequently on the distribution of shear stress. It is noted that the static pressure distributions plotted in Fig. 14 show a favorable pressure gradient over the forward portions of each body of revolution. The results of Fig. 13 are taken from a free stream velocity of 57.0 feet per second.

The flat plate curve in Fig. 13 shows a steep slope for the boundary layer profile near the leading edge with an immediate drop indicated with increases in local Reynolds number caused by distance aft. The behavior of the curve indicates a thickening of the boundary layer and reduction in slope of the profiles at the surface. This is the result of losses in momentum of the air in contact with the plate and the propagation of the losses through additional layers of air by the action of viscous shearing forces between molecules.

The negative pressure gradients along the forward portion of the bodies of revolution caused an acceleration of air flow around the body, adding to the momentum and inertia forces of the free stream. The result of this favorable pressure gradient delayed boundary layer thickening and caused steep velocity profiles to persist further aft along the body as shown in Fig. 13. In the regions where the pressure gradient became less negative, as indicated in Fig. 14 acceleration of air was reduced permitting increased viscous thickening of the boundary layer and reduction in slopes of the velocity profiles. Acceleration around the shorter body of revolution was greater since the air flow increased to approximately the same super-velocity at the maximum diameter. The result of the acceleration occurring over shorter distances from nose to maximum diameter caused steeper velocity gradients in the boundary layer of the shorter model.

It is noted from the velocity profile slopes versus local Reynolds number in Fig. 13 that neither of the streamlined bodies reached that of the flat plate before turbulent transition occurred. This could be the result of transition caused by the onset of an adverse pressure gradient aft of the maximum diameter of the model. A positive pressure gradient would cause losses of momentum in the boundary layer and cause increased thickness. The resulting instability in a laminar boundary layer promotes transition to turbulent flow and eventually separation if adverse pressures persist.

The most important conclusion which can be reached from the results presented in Fig. 13 is that any quantitative comparison of the local shear stress of an arbitrary body of revolution with the known results of a flat plate may be difficult and give questionable results. A qualitative estimate of effects caused by negative pressure gradients and super-velocities can, however, be obtained. The value of this information in accurately relating the magnitude of local friction intensity of an arbitrary body to that of a flat plate is doubtful.

In addition to limited ability to compare the three dimensional boundary layers on bodies of revolution to that of a flat plate, little experimental data are available from subsonic tests on three dimensional bodies. In recent years the NACA has conducted numerous drag and pressure distribution experiments on bodies of revolution in supersonic tunnels and in compressible subsonic flow [9] [10]. This information is of little interest here, however. Various two dimensional boundary layer experiments conducted by the NACA on airfoil sections and flat plates provided additional evidence as to the qualitative effects of pressure gradient and local acceleration of flow on the velocity profiles in incompressible flow [11] [12] [13] [14]. The results of these experiments on different curvilinear profiles do not provide sufficient basis for the application to arbitrary three dimensional bodies in estimating the local distribution of shear stresses with any assured degree of accuracy.

a. Analytical and Theoretical Methods.

For fluids with relatively small viscosity the affect of internal fluid friction is important only in the narrow regions surrounding flow boundaries called the boundary layer. Since the fluid has zero velocity at the surface there is a steep velocity gradient from the boundary into the main stream of flow. In real fluids the velocity gradient sets up boundary shear forces causing resistance to flow and losses of fluid momentum in the boundary layer. The boundary layer is very thin at the upstream end of a streamlined body. With motion downstream the continuous action of shear stress slows down additional fluid causing increases in boundary layer thickness. The flow is subjected to pressure gradients which serve to increase fluid momentum if the pressure decreases downstream and decreases momentum if a positive pressure gradient exists. The boundary layer is initially laminar on the forward portion of the body. As the boundary layer thickness increases, laminar instability develops and a transition to turbulent flow occurs, after which fluid particles move in random paths throughout the boundary layer except for a thin layer next to the surface referred to as the laminar sub-layer.

From an analytical viewpoint the requirement to establish a distribution for local shear stresses is to solve theoretical boundary layer equations to determine the velocity

gradient at the surface. The local shear stress which is a function of the velocity gradient can then be obtained from the following relation:

$$\tau_0 = \mu \left(\frac{\partial V}{\partial y} \right)_0$$

where μ = absolute viscosity lb.-sec./ft.^{2}

$\left(\frac{\partial V}{\partial y} \right)_0$ = slope of velocity profile at the surface ft./sec.

Not only is this equation applicable to laminar boundary layers but the existence of the laminar sub-layer in turbulent boundary layers [15] permits its use in calculating local shear stresses throughout regions of both laminar and turbulent flow.

Various theoretical methods such as potential flow and the solution of the Navier-Stokes equations have been used for predicting the point of transition to turbulent flow. The calculation of turbulent boundary layer flow and shear stresses are based on the theoretical assumptions of Prandtl's mixing length theory, von Karman's similarity hypothesis and others such as momentum thickness theorems.

The application of potential and stream function theorems which are relatively easy to apply in two dimensions, causes added complexity when applied to arbitrary three dimensional flow conditions. The axially symmetric boundary layer on the simplest case of a sphere is discussed in Schlichting [2] where it is indicated that the body contour and the Blasius

solution for the velocity potential must be represented by a power series to the seventh power to obtain an acceptable degree of accuracy.

Slender bodies require considerably more terms in the Blasius power series to adequately represent conditions on the long afterbody. It was concluded [2] that the calculation of functional coefficients for the Blasius series beyond the seventh term involves an unacceptable amount of computation. For this reason the method is considered to be severely limited for practical application to slender bodies.

In addition, potential flow theorems and velocity potential functions have been applied to the two dimensional case of streamlined bodies to determine the influences of profile shape on the location of transition. The Pohlhausen method and potential flow were applied by Bussman and Ulrich [16] to various Joukowsky profiles. The potential flow about a Joukowsky airfoil section is obtained through the complex transformation and conformal mapping of the flow about a circular cylinder. The instability or transition point obtained from this detailed analysis only approximated the experimental results on the same airfoil section. Since the onset of turbulent flow is a major factor in determining total skin friction drag on a body; the accuracy with which the transition point can be located is reflected in the accuracy with which skin friction drag can be predicted.

From Prandtl's mixing length theory [17] the expression given for shear stress in turbulent flow is:

$$\tau = \rho \ell^2 \left(\frac{dv}{dy}\right)^2$$

where the distance (ℓ) is referred to as the mixing length and represents a magnitude which is analogous to the mean free path of a molecule in the kinetic theory of gases. The mixing length has a magnitude proportional to the displacements of aggregate volumes of fluid transverse to the direction of general flow [2]. Prandtl made the additional assumption that the shear was constant throughout the turbulent boundary layer, therefore; the above equation becomes the local shear stress at the surface.

Different viewpoints as to the variables upon which the mixing length is dependent have been expressed. Prandtl, for his case where the shear is constant across the boundary layer, considered the mixing length to be determined simply by the distance from the surface [18]. von Karman, in his similarity hypothesis, considered the mixing length to be determined by the ratio of the first derivative of velocity with respect to distance to the second derivative. Experimental evidence quoted by Fediaevsky [18] indicates that the mixing length is apparently a function only of a non-dimensional distance from the surface.

The complexity of application of these theoretical methods and the volume of calculations necessary in adapting

them to any practical engineering problems appear to limit these methods to more of an academic interest. More easily applied and practical approaches should be used for general engineering solutions.

b. Experimental Estimate of Shear Stresses.

Difficulties encountered in extrapolating existing two dimensional shear stress distributions to three dimensional flow conditions in conjunction with limited applications of theoretical solutions to boundary layer flow prompted an experimental approach toward direct determination of skin friction distribution. The combination of a wind tunnel boundary layer probe at several low Reynolds numbers and rational extrapolation to higher velocities provide the basis for the following direct evaluation of local skin friction intensity. The local shear stresses were subsequently integrated over the entire surface area of each body of revolution to obtain total skin friction drag and drag coefficients. These results are then compared for agreement with the previous method of subtracting pressure drag contributions from total drag.

The bodies of revolution with fineness ratios of one and two are considered to be extreme cases of streamlined bodies. The skin friction drag is of less interest than on longer bodies; therefore, no effort was made to predict local shear distributions for these bodies. It is felt, however, from the results of total drag measurements and pressure distributions,

that the L/D ratio of one; and the L/D ratio of two to a lesser degree; would demonstrate characteristics very similar to a sphere.

For the four longer models a boundary layer probe was made at a point 0.009 inches from the surface to determine the lengthwise velocity distribution in the boundary layer near the surface of the body. Boundary layer probes were taken for free stream velocities of 57, 90, and 140 feet per second. The data are recorded in Table XVI and plotted in Figs. 15 and 16 as V/V_o versus distance along the models. The curves show high values of V/V_o near the nose of the bodies where the boundary layer is thin and an increase in momentum by acceleration of the free stream has caused a steep velocity gradient. With progress downstream the magnitude of V/V_o decreases which is the result of momentum losses in the boundary layer from viscous shearing forces. The distance downstream where the velocity at 0.009 inches from the body reverses its decreasing trend and becomes greater indicates the point where transition to turbulent flow has occurred. A comparison of the velocity distribution curves of Figs. 15 and 16 with graphs of pressure distribution in Fig. 14 shows that the transition points indicated from velocity distributions at the lowest Reynolds number coincide in each case to the onset of a positive pressure gradient on the afterbody of the model. This coincidence would suggest that the positive pressure gradient was the influencing factor in causing transition. At higher velocities and Reynolds

number the transition point is seen to move forward of the positive pressure gradient region indicating that the critical Reynolds number for laminar flow has been reached.

Limitations of the test set up did not permit boundary layer probes at higher velocities. It is expected, however, that forward translation of the transition point would continue with increases in Reynolds number. Forward translation to the region of negative pressure gradient could reasonably be expected if sufficiently high Reynolds numbers are attained.

For the Reynolds numbers at which lengthwise velocity distributions were taken the velocity gradients at the surface can be approximated with the assumption that the velocity varies linearly from zero at the surface to the value measured at the 0.009 inch distance from the body. The intensity of skin friction (τ) in pounds per square foot is then obtained by multiplying the velocity gradient by the viscosity of air.

$$\tau_0 = \mu \left(\frac{\partial v}{\partial y} \right)_0$$

Goldstein [5] quotes good experimental results obtained from the application of this formula throughout both the laminar and turbulent regions. The presence of the laminar sub-layer permits application to the turbulent region [15].

The results from all tests within the capabilities of the equipment are evaluated and recorded in Table XVII through XX. τ_0 was divided by the free stream dynamic pressure to obtain a non-dimensional shear distribution. The non-dimensional values are plotted in Figs. 17, 18, 19, and 20 as $\frac{\tau_0}{q_0}$ versus

s/L for each test Reynolds number. The intensity of friction rises rapidly from zero at the stagnation point on the nose to a maximum value located very near the nose where the greatest acceleration of air is occurring and the steeper velocity gradients are apparent. The rapid decrease to zero friction at the stagnation point is not shown in the figures. The curves start at the peak located near the nose which is associated with laminar flow.

Frictional intensity is seen to fall steadily with distance aft of the nose until the point of laminar instability is reached and transition to turbulent flow has occurred. At transition there is a rise in frictional intensity to a second peak after which the intensity of friction falls as the tail of the model is approached.

A characteristic pattern among the three experimental curves for each model is apparent. The maximum magnitude of non-dimensional friction intensity on the forward body is reduced with increasing Reynolds number as a result of the velocity squared term in the denominator of $\frac{\tau_0}{q_0}$. The transition point is seen to move forward on the body with increasing Reynolds number and the peak intensity associated with turbulent boundary layer shows an increase in magnitude with forward shifts in transition point. These distinct characteristics, with the aid of local Reynolds numbers for predicting transition, were used for extrapolating frictional intensity to higher velocities. Local Reynolds numbers based on local super-velocities and the developed length aft of the nose are tabulated in Tables X through XV.

In the extrapolation procedure emphasis was placed on local Reynolds number and static pressure gradient in locating the transition point. Initial estimates for the critical Reynolds number for each model were taken as the Reynolds number at the point on the experimental curves where transition is first indicated forward of the region of positive pressure gradient. For a fineness ratio of six this condition appears to have occurred at an s/L of 0.45 with a local Reynolds number of approximately 1.0 X 10^6. With increasing free stream velocity the local super-velocity is greater, therefore, the local Reynolds number at a given point is higher. On this basis it is expected that the transition point will shift forward through the region of approximately zero pressure gradient. With movement of the transition point toward the forward region of negative pressure gradient the critical R_s, which will cause laminar instability and transition, increases. In extrapolating for the L/D ratio of six, the transition point was moved forward in decreasing increments to an s/L of 0.33 where R_s is approximately 1.55 X 10^6 when the free stream velocity was 249 feet per second.

A similar procedure was applied to all bodies. This resulted in a forward shift in transition point on the L/D ratio of five from s/L of 0.57 to 0.35 through a range of R_s from 1.15 X 10^6 to 1.6 X 10^6. The range of R_s for fineness ratios of three and four is of similar magnitude, however, forward shift of transition in terms of s/L was slightly less

in order to account for a more extensive range of negative pressure gradient on the forward body.

The second critical point in the extrapolation was the peak magnitude of friction intensity associated with the turbulent boundary layer after transition. Hoerner [19] discusses the influences on friction intensity of shrinking the body radius aft of the maximum diameter on a body of revolution. These influences are not apparent from the tapering of a two dimensional profile. The most significant factor influencing friction drag on the aft portion of a three dimensional body, other than separation where friction vanishes, is the geometric shape of the afterbody. On the forebody where the diameter is increasing in the direction of flow, the volume of the boundary layer is thinly distributed over the growing circumference. Along the afterbody the thickness of the boundary layer increases because of pressure gradient and the additional influence of reducing the body diameter. The requirement for an increasing volume of boundary layer air to be forced into a decreasing circumference causes rapid increases in thickness if separation does not occur. Upon reaching the pointed end of the body a circular wake has developed. Experience has indicated that the wake diameter will generally be about one half the maximum diameter of the body.

Associated with transition to turbulent boundary layer flow there is an increase in local friction intensity over that of the immediately preceding laminar flow. Goldstein [5] quotes experimental evidence that the peak intensity for turbulent flow may be greater on curvilinear bodies than the

peak intensity for laminar flow. Conditions of boundary layer thickness and geometry of the body at transition will also influence the magnitude to which turbulent flow increases frictional intensity.

When transition occurs well aft on a three-dimensional streamlined body the peak friction intensity is reduced by thick boundary layers and geometric shrinking of the surface away from the flow with distance downstream. This trend is indicated by those curves in Figs. 17 through 20, which were estimated from experimental data. As the transition point moves forward on a body of revolution and approaches the point of maximum diameter the effect would be reversed. This characteristic was considered in the extrapolation of $\frac{\tau_0}{q_0}$ curves for each model at higher free stream velocities.

Using these increased peak intensities in conjunction with previously estimated transition points the extrapolated data was drawn into a smooth family of curves. The family of curves for each body with fineness ratios from three to six are given in Figs. 17 through 20, respectively.

These data represent the non-dimensional shearing stress acting tangent to the surface at every point on the body. The drag caused by viscous forces is obtained by integration of the axial components over the surface area of the body. The frictional drag coefficient is obtained from the integral:

$$C_{D_f} = \frac{2\pi}{S_w} \int_0^S \frac{\tau_0}{q_0} r \cos\theta \, ds$$

where S = developed length from nose to tail (ft.)

S_W = wetted surface (sq. ft.)

r = radius (ft.)

θ = angle between body axis and surface tangent (degrees)

ds = differential of developed length

This equation cannot be integrated directly, and requires either a graphical or a numerical solution. A numerical formulation of the equation could be written as:

$$C_{D_f} \cong \frac{2\pi}{S_w} \sum_{i=0}^{12} \left(\frac{\tau_0}{q_0}\right)_i r_i \cos\theta_i \, \Delta s_i$$

Where i refers to the twelve pressure orifice locations along the model and Δs is the developed length from mid-point to mid-point between the orifice in question and two adjacent points.

The equation was evaluated by graphical methods to obtain skin friction drag coefficients for Reynolds numbers corresponding to the five free stream dynamic pressures considered. The coefficients are given in Tables XVII through XX for L/D ratios of three through six. Curves of the estimated skin friction coefficients plotted in Fig. 21 represent the objective of this portion of the analysis. Fig. 21 shows a family of curves similar to those previously obtained and shown in Fig. 11. Detailed comparison of the agreement between these data and that obtained from the difference between total and pressure drag is discussed in the following section.

6. Comparison of Results.

The degree of correlation which can be obtained by a comparison of the results derived through two different methods of analysis is a good indication of the relative accuracy which could be expected from either approach. Small errors necessarily introduced by limits in accuracy of equipment and procedure employed precludes exact agreement between the two methods.

Figs. 22 and 23 are a combination of the curves for individual bodies taken from Figs. 11 and 21. This permits a direct comparison of the final results obtained by the two methods of analysis. From the figures it is seen that the shapes of the two curves for each body are very similar. The minimum drag coefficient for an individual body is seen to occur at approximately the same Reynolds number for both the method of subtracting friction from total drag and the direct estimate of skin friction drag from boundary layer data. The families of drag coefficient curves obtained by either analysis show similar characteristics of shape and points of minimum drag. This would indicate that factors causing major influences in skin friction drag have been considered and that inconsistencies in results would appear essentially in differences of magnitude.

The estimated curves for all models in Figs. 22 and 23 are seen to be lower in each case than the corresponding curve taken from the difference between total and pressure drag. The higher curves are approximately 1.1 to 1.25 times as great

as the estimated curves for the L/D ratios of four, five, and six. For the L/D ratio of three the discrepancy factor between curves is 1.5 to 1.6. Larger total drag measurements encountered for L/D of three would tend to reflect larger percentage errors in final results for any experimental inaccuracies perhaps explaining the larger discrepancy in results for this model.

The general discrepancies between results could be the result of many factors. The low drag models caused very little pressure drag for the higher L/D ratios where separation did not occur. Inaccuracies involved in graphical integration of such small quantities could introduce errors in results. In addition, the percentage of error in determining pressure drag is directly related to the number of orifices used to obtain points for integration [5]. For the smaller bodies the 12 orifices may have been sufficient but for the larger bodies the distance between points was excessive. Total drag measurements are considered accurate, therefore errors in results from this phase are negligible.

A possible source of error is the integration of tangential shear stress and the assumption on which the extrapolated local shear intensities were based. Some error was introduced by the finite size of the pitot tube used for the boundary layer profiles and the assumption of a linear variation of velocity gradient between the body surface and the point where velocity was measured. The character of boundary layer profiles would cause this approximation for the slope of the

velocity profile at the surface to be lower than that which actually occurs.

von Doenhoff [12] and Dhawan [15] applied correction factors to all velocity profile data obtained by this method to correct for the steep velocity gradients at the surface. The correction applied by Dhawan was an increase in the slopes of measured profiles by a factor of approximately 15 to 20 percent.

A correction factor of this nature applied to the boundary layer probes taken would have reduced the 10 to 25 percent discrepancy in the final results which are compared in Figs. 22 and 23. These trends suggest that errors, which lead to the discrepancy noted between results of the two methods, were introduced by the distance from the body at which the boundary layer probe was taken. The accuracy of the boundary layer probe method can be greatly improved, giving closer agreement between results, by fitting the models with smaller flush mounted pitot tubes or using specially adapted hot-wire anemometers. A distance of 0.003 to 0.005 inches from the surface is suggested as a more appropriate point for a boundary layer probe.

7. Conclusion.

The skin friction coefficient of drag as a function of Reynolds number and fineness ratio were experimentally determined for several axially symmetric bodies of revolution at zero angle of attack. The results of two separate methods were obtained, compared and form the basis for the following conclusions:

The results indicate that first approximations for the total coefficient of skin friction drag for fineness ratios greater than about three can be made using zero pressure gradient flat plate values at comparable Reynolds numbers. The distribution of frictional drag forces on the streamlined bodies can not be quantitatively compared with the distribution of viscous forces on a flat plate.

Total skin friction drag and the accuracy with which the distribution of friction drag over the surface can be predicted depends largely on the locations of the transition and flow separation points. These points are largely determined by static pressure gradient and Reynolds number.

The assumption of a linear boundary layer velocity profile from the surface to the point of measurement leads to good estimates of skin friction drag coefficients. Agreement in results suggests that either method can be used for a reliable analysis of skin friction drag.

Separation of flow occurred on the afterbody of L/D ratios one and two and to a lesser degree in the range of low Reynolds numbers for L/D ratio of three. The percentage of total drag attributed to frictional forces is high for the models without separation. It is concluded that flow separation caused the abrupt decrease in the ratio of friction drag to total drag between L/D ratios of two and three. Flow separation reduced the surface area subjected to shear stresses and caused an added increment of pressure drag.

It is suggested that better agreement in results can be obtained with two simple modifications of equipment. The longer bodies should be fitted with additional pressure taps. Smaller flush-mounted pitot tubes or specially adapted hot-wire anemometers are recommended for improvements in the equipment used for the boundary layer probe.

REFERENCES

1. Pope, Alan: Wind-Tunnel Testing, 1954, 2nd. ed., John Wiley and Sons, Inc., New York.
2. Schlichting, H.: Boundary Layer Theory, 1955, McGraw-Hill Book Co., Inc., New York.
3. Smith, D. W. and Walker, J. H.: Skin-Friction Measurements In Incompressible Flow, NACA TN 4231, 1958.
4. Hunsaker, J. C. and Rightmire, B. G.: Engineering Applications of Fluid Mechanics, 1947, McGraw-Hill Book Co., Inc., New York.
5. Goldstein, S.: Modern Developments In Fluid Dynamics, Vols. I and II, 1938, The Clarendon Press, Oxford.
6. Dodge, R. A. and Thompson, M. J.: Fluid Mechanics, 1937, McGraw-Hill Book Co., Inc., New York.
7. Shapiro, Ascher, H.: Shape and Flow, The Fluid Dynamics of Drag, 1961, Doubleday and Company, Inc., Garden City, New York.
8. Miller, James A.: Transition in Oscillating Blausis Flow, 1963, Phd Thesis, Illinois Institute of Technology, Chicago.
9. McDevitt, J. B. and Taylor, R. A.: Pressure Distribution at Transonic Speeds for Slender Bodies Having Various Axial Locations of Maximum Diameter, NACA TN 4280, 1958.
10. McLean, F. E. and Rennemann, C. Jr.: Supersonic Flow Past Nonlifting Bumped and Indented Bodies of Revolution, NACA TN 3744, 1956.
11. Mottard, E. J. and Loposer, J. D.: Average Skin-Friction Drag Coefficients from Tank Tests of a Parabolic Body of Revolution, NACA Report 1161, 1954.
12. von Doenhoff, A. E.: Investigation of the Boundary Layer About a Symmetrical Airfoil in a Wind Tunnel of Low Turbulence, NACA Wartime Report L-507, 1940.
13. von Doenhoff, A. E. and Tetervin, N.: Determination of General Relations for the Behavior of Turbulent Boundary Layers, NACA Report 772, 1943.
14. Schubauer, G. B.: AirFlow In the Boundary Layer of an Elliptical Cylinder, NACA Report 652, 1939.
15. Dhawan, S.: Direct Measurements of Skin Friction, NACA TN 2567, 1952.

16. Bussmann, K. and Ulrich, A.: Systematic Investigations of the influence of the Shape of the Profile Upon the Position of the Transition Point. NACA TM 1185, 1947.

17. Streeter, V. L.: Fluid Mechanics, 3rd. ed., 1962, McGraw-Hill Book Co., Inc., New York.

18. Fediaevsky, K.: Turbulent Boundary Layer of an Airfoil, NACA TM 822, 1937.

19. Hoerner, S. F.: Fluid Dynamic Drag, 1958, Published by the Author, Midland Park, New Jersey.

TABLE I

DIAMETER - LENGTH COORDINATES
STREAMLINED BODIES
66(215) - OXX

STATION X, %L	DIAMETER INCHES	STATION X, %L	DIAMETER INCHES
00.00	0.000	40.0	5.937
00.50	0.906	45.0	6.000
00.75	1.087	50.0	5.965
01.25	1.358	55.0	5.836
02.50	1.808	60.0	5.588
05.00	2.496	65.0	5.139
07.50	3.037	70.0	4.515
10.00	3.496	75.0	3.767
15.00	4.234	80.0	2.944
20.00	4.801	85.0	2.083
25.00	5.238	90.0	1.234
30.00	5.568	95.0	0.474
35.00	5.803	100.0	0.062

L/D	1	2	3	4	5	6
L, inches	6	12	18	24	30	36

TABLE II

MODEL CHARACTERISTICS
66(215) - OXX

BODY L/D	L INCHES	S_{wet} Sq. ft.	S/S_{wet}	VOLUME cu. ft.	$\Delta C_{D_B}^*$ BUOYANCY
1	6	0.534	.3670	.0546	.00005
2	12	1.068	.1835	.1093	.00007
3	18	1.602	.1224	.1640	.00008
4	24	2.137	.0918	.2180	.00010
5	30	2.670	.0734	.2730	.00011
6	36	3.458	.0567	.3280	.00009

* Buoyancy drag based on wetted area

S_o = .1963 sq. ft. Frontal Area

Wetted surface area:
$S_{wet} = .089\ L(in.) = .741\ L(ft.)$ sq. ft.

Volume:
$V = .00911\ L(in.) = .01092\ L(ft.)$ cu. ft.

TABLE III

PRESSURE ORIFICE LOCATIONS
STREAMLINED BODIES
66(215) - OXX

ORIFICE	STATION X, %L	DIAMETER INCHES	RADIUS INCHES
1	0.00	0.000	0.000
2	1.00	1.200	0.600
3	6.00	2.730	1.365
4	15.00	4.234	2.117
5	25.00	5.238	2.619
6	35.00	5.803	2.902
7	45.00	6.000	3.000
8	55.00	5.836	2.918
9	65.00	5.139	2.569
10	75.00	3.767	1.884
11	87.50	1.600	0.800
12	100.00	0.062	0.031

TABLE IV

COEFFICIENT OF DRAG
STREAMLINED BODY OF REVOLUTION
L/D = 1

December 30, 1963

Barometric Pressure 30.48 in. Hg.
Temperature 66°-74° F.

q cm	R_L X 10^{-5}	DRAG, lbs.	C_{D_t}	$\Delta C_{D_{S+B}}$	$C_{D_{wet}}$
.85	1.165	.192	.2221	.00078	.22132
1.50	1.531	.335	.2198	.00088	.21892
2.08	1.800	.456	.2178	.00098	.21692
2.57	2.002	.568	.2177	.00110	.21380
3.07	2.19	.670	.2149	.00110	.21380
3.51	2.34	.766	.2145	.00112	.21338
4.03	2.51	.858	.2110	.00115	.20985
5.09	2.81	1.094	.2120	.00128	.21072
3.02	2.17	.648	.2121	.00110	.21100
5.06	2.81	1.092	.2130	.00128	.21172
6.04	3.08	1.312	.2140	.00149	.21251
7.00	3.31	1.519	.2135	.00160	.21190
7.99	3.54	1.717	.2115	.00175	.20975
8.98	3.75	1.942	.2125	.00175	.20975
10.03	3.96	2.161	.2065	.00186	.20464
11.97	4.32	2.492	.2055	.00185	.20365
14.19	4.71	2.642	.1835	.00178	.18180
16.07	5.01	2.979	.1823	.00164	.18066
18.08	5.32	3.310	.1805	.00158	.17892
17.00	5.17	3.014	.1740	.00160	.17240
18.90	5.44	3.090	.1570	.00152	.15548
19.45	5.52	2.791	.1412	.00150	.13970
20.03	5.60	2.422	.1190	.00149	.11751
20.94	5.72	2.440	.1147	.00152	.11318
21.91	5.85	2.508	.1126	.00155	.11105
24.12	6.14	2.718	.1110	.00160	.10940
25.88	6.36	2.896	.1100	.00167	.10833
28.00	6.62	3.131	.1100	.00173	.10827
30.89	6.95	3.458	.1101	.00177	.10833
33.92	7.27	3.810	.1104	.00180	.10860
36.64	7.58	4.206	.1128	.00207	.11073
40.12	7.93	4.860	.1191	.00208	.11702

TABLE V

COEFFICIENT OF DRAG
STREAMLINED BODY OF REVOLUTION
L/D = 2

December 27, 1963

Barometric Pressure 30.38 in. Hg.
Temperature 65°-75° F.

q cm	$R_L \times 10^{-5}$	DRAG, lbs.	C_{D_t}	$\Delta C_{D_{S+B}}$	$C_{D_{wet}}$
1.09	2.67	0.118	.05220	.00040	.05180
2.02	3.64	.173	.04145	.00050	.04095
3.15	4.55	.230	.03535	.00055	.03480
4.06	5.16	.261	.03110	.00059	.03051
5.02	5.72	.263	.02540	.00064	.02476
2.95	4.40	.232	.03810	.00055	.03755
3.97	5.11	.243	.02965	.00059	.02906
4.99	5.72	.241	.02340	.00064	.02276
6.06	6.31	.253	.02020	.00076	.01944
7.03	6.79	.279	.01921	.00082	.01839
8.07	7.28	.311	.01866	.00089	.01777
9.08	7.72	.342	.01824	.00092	.01732
10.97	8.48	.411	.01814	.00091	.01723
11.98	8.87	.454	.01835	.00089	.01746
13.02	9.25	.473	.01759	.00088	.01671
14.09	9.62	.501	.01721	.00086	.01635
15.05	9.94	.556	.01789	.00085	.01704
16.92	10.55	.625	.01790	.00081	.01709
18.00	10.87	.676	.01818	.00080	.01738
19.09	11.19	.723	.01834	.00078	.01756
20.11	11.50	.763	.01837	.00076	.01761
21.10	11.76	.811	.01862	.00078	.01784
23.07	12.31	.897	.01884	.00080	.01804
24.08	12.57	.945	.01902	.00082	.01814
26.04	12.72	1.033	.01957	.00087	.01870
28.11	13.22	1.134	.01988	.00090	.01898
29.88	13.63	1.231	.02032	.00095	.01937
31.82	14.07	1.342	.02078	.00099	.01979
34.00	14.54	1.441	.02090	.00101	.01989
35.89	14.94	1.531	.02103	.00103	.02000
37.92	15.36	1.633	.02123	.00105	.02018
39.99	15.76	1.729	.02132	.00105	.02027
44.05	16.11	1.934	.02196	.00106	.02090
46.20	16.50	2.047	.02218	.00107	.02111
48.83	16.97	2.176	.02232	.00108	.02124

TABLE VI

COEFFICIENT OF DRAG
STREAMLINED BODY OF REVOLUTION
L/D = 3

December 26, 1963

Barometric Pressure 30.40 in. Hg.
Temperature 72°-80° F.

q cm	$R_L \times 10^{-5}$	DRAG, lbs.	C_{D_t}	$\Delta C_{D_{S+B}}$	$C_{D_{wet}}$
1.00	3.72	.042	.01373	.00085	.01288
2.00	5.26	.079	.01138	.00088	.01050
3.00	6.44	.096	.01060	.00090	.00970
4.04	7.47	.121	.00985	.00090	.00875
5.05	8.36	.151	.00985	.00092	.00893
3.00	6.44	.091	.01000	.00090	.00910
4.00	7.40	.113	.00940	.00090	.00850
5.00	8.32	.149	.00984	.00092	.00892
5.94	9.06	.173	.00960	.00095	.00865
7.03	9.86	.198	.00930	.00095	.00835
7.94	10.48	.227	.00941	.00096	.00845
9.09	11.20	.255	.00925	.00098	.00827
9.98	11.72	.279	.00922	.00101	.00821
10.99	12.30	.311	.00932	.00099	.00833
12.06	12.90	.333	.00910	.00097	.00813
13.01	13.40	.359	.00909	.00096	.00813
13.93	13.88	.385	.00909	.00095	.00814
14.95	14.38	.412	.00908	.00094	.00814
16.01	14.88	.444	.00912	.00089	.00823
17.04	15.35	.475	.00918	.00088	.00830
19.03	16.22	.531	.00920	.00086	.00834
18.00	15.78	.507	.00926	.00086	.00844
18.96	16.19	.535	.00929	.00086	.00843
20.06	16.85	.564	.00927	.00082	.00845
21.02	17.05	.593	.00929	.00082	.00847
22.09	17.48	.621	.00926	.00078	.00848
24.00	18.21	.683	.00938	.00073	.00865
26.00	18.95	.742	.00940	.00067	.00873
27.99	19.68	.803	.00940	.00066	.00880
29.95	20.04	.864	.00951	.00067	.00884
31.92	21.00	.927	.00957	.00068	.00889
33.89	21.62	.990	.00962	.00068	.00894
36.94	22.59	1.097	.00978	.00069	.00909
40.01	23.35	1.206	.00993	.00072	.00921
42.93	24.35	1.329	.01020	.00074	.00946

TABLE VII

COEFFICIENT OF DRAG
STREAMLINED BODY OF REVOLUTION
L/D = 4

December 26, 1963

Barometric Pressure 30.34 in. Hg.
Temperature 80° F.

q cm	$R_L \times 10^{-5}$	DRAG, lbs.	C_{D_t}	$\Delta C_{D_{S+B}}$	$C_{D_{wet}}$
1.09	5.01	.032	.00739	.00131	.00608
2.08	6.83	.061	.00739	.00137	.00602
2.94	8.24	.080	.00685	.00137	.00548
3.92	9.56	.108	.00694	.00137	.00557
5.01	10.79	.131	.00660	.00137	.00523
2.98	8.28	.079	.00668	.00137	.00531
3.95	9.60	.109	.00695	.00137	.00558
5.00	10.78	.127	.00640	.00137	.00503
5.92	11.73	.150	.00639	.00137	.00502
6.92	12.72	.176	.00637	.00139	.00498
7.93	13.59	.194	.00616	.00141	.00475
8.88	14.40	.213	.00604	.00144	.00460
9.90	15.19	.231	.00587	.00147	.00440
11.07	16.05	.256	.00583	.00147	.00436
12.11	16.80	.282	.00585	.00146	.00439
12.99	17.38	.299	.00580	.00146	.00434
14.00	18.05	.327	.00587	.00146	.00441
14.99	18.65	.354	.00594	.00144	.00450
16.22	19.43	.379	.00588	.00142	.00446
18.05	20.50	.419	.00585	.00139	.00456
19.19	21.15	.457	.00600	.00138	.00462
17.00	19.90	.405	.00601	.00139	.00472
19.01	21.04	.466	.00606	.00134	.00482
20.16	21.62	.497	.00615	.00131	.00484
21.99	22.60	.551	.00631	.00125	.00506
24.17	23.70	.613	.00639	.00119	.00520
26.04	24.61	.675	.00627	.00108	.00519
28.01	25.55	.729	.00655	.00104	.00541
30.00	26.42	.782	.00656	.00097	.00559
33.01	27.75	.870	.00663	.00090	.00573
36.02	28.95	.958	.00668	.00080	.00588
39.06	30.19	1.049	.00660	.00071	.00589
42.19	31.35	1.147	.00676	.00060	.00616
45.08	32.40	1.241	.00694	.00051	.00643
48.01	33.45	1.338	.00703	.00045	.00658

TABLE VIII

COEFFICIENT OF DRAG
STREAMLINED BODY OF REVOLUTION
L/D = 5

December 26, 1963

Barometric Pressure 30.34 in. Hg.
Temperature 75° F.

q cm	R_L X 10^{-5}	DRAG, lbs.	C_{D_t}	$\Delta C_{D_{S+B}}$	$C_{D_{wet}}$
1.05	6.29	0.027	.00512	.00110	.00402
2.00	8.60	.049	.00488	.00115	.00373
2.86	10.46	.076	.00529	.00115	.00414
4.08	12.39	.095	.00464	.00115	.00349
5.00	13.71	.117	.00466	.00115	.00351
3.09	10.78	.075	.00484	.00115	.00369
4.01	12.28	.101	.00502	.00115	.00387
5.02	13.74	.124	.00492	.00115	.00377
6.01	15.04	.140	.00465	.00116	.00349
6.97	16.18	.163	.00466	.00118	.00348
8.05	17.40	.179	.00443	.00120	.00323
9.04	18.43	.197	.00435	.00121	.00314
9.98	19.36	.208	.00416	.00122	.00294
11.00	20.32	.234	.00424	.00122	.00302
11.99	21.21	.256	.00425	.00121	.00304
13.00	22.10	.279	.00427	.00121	.00306
14.04	22.98	.301	.00428	.00119	.00309
16.03	24.52	.349	.00434	.00117	.00317
18.11	26.09	.391	.00430	.00115	.00315
16.96	25.22	.367	.00431	.00112	.00319
19.00	26.72	.417	.00437	.00110	.00327
21.16	28.19	.471	.00444	.00110	.00334
22.94	29.35	.519	.00451	.00100	.00351
25.03	30.68	.574	.00457	.00091	.00366
27.88	32.37	.654	.00468	.00086	.00382
30.98	34.10	.752	.00484	.00082	.00402
34.06	35.77	.848	.00496	.00070	.00426
37.04	37.30	.954	.00513	.00060	.00453
40.00	38.75	1.042	.00519	.00050	.00469
42.71	40.08	1.129	.00527	.00050	.00477
45.98	41.54	1.224	.00531	.00045	.00486
48.06	42.50	1.284	.00533	.00040	.00493

TABLE IX

COEFFICIENT OF DRAG
STREAMLINED BODY OF REVOLUTION
L/D = 6

December 26, 1963

Barometric Pressure 30.34 in. Hg.
Temperature 73°-83° F.

q cm	R_L X 10^{-5}	DRAG, lbs.	C_{D_t}	$\Delta C_{D_{S+B}}$	$C_{D_{wet}}$
1.03	7.44	.025	.00372	.00085	.00287
1.49	8.91	.037	.00381	.00086	.00295
1.98	10.21	.050	.00387	.00088	.00299
2.46	11.43	.062	.00386	.00088	.00298
2.97	12.58	.074	.00381	.00088	.00293
3.98	14.55	.100	.00386	.00088	.00298
4.91	16.18	.121	.00376	.00089	.00285
3.97	14.55	.097	.00374	.00088	.00286
4.93	16.20	.119	.00370	.00089	.00281
5.92	17.78	.140	.00364	.00089	.00275
6.93	19.21	.160	.00356	.00091	.00265
7.90	20.51	.187	.00363	.00092	.00271
8.93	21.80	.207	.00356	.00093	.00263
9.95	23.00	.229	.00355	.00094	.00261
10.90	24.10	.249	.00350	.00094	.00256
11.89	25.15	.271	.00350	.00093	.00257
12.91	26.21	.294	.00349	.00093	.00256
14.00	27.30	.325	.00356	.00093	.00263
14.92	28.20	.346	.00373	.00092	.00271
16.94	30.00	.407	.00368	.00091	.00277
17.00	30.10	.398	.00358	.00088	.00270
19.00	31.80	.452	.00364	.00087	.00297
21.00	33.44	.490	.00358	.00086	.00272
22.90	34.90	.557	.00371	.00077	.00294
25.00	36.49	.617	.00378	.00077	.00301
26.90	37.85	.666	.00380	.00070	.00310
28.79	39.20	.705	.00377	.00063	.00314
30.94	40.60	.774	.00383	.00061	.00322
33.80	42.40	.843	.00382	.00050	.00332
35.96	43.70	.899	.00384	.00049	.00335
37.82	44.85	.952	.00386	.00045	.00341
41.90	47.25	1.124	.00412	.00039	.00373

TABLE Xa

DISTRIBUTION OF NORMAL PRESSURE FORCES AND LOCAL VELOCITIES L/D = 1

q_o = 2 cm silicone
V_o = 56.4 ft./sec.
Length = .5 feet
$R_L = 1.80 \times 10^5$

December 24, 1963
Barometric Pressure 30.42 in. Hg.
Temperature 63° F.
C_{D_p} = .825

Orifice	s/L	Δp cm	$\Delta p/q_o$	V_{local} ft/sec	V/V_o	$R_s \times 10^{-4}$
1	.000	2.00	1.00	0.00	0.00	0.00
2	.100	1.80	.90	17.8	0.32	0.57
3	.237	1.23	.615	35.0	0.62	2.65
4	.385	.12	.06	54.7	0.47	6.74
5	.517	- .66	- .33	65.1	1.15	11.10
6	.633	-1.02	- .51	69.4	1.23	14.05
7	.734	- .74	- .37	66.1	1.17	15.53
8	.836	- .75	- .375	66.2	1.17	17.70
9	.955	- .81	- .405	67.0	1.18	20.43
10	1.111	- .82	- .41	67.0	1.18	23.75
11	1.331	- .87	- .435	67.6	1.19	28.79
12	1.512	- .89	- .445	67.8	1.20	32.83

TABLE Xb

DISTRIBUTION OF NORMAL PRESSURE FORCES AND LOCAL VELOCITIES L/D = 1

q_o = 5 cm silicone
V_o = 89.2 ft./sec.
Length = 0.5 feet
$R_L = 2.85 \times 10^5$

December 24, 1963
Barometric Pressure 30.42 in. Hg.
Temperature 63° F.
$C_{D_p} = 0.1710$

Orifice	s/L	Δp cm	$\Delta p/q_o$	V_{local} ft/sec	V/V_o	$R_s \times 10^{-4}$
1	.000	5.00	1.00	0.0	0.00	0.00
2	.100	4.55	.91	26.7	.30	.86
3	.237	3.15	.63	54.3	.61	4.11
4	.385	.45	.09	85.1	.95	10.48
5	.517	-1.70	- .34	99.4	1.11	16.95
6	.633	-2.35	- .47	108.2	1.21	21.91
7	.734	-1.85	- .37	104.5	1.17	24.55
8	.836	-1.85	- .37	104.5	1.17	27.94
9	.955	-1.90	- .38	104.8	1.17	32.01
10	1.111	-2.05	- .41	105.9	1.18	37.55
11	1.331	-2.10	- .42	106.0	1.19	45.28
12	1.512	-2.65	- .53	110.4	1.23	53.42

TABLE Xc

DISTRIBUTION OF NORMAL PRESSURE FORCES AND LOCAL VELOCITIES L/D = 1

q_o = 12.00 cm silicone
V_o = 138.3 ft./sec.
Length = 0.5 feet
$R_L = 4.42 \times 10^5$

December 24, 1963
Barometric Pressure 30.42 in. Hg.
Temperature 63° F.
$C_{D_p} = 0.1680$

Orifice	s/L	Δp cm	$\Delta p/q_o$	V_{local} ft/sec	V/V_o	$R_s \times 10^{-5}$
1	.000	12.00	1.00	0.00	0.00	0.00
2	.100	10.90	.909	41.8	.30	.13
3	.237	7.45	.621	85.1	.61	.64
4	.385	.80	.067	133.6	.97	1.64
5	.517	- 5.00	- .417	164.5	1.19	2.80
6	.633	- 7.90	- .658	178.0	1.29	3.60
7	.734	- 6.25	- .521	170.5	1.23	4.00
8	.836	- 5.05	- .421	164.8	1.19	4.41
9	.955	- 5.00	- .417	164.6	1.19	5.03
10	1.111	- 5.50	- .458	166.9	1.20	5.92
11	1.331	- 5.85	- .487	168.6	1.21	7.18
12	1.512	- 7.00	- .583	173.9	1.25	8.42

TABLE Xd

DISTRIBUTION OF NORMAL PRESSURE FORCES AND LOCAL VELOCITIES L/D = 1

q_o = 25.0 cm silicone
V_o = 199.5 ft./sec.
Length = 0.5 feet
R_L = 6.38 X 10^5

December 24, 1963
Barometric Pressure 30.42 in. Hg.
Temperature 63° F.
C_{D_p} = .0841

Orifice	s/L	Δp cm	$\Delta p/q_o$	V_{local} ft/sec	V/V_o	R_s X 10^{-5}
1	.000	25.00	1.00	0.00	0.00	0.00
2	.100	21.95	.878	69.7	.35	.22
3	.237	14.05	.562	132.1	.66	1.00
4	.385	- 1.90	- .076	207.0	1.04	2.55
5	.517	-16.25	- .650	258.3	1.28	4.37
6	.633	-30.40	-1.215	297.1	1.49	6.02
7	.734	-34.15	-1.365	306.9	1.54	7.21
8	.836	-27.45	-1.097	289.1	1.45	7.73
9	.955	- 4.40	- .176	216.4	1.08	6.61
10	1.111	- 4.25	- .170	215.8	1.08	7.65
11	1.331	- 5.30	- .212	219.7	1.10	9.36
12	1.512	- 8.40	- .336	230.7	1.15	11.16

TABLE Xe

DISTRIBUTION OF NORMAL PRESSURE FORCES AND LOCAL VELOCITIES L/D = 1

q_o = 38.0 cm silicone
V_o = 246.0 ft./sec.
Length = 0.5 feet
R_L = 7.87 X 10^5

December 24, 1963
Barometric Pressure 30.42 in. Hg.
Temperature 63° F.
C_{D_p} = 0.099

Orifice	s/L	Δp cm	$\Delta p/q_o$	V local ft/sec	V/V_o	R_s X 10^{-6}
1	.000	38.00	1.00	0.00	0.00	0.00
2	.100	33.65	.885	83.2	.34	.27
3	.237	21.30	.560	163.1	.66	1.23
4	.385	- 2.75	- .072	254.8	1.04	3.14
5	.517	-25.00	- .658	316.8	1.28	5.40
6	.633	-46.95	-1.235	367.9	1.49	7.45
7	.734	-52.95	-1.394	380.6	1.54	8.94
8	.836	-27.25	- .717	322.4	1.31	8.62
9	.955	-10.20	- .268	277.1	1.12	8.46
10	1.111	- 7.05	- .185	267.9	1.08	9.49
11	1.331	- 7.10	- .187	268.0	1.09	11.41
12	1.512	- 8.35	- .220	271.7	1.10	13.15

TABLE XIa

DISTRIBUTION OF NORMAL PRESSURE FORCES AND LOCAL VELOCITIES L/D = 2

q_o = 2.0 cm silicone
V_o = 56.2 ft./sec.
Length = 1.0 feet
R_L = 3.66 X 10^5

December 24, 1963
Barometric Pressure 30.35 in. Hg.
Temperature 57° F.
C_{D_p} = 0.0180

Orifice	s/L	Δp cm	$\Delta p/q_o$	V_{local} ft/sec	V/V_o	R_s X 10^{-4}
1	.000	2.00	1.00	00.0	0.00	0.00
2	.052	1.45	.725	29.5	.52	.99
3	.135	.55	.275	47.9	.85	4.21
4	.245	- .20	- .100	58.9	1.05	9.41
5	.354	- .75	- .375	65.9	1.17	15.20
6	.458	-1.00	- .500	68.8	1.22	20.50
7	.558	-1.05	- .525	69.4	1.23	25.20
8	.659	- .80	- .400	66.5	1.18	28.50
9	.766	- .60	- .300	64.1	1.14	32.00
10	.880	- .25	- .125	59.6	1.06	34.20
11	1.035	+ .20	+ .100	53.3	.95	35.90
12	1.180	.25	.125	52.5	.94	40.40

[illegible]

[illegible]

[illegible]	[illegible]	[illegible]	[illegible]	[illegible]	[illegible]	[illegible]
[illegible]	[illegible]	[illegible]	[illegible]	[illegible]	[illegible]	[illegible]
[illegible]	[illegible]	[illegible]	[illegible]	[illegible]	[illegible]	[illegible]
[illegible]	[illegible]	[illegible]	[illegible]	[illegible]	[illegible]	[illegible]
[illegible]	[illegible]	[illegible]	[illegible]	[illegible]	[illegible]	[illegible]
[illegible]	[illegible]	[illegible]	[illegible]	[illegible]	[illegible]	[illegible]
[illegible]	[illegible]	[illegible]	[illegible]	[illegible]	[illegible]	[illegible]
[illegible]	[illegible]	[illegible]	[illegible]	[illegible]	[illegible]	[illegible]
[illegible]	[illegible]	[illegible]	[illegible]	[illegible]	[illegible]	[illegible]
[illegible]	[illegible]	[illegible]	[illegible]	[illegible]	[illegible]	[illegible]
[illegible]	[illegible]	[illegible]	[illegible]	[illegible]	[illegible]	[illegible]
[illegible]	[illegible]	[illegible]	[illegible]	[illegible]	[illegible]	[illegible]

TABLE XIb

DISTRIBUTION OF NORMAL PRESSURE FORCES AND LOCAL VELOCITIES L/D = 2

q_o = 5.0 cm silicone
V_o = 88.9 ft./sec.
Length = 1.0 feet
R_L = 5.79 X 10^5

December 24, 1963
Barometric Pressure 30.35 in. Hg.
Temperature 57° F.
C_{D_p} = .0110

Orifice	s/L	Δp cm	$\Delta p/q_o$	V_{local} ft/sec	V/V_o	R_s X 10^{-5}
1	.000	5.00	1.00	00.0	0.00	0.00
2	.052	3.75	.75	44.4	0.50	0.15
3	.135	1.35	.27	75.9	.85	.67
4	.245	- .60	- .12	94.1	1.06	1.50
5	.354	-1.90	- .38	104.4	1.17	2.41
6	.458	-2.70	- .54	110.3	1.24	3.29
7	.558	-2.95	- .59	112.1	1.26	4.07
8	.659	-2.50	- .50	108.9	1.22	4.67
9	.766	-2.00	- .40	105.2	1.18	5.25
10	.880	+ .25	+ .05	86.6	.97	4.97
11	1.035	1.10	.22	78.5	.88	5.29
12	1.180	1.05	.21	79.0	.89	6.07

TABLE XIc

DISTRIBUTION OF NORMAL PRESSURE FORCES AND LOCAL VELOCITIES L/D = 2

q_o = 12.0 cm silicone
V_o = 137.7 ft./sec.
Length = 1.0 feet
$R_L = 8.96 \times 10^6$

December 24, 1963
Barometric Pressure 30.35 in. Hg.
Temperature 57° F.
C_{D_p} = .0094

Orifice	s/L	Δp cm	$\Delta p/q_o$	V_{local} ft/sec	V/V_o	$R_s \times 10^{-5}$
1	.000	12.00	1.00	0.0	0.00	0.00
2	.052	8.95	.746	69.4	.50	.23
3	.135	3.20	.266	117.9	.85	1.04
4	.345	- 1.65	- .138	146.8	1.06	2.34
5	.354	- 5.00	- .417	163.9	1.19	3.78
6	.458	- 7.00	- .584	173.3	1.26	5.17
7	.558	- 7.85	- .653	177.1	1.29	6.44
8	.659	- 7.90	- .658	177.3	1.29	7.61
9	.766	- 6.70	- .558	171.9	1.25	8.58
10	.880	+ 1.90	+ .158	126.3	.92	7.25
11	1.035	3.85	.321	113.5	.82	7.65
12	1.180	3.10	.258	118.8	.86	9.12

TABLE XId

DISTRIBUTION OF NORMAL PRESSURE FORCES AND LOCAL VELOCITIES L/D = 2

q_o = 25.0 cm silicone
V_o = 198.7 ft./sec.
Length = 1.0 feet
R_L = 1.29 X 10^6

December 24, 1963
Barometric Pressure 30.35 in. Hg.
Temperature 57° F.
C_{D_p} = .0076

Orifice	s/L	Δp cm	$\Delta p/q_o$	V_{local} ft/sec	V/V_o	R_s X 10^{-5}
1	.000	25.00	1.00	0.0	0.00	0.00
2	.052	18.65	.747	100.2	.50	.34
3	.135	6.40	.256	184.7	.93	1.62
4	.245	- 3.75	- .150	213.1	1.07	3.40
5	.354	-10.65	- .426	237.3	1.19	5.47
6	.458	-14.85	- .595	238.0	1.20	7.10
7	.558	-16.25	- .651	255.3	1.28	9.28
8	.659	-17.10	- .685	257.9	1.29	11.07
9	.766	-10.10	- .404	235.5	1.18	11.75
10	.880	+ 3.25	+ .130	185.4	.93	10.64
11	1.035	7.80	.312	164.8	.82	11.11
12	1.180	6.00	.240	173.3	.87	13.32

TABLE XIe

DISTRIBUTION OF NORMAL PRESSURE FORCES AND LOCAL VELOCITIES L/D = 2

q_o = 38.0 cm silicone
V_o = 245.0 ft./sec.
Length = 1.0 feet
R_L = 1.59 X 10^6

December 24, 1963
Barometric Pressure 30.35 in. Hg.
Temperature 57° F.
C_{D_p} = .0080

Orifice	s/L	Δp cm	$\Delta p/q_o$	V_{local} ft/sec	V/V_o	R_s X 10^{-5}
1	.000	38.00	1.00	0.0	0.00	0.00
2	.052	28.10	.741	125.0	.51	.42
3	.135	9.60	.253	211.8	.86	1.86
4	.245	- 6.20	- .164	264.3	1.08	4.22
5	.354	-16.05	- .423	292.2	1.19	6.74
6	.458	-22.90	- .604	310.2	1.26	9.26
7	.558	-24.90	- .656	315.3	1.28	11.46
8	.659	-26.45	- .696	319.1	1.30	13.70
9	.766	-10.60	- .279	277.1	1.13	13.83
10	.880	+ 3.95	+ .104	231.9	.95	13.32
11	1.035	11.95	.315	202.9	.83	13.67
12	1.180	8.70	.229	215.2	.89	16.54

TABLE XIIa

DISTRIBUTION OF NORMAL PRESSURE FORCES AND LOCAL VELOCITIES L/D = 3

q_o = 2.0 cm silicone
V_o = 56.4 ft./sec.
Length = 1.5 feet
R_L = 5.4 X 10^5

December 23, 1963
Barometric Pressure 30.40 in. Hg.
Temperature 62° F.
C_{D_p} = .00395

Orifice	s/L	$\triangle p$ cm	$\triangle p/q_o$	V_{local} ft/sec	V/V_o	R_s X 10^{-5}
1	.000	2.00	1.000	0.0	0.00	0.00
2	.036	1.35	.676	32.2	.57	.11
3	.101	.20	.100	53.5	.95	.52
4	.204	- .20	- .100	59.2	1.05	1.16
5	.308	- .50	- .250	63.1	1.12	1.86
6	.408	- .65	- .325	64.9	1.15	2.55
7	.506	- .70	- .350	65.6	1.16	3.19
8	.607	- .70	- .350	65.6	1.16	3.84
9	.709	- .55	- .275	63.7	1.13	4.35
10	.816	+ .25	+ .125	52.8	.94	4.15
11	.954	.50	.250	48.9	.87	4.49
12	1.082	.40	.200	50.5	.89	5.26

TABLE XIIb

DISTRIBUTION OF NORMAL PRESSURE FORCES AND LOCAL VELOCITIES L/D = 3

q_o = 5.0 cm silicone
V_o = 89.2 ft./sec.
Length = 1.5 feet
R_L = 8.58 X 10^5

December 23, 1963
Barometric Pressure 30.40 in. Hg.
Temperature 62° F.
C_{D_p} = .00345

Orifice	s/L	Δp cm	$\Delta p/q_o$	V_{local} ft/sec	V/V_o	$R_s \times 10^{-5}$
1	.000	5.00	1.00	0.0	0.00	0.00
2	.036	3.40	.68	50.5	.57	.18
3	.101	.40	.08	85.6	.95	.83
4	.204	- .70	- .14	92.3	1.06	1.86
5	.308	-1.25	- .25	99.7	1.11	2.93
6	.408	-1.65	- .33	102.8	1.15	4.04
7	.506	-1.85	- .37	104.4	1.17	5.08
8	.607	-1.90	- .38	104.8	1.17	6.10
9	.709	-1.45	- .29	101.3	1.14	6.96
10	.816	+ .70	+ .14	82.7	.93	6.47
11	.954	1.35	.27	76.22	.85	6.96
12	1.082	.90	.18	80.8	.91	8.40

TABLE XIIc

DISTRIBUTION OF NORMAL PRESSURE FORCES AND LOCAL VELOCITIES L/D = 3

q_o = 12.0 cm silicone	December 23, 1963
V_o = 138.2 ft./sec.	Barometric Pressure 30.40 in. Hg.
Length = 1.5 feet	Temperature 62° F.
$R_L = 1.33 \times 10^6$	C_{D_p} = .00335

Orifice	s/L	Δp cm	$\Delta p/q_o$	V_{local} ft/sec	V/V_o	$R_s \times 10^{-5}$
1	.000	12.00	1.00	0.0	0.00	0.00
2	.036	8.10	.675	78.8	.57	.27
3	.101	.80	.066	133.5	.96	1.30
4	.204	- 1.85	- .154	148.5	1.07	2.91
5	.308	- 3.25	- .271	155.8	1.13	4.59
6	.408	- 4.30	- .358	161.1	1.16	6.33
7	.506	- 4.50	- .375	162.0	1.17	7.90
8	.607	- 4.85	- .404	163.7	1.18	9.58
9	.709	- 4.00	- .333	159.6	1.15	10.90
10	.816	+ 1.35	+ .112	130.2	.94	10.23
11	.954	3.25	.271	118.0	.85	10.83
12	1.082	1.65	.137	128.3	.93	13.37

TABLE XIId

DISTRIBUTION OF NORMAL PRESSURE FORCES AND LOCAL VELOCITIES L/D = 3

q_o = 25.0 cm silicone
V_o = 199.5 ft./sec.
Length = 1.5 feet
R_L = 1.92 X 10^6

December 23, 1963
Barometric Pressure 30.40 in. Hg.
Temperature 62° F.
C_{D_p} = .00335

Orifice	s/L	Δp cm	$\Delta p/q_o$	V_{local} ft/sec	V/V_o	R_s X 10^{-5}
1	.000	25.00	1.00	0.0	0.00	0.00
2	.036	16.95	.679	113.2	.57	.39
3	.101	1.70	.068	192.6	.96	1.87
4	.204	- 3.85	- .154	214.3	1.07	4.20
5	.308	- 6.70	- .268	224.6	1.13	6.61
6	.408	- 8.80	- .352	231.9	1.16	9.11
7	.506	- 9.50	- .380	234.3	1.17	11.42
8	.607	-10.35	- .414	237.2	1.19	13.89
9	.709	- 8.45	- .338	230.7	1.16	15.76
10	.816	+ 2.45	+ .098	189.4	.95	14.88
11	.954	6.65	.266	170.9	.86	15.69
12	1.082	3.45	.138	185.2	.93	19.30

TABLE XIIe

DISTRIBUTION OF NORMAL PRESSURE FORCES AND LOCAL VELOCITIES L/D = 3

q_o = 38.0 cm silicone
V_o = 245.9 ft./sec.
Length = 1.5 feet
R_L = 2.36 X 10^6

December 23, 1963
Barometric Pressure 30.40 in. Hg.
Temperature 62° F.
C_{D_p} = .0031

Orifice	s/L	Δp cm	$\Delta p/q_o$	V_{local} ft/sec	V/V_o	R_s X 10^{-5}
1	000	38.00	1.00	0.0	.00	.00
2	.036	25.45	.672	141.3	.57	.49
3	.101	2.40	.063	238.0	.96	2.32
4	.204	- 6.15	- .162	265.0	1.08	5.20
5	.308	-10.10	- .266	276.7	1.13	8.15
6	.408	-13.45	- .354	286.1	1.16	11.24
7	.506	-14.60	- .384	289.3	1.17	14.10
8	.607	-15.80	- 416	292.6	1.18	17.12
9	.709	-12.75	- .336	284.2	1.15	19.41
10	.816	+ 3.40	+ .089	234.6	.95	18.43
11	.954	9.55	.251	275.1	1.11	25.25
12	1.082	5.35	.141	227.9	.93	23.75

TABLE XIIIa

DISTRIBUTION OF NORMAL PRESSURE FORCES AND LOCAL VELOCITIES L/D = 4

q_o = 2 cm silicone
V_o = 56.58 ft./sec.
Length = 2.0 feet
R_L = 7.18 X 10^5

December 23, 1963
Barometric Pressure 30.40 in. Hg.
Temperature 65° F.
C_{D_p} = .00123

Orifice	s/L	Δp cm	$\Delta p/q_o$	V_{local} ft/sec	V/V_o	R_s X 10^{-4}
1	.00	2.00	1.00	0.00	0.000	0.00
2	.028	.95	.475	41.00	.724	1.47
3	.088	.20	.100	53.67	.948	5.96
4	.183	- .20	- .100	59.34	1.048	13.81
5	.286	- .35	- .175	61.33	1.084	22.26
6	.387	- .40	- .200	61.98	1.095	30.43
7	.487	- .45	- .225	62.62	1.107	38.73
8	.587	- .50	- .050	63.26	1.118	47.08
9	.688	- .35	- .175	61.33	1.084	53.60
10	.794	+ .30	+ .150	52.16	.922	52.57
11	.927	.45	.225	49.81	.880	58.63
12	1.060	.10	.050	55.15	.975	74.13

TABLE XIIIb

DISTRIBUTION OF NORMAL PRESSURE FORCES AND LOCAL VELOCITIES L/D = 4

q_o = 5 cm silicone
V_o = 89.46 ft./sec.
Length = 2.0 feet
R_L = 1.136 X 10^6

December 23, 1963
Barometric Pressure 30.40 in. Hg.
Temperature 65° F.
C_{D_p} = .00133

Orifice	s/L	Δp cm	$\Delta p/q_o$	V_{local} ft/sec	V/V_o	R_s X 10^{-4}
1	.00	5.00	1.00	0.00	0.000	0 000
2	.028	2.36	.472	65.01	.726	2.338
3	.086	.35	.070	86.28	.964	9.584
4	.183	- .50	- .100	93.83	1.049	21.84
5	.286	- .80	- .160	96.35	1.077	34.97
6	.387	-1.10	- .220	98.82	1.104	48.50
7	.487	-1.15	- .230	99.22	1.109	61.35
8	.587	-1.30	- .260	100.40	1.122	74.74
9	.688	- .95	- .190	97.59	1.091	85.29
10	.794	+ .50	+ .100	84.87	.949	85.52
11	.927	1.05	.210	79.52	.889	93.59
12	1.06	.15	.030	88.11	.985	118.40

TABLE XIIIc

DISTRIBUTION OF NORMAL PRESSURE FORCES AND LOCAL VELOCITIES L/D = 4

q_o = 12 cm silicone
V_o = 138.59 ft./sec.
Length = 2 feet
R_L = 1.76 X 10^6

December 23, 1963
Barometric Pressure 30.40 in. Hg.
Temperature 65° F.
C_{D_p} = .00155

Orifice	s/L	Δp cm	$\Delta p/q_o$	V_{local} ft/sec	V/V_o	R_s X 10^{-5}
1	.00	12.00	1.00	0.0	0.000	0.000
2	.028	5.65	.47	100.8	.727	.362
3	.086	.80	.067	133.9	.966	1.487
4	.183	- 1.25	- .104	145.6	1.051	3.390
5	.286	- 2.20	- .184	150.8	1.088	5.471
6	.387	- 2.85	- .238	154.2	1.112	7.569
7	.487	- 3.10	- .258	155.5	1.122	9.614
8	.587	- 3.45	- .288	157.3	1.134	11.70
9	.688	- 2.75	- .229	153.7	1.109	13.43
10	.794	+ .75	+ .065	134.2	.968	13.52
11	.927	2.35	.196	124.3	.897	14.63
12	1.06	.15	.013	137.7	.994	18.51

TABLE XIIId

DISTRIBUTION OF NORMAL PRESSURE FORCES AND LOCAL VELOCITIES L/D = 4

q_o = 25 cm silicone
V_o = 200.0 ft./sec.
Length = 2 feet
$R_L = 2.54 \times 10^6$

December 23, 1963
Barometric Pressure 30.40 in. Hg.
Temperature 65° F.
C_{D_p} = .00169

Orifice	s/L	Δp cm	$\Delta p/q_o$	V_{local} ft/sec	V/V_o	$R_s \times 10^{-5}$
1	.000	25.00	1.00	0.00	.000	.000
2	.028	11.80	.472	145.4	.726	.523
3	.086	1.65	.066	193.3	.966	2.148
4	.183	- 2.65	- .106	210.4	1.052	4.897
5	.286	- 4.45	- .178	217.1	1.085	7.879
6	.387	- 5.85	- .234	222.2	1.111	10.91
7	.487	- 6.45	- .258	224.4	1.122	13.87
8	.587	- 7.30	- .292	227.4	1.136	16.92
9	.688	- 5.75	- .230	221.9	1.109	19.39
10	.794	+ 1.30	+ .052	194.8	.974	19.63
11	.927	5.05	.202	178.7	.893	21.03
12	1.060	0.60	.024	197.6	.988	26.56

TABLE XIIIe

DISTRIBUTION OF NORMAL PRESSURE FORCES AND LOCAL VELOCITIES L/D = 4

q_o = 38.0 cm silicone
V_o = 246.6 ft./sec.
Length = 2.0 feet
R_L = 3.13 X 10^6

December 23, 1963
Barometric Pressure 30.40 in. Hg.
Temperature 65 ° F.
C_{D_p} = .00199

Orifice	s/L	Δp cm	$\Delta p/q_o$	V_{local} ft/sec	V/V_o	R_s X 10^{-5}
1	.000	38.00	1.00	0.0	0.00	0.00
2	.028	18.00	.475	178.9	.735	.64
3	.086	2.30	.061	239.0	.969	2.65
4	.183	- 4.15	- .110	259.7	1.053	6.05
5	.286	- 6.90	- .182	268.1	1.087	9.74
6	.387	- 9.05	- .238	274.4	1.113	13.47
7	.487	- 9.80	- .258	276.6	1.121	17.10
8	.587	-11.10	- .292	280.3	1.137	20.87
9	.688	- 8.35	- .233	273.8	1.110	23.93
10	.794	+ 1.50	+ .039	241.7	.980	20.36
11	.927	7.35	.194	221.5	.898	26.07
12	1.060	.85	.022	243.8	.989	32.78

TABLE XIV a

DISTRIBUTION OF NORMAL PRESSURE FORCES AND LOCAL VELOCITIES L/D = 5

q_o = 2 cm silicone
V_o = 56.68 ft./sec.
Length = 2.5 feet
R_L = 8.935 X 10^5

December 23, 1963
Barometric Pressure 30.40 in. Hg.
Temperature 67 ° F
C_{D_p} = .00035

Orifice	s/L	Δp cm	$\Delta p/q_o$	V_{local} ft/sec	V/V_o	R_s X 10^{-5}
1	.000	2.00	1.00	0.00	0.00	0.00
2	.023	.80	.40	43.90	.775	.159
3	.079	.15	.075	54.51	.962	.679
4	.173	- .15	- .075	58.77	1.037	1.599
5	.276	- .25	- .125	60.12	1.061	2.612
6	.376	- .30	- .150	60.78	1.072	3 606
7	.476	- .35	- .175	61.44	1.084	4.610
8	.576	- .35	- .175	61.44	1.084	5.582
9	.677	- .25	- .125	60.12	1.061	6.422
10	.779	+ .20	+ .10	53.77	.948	6.609
11	.909	.35	.175	51.48	.908	7.377
12	1.035	.10	.05	55.25	.975	9.019

TABLE XIVb

DISTRIBUTION OF NORMAL PRESSURE FORCES AND LOCAL VELOCITIES L/D $\cong$ 5

$q_o \cong 5$ cm silicone
$V_o \cong 89.6$ ft./sec.
Length $\cong$ 2.5 feet
$R_L \cong 1.41 \times 10^6$

December 23, 1963
Barometric Pressure 30.40 in. Hg.
Temperature 67° F.
$C_{D_p} \cong .00098$

Orifice	s/L	Δp cm	$\Delta p/q_o$	V_{local} ft/sec	V/V_o	$R_s \times 10^{-5}$
1	0.000	5.00	1.00	0.00	0.000	0.00
2	.023	1.85	.37	71.14	.794	.258
3	.079	.30	.06	86.89	.969	1.082
4	.173	− .50	− .10	94.00	1.049	2.558
5	.276	− .65	− .13	95.27	1.063	4.140
6	.376	− .80	− .16	96.53	1.077	5.726
7	.476	− .85	− .17	96.94	1.082	7.274
8	.576	− .95	− .19	97.77	1.091	8.882
9	.677	− .70	− .14	95.69	1.068	10.220
10	.779	+ .30	+ .06	86.89	.969	10.680
11	.909	.80	.16	82.14	.916	11.770
12	1.035	.15	.03	88.27	.983	14.410

TABLE XIVc

DISTRIBUTION OF NORMAL PRESSURE FORCES AND LOCAL VELOCITIES L/D = 5

q_o = 12 cm silicone
V_o = 138.8 ft./sec.
Length = 2.5 feet
$R_L = 2.188 \times 10^6$

December 23, 1963
Barometric Pressure 30.40 in. Hg.
Temperature 67° F.
$C_{D_p} = .00125$

Orifice	s/L	Δp cm	$\Delta p/q_o$	V_{local} ft/sec	V/V_o	$R_s \times 10^{-5}$
1	0.000	12.00	1.00	0.00	0.00	.00
2	.023	4.55	.379	109.4	.789	.396
3	.079	.75	.063	134.4	.968	1.674
4	.173	- 1.10	.092	145.1	1.045	3.948
5	.276	- 1.60	- .133	147.8	1.064	6.423
6	.376	- 2.15	- .179	150.8	1.086	8.944
7	.476	- 2.25	- .187	151.3	1.090	11.350
8	.576	- 2.50	- .208	152.6	1.099	13.860
9	.677	- 1.95	- .163	149.7	1.078	15.990
10	.779	+ .60	+ .05	135.3	.975	16.630
11	.909	1.90	.159	127.4	.917	18.250
12	1.035	.25	.021	137.4	.989	22.430

TABLE XIVd

DISTRIBUTION OF NORMAL PRESSURE FORCES AND LOCAL VELOCITIES L/D = 5

q_o = 25 cm silicone
V_o = 200.4 ft./sec.
Length = 2.5 feet
R_L = 3.159 X 10^6

December 23, 1963
Barometric Pressure 30.40 in. Hg.
Temperature 67° F.
C_{D_p} = .0013

Orifice	s/L	Δp cm	$\Delta p/q_o$	V_{local} ft/sec	V/V_o	R_s X 10^{-5}
1	0.000	25.00	1.00	0.0	.00	.00
2	.023	9.40	.376	158.3	.790	.574
3	.079	1.50	.060	194.3	.969	2.419
4	.173	- 2.50	- .10	210.2	1.049	5.721
5	.276	- 3.30	- .132	213.2	1.064	9.265
6	.376	- 4.40	- .176	217.3	1.084	12.89
7	.476	- 4.65	- .186	218.3	1.089	16.37
8	.576	- 5.35	- .214	220.8	1.102	20.06
9	.677	- 4.10	- .164	216.2	1.079	23.09
10	.779	+ .80	+ .032	197.2	.984	24.23
11	.909	3.75	.150	184.7	.923	26.47
12	1.035	.20	.008	199.6	.996	32.58

TABLE XIVe

DISTRIBUTION OF NORMAL PRESSURE FORCES AND LOCAL VELOCITIES L/D = 5

q_o = 38 cm silicone
V_o = 247.1 ft./sec.
Length = 2.5 feet
R_L = 3.89×10^6

December 23, 1963
Barometric Pressure 30.40 in. Hg.
Temperature 67° F.
C_{D_p} = .0015

Orifice	s/L	Δp cm	$\Delta p/q_o$	V_{local} ft/sec	V/V_o	$R_s \times 10^{-5}$
1	0.000	38.0	1.00	0.0	.00	.00
2	.023	14.4	.399	194.7	.788	.706
3	.079	2.3	.061	239.5	.969	2.982
4	.173	− 3.75	− .097	259.0	1.048	7.049
5	.276	− 4.85	− .127	262.4	1.062	11.40
6	.376	− 6.70	− .176	268.0	1.084	15.90
7	.476	− 7.40	− .195	270.0	1.093	20.26
8	.576	− 8.15	− .215	272.3	1.102	24.74
9	.677	− 6.10	− .161	266.2	1.077	28.43
10	.779	+ 1.05	+ .028	243.6	.986	29.94
11	.909	5.50	.145	228.5	.924	32.74
12	1.035	.15	.004	246.6	.998	40.26

TABLE XVa

DISTRIBUTION OF NORMAL PRESSURE FORCES AND LOCAL VELOCITIES L/D = 6

q_o = 2 cm silicone
V_o = 57.0 ft./sec.
Length = 3.0 feet
$R_L = 1.05 \times 10^6$

December 23, 1963
Barometric Pressure 30.4 in. Hg.
Temperature 75° F.
$C_{D_p} = 0.00056$

Orifice	s/L	Δp cm	$\Delta p/q_o$	V_{local} ft/sec	V/V_o	$R_s \times 10^{-5}$
1	.000	2.00	1.000	00.0	0.00	0.00
2	.021	.55	.275	48.6	.85	.188
3	.073	.05	.025	56.4	.99	.755
4	.169	- .15	- .075	59.2	1.04	1.84
5	.269	- .25	- .125	60.5	1.06	3.00
6	.369	- .25	- .125	60.5	1.06	4.12
7	.469	- .35	- .175	61.9	1.08	5.35
8	.569	- .40	- .200	62.5	1.09	6.55
9	.669	- .25	- .125	60.5	1.06	7.47
10	.772	+ .10	+ .050	55.6	.97	7.91
11	.901	.20	.100	54.1	.94	8.98
12	1.029	.30	.150	52.6	.92	9.99

[illegible]

[illegible]

[illegible]

[illegible]	[illegible]	[illegible]	[illegible]	[illegible]	[illegible]	[illegible]
[illegible]	[illegible]	[illegible]	[illegible]	[illegible]	[illegible]	[illegible]
[illegible]	[illegible]	[illegible]	[illegible]	[illegible]	[illegible]	[illegible]
[illegible]	[illegible]	[illegible]	[illegible]	[illegible]	[illegible]	[illegible]
[illegible]	[illegible]	[illegible]	[illegible]	[illegible]	[illegible]	[illegible]
[illegible]	[illegible]	[illegible]	[illegible]	[illegible]	[illegible]	[illegible]
[illegible]	[illegible]	[illegible]	[illegible]	[illegible]	[illegible]	[illegible]
[illegible]	[illegible]	[illegible]	[illegible]	[illegible]	[illegible]	[illegible]
[illegible]	[illegible]	[illegible]	[illegible]	[illegible]	[illegible]	[illegible]
[illegible]	[illegible]	[illegible]	[illegible]	[illegible]	[illegible]	[illegible]
[illegible]	[illegible]	[illegible]	[illegible]	[illegible]	[illegible]	[illegible]
[illegible]	[illegible]	[illegible]	[illegible]	[illegible]	[illegible]	[illegible]

TABLE XVb

DISTRIBUTION OF NORMAL PRESSURE FORCES AND LOCAL VELOCITIES $L/D \cong 6$

$q_o \cong 5$ cm silicone
$V_o \cong 90.2$ ft./sec.
Length $\cong 3.0$ feet
$R_L \cong 1.66 \times 10^6$

December 23, 1963
Barometric Pressure 30.40 in. Hg.
Temperature 75° F.
$C_{D_p} \cong 0.00061$

Orifice	s/L	Δp cm	$\Delta p/q_o$	V_{local} ft/sec	V/V_o	$R_s \times 10^{-5}$
1	0.000	5.00	1.000	00.0	0.00	0.00
2	.021	1.31	.262	77.5	.86	.30
3	.073	0.17	.034	88.7	.98	1.19
4	.169	− .33	− .066	93.2	1.03	2.90
5	.269	− .60	− .120	95.5	1.06	4.75
6	.369	− .64	− .128	95.8	1.06	6.52
7	.469	− .71	− .142	96.4	1.07	8.34
8	.569	− .80	− .160	97.2	1.08	16.19
9	.699	− .57	− .114	95.3	1.05	11.75
10	.772	+ .28	+ .056	87.6	.97	12.47
11	.901	.61	.122	84.6	.94	14.03
12	1.029	.21	.042	88.3	.98	16.74

TABLE XVc

DISTRIBUTION OF NORMAL PRESSURE FORCES AND LOCAL VELOCITIES L/D = 6

q_o = 12 cm silicone
V_o 139.8 ft./sec
Length = 3.0 feet
R_L = 2.57 X 10^6

December 23, 1963
Barometric Pressure 30.40 in. Hg.
Temperature 75° F.
C_{D_p} = 0.00059

Orifice	s/L	Δp cm	$\Delta p/q_o$	V_{local} ft/sec	V/V_o	R_s X 10^{-5}
1	0.000	12.00	1.000	000.0	0.00	0.00
2	.021	2.90	.242	121.7	.87	.47
3	.073	.30	.025	138.0	.98	1.85
4	.169	- .90	- .075	144.9	1.04	4.51
5	.269	-1.50	- .125	148.3	1.06	7.36
6	.369	-1.60	- .133	149.0	1.06	10.13
7	.469	-.185	- .154	150.2	1.07	12.99
8	.569	-2.00	- .167	151.0	1.08	15.84
9	.669	-1.50	- .125	148.3	1.06	18.30
10	.772	+ .51	+ .043	136.8	.98	19.46
11	.901	1.45	.121	131.1	.94	21.75
12	1.029	.44	.037	137.2	.98	26.01

TABLE XVd

DISTRIBUTION OF NORMAL PRESSURE FORCES AND LOCAL VELOCITIES L/D = 6

q_o = 25 cm silicone
V_o = 201.8 ft./sec.
Length = 3.0 feet
R_L = 3.72 X 10^6

December 23, 1963
Barometric Pressure 30.40 in. Hg.
Temperature 75° F.
C_{D_p} = .00073

Orifice	s/L	Δp cm	$\Delta p/q_o$	V_{local} ft/sec	V/V_o	R_s X 10^{-5}
1	.000	25.00	1.000	000.0	.00	.00
2	.021	6.20	.248	175.0	.87	.68
3	.073	.60	.024	199.4	.99	2.67
4	.169	- 1.80	- .072	209.0	1.04	6.50
5	.269	- 3.00	- .120	213.6	1.06	10.60
6	.369	- 3.30	- .132	214.7	1.06	14.61
7	.469	- 3.75	- .150	216.4	1.07	18.71
8	.569	- 4.15	- .166	217.9	1.08	22.85
9	.669	- 3.10	- .124	214.0	1.06	26.40
10	.772	+ .95	+ .038	197.9	.98	28.15
11	.901	3.10	.124	188.8	.94	31.33
12	1.029	.70	.028	198.9	.98	37.72

TABLE XVe

DISTRIBUTION OF NORMAL PRESSURE FORCES AND LOCAL VELOCITIES L/D = 6

q_o = 38 cm silicone
V_o = 248.8 ft./sec.
Length = 3.0 feet
R_L = 4.58×10^6

December 23, 1963
Barometric Pressure 30.40 in. Hg.
Temperature 75 ° F.
C_{D_p} = .00070

Orifice	s/L	Δp cm	$\Delta p/q_o$	V_{local} ft/sec	V/V_o	$R_s \times 10^{-5}$
1	.000	38.00	1.00	0.0	.00	.00
2	.021	8.25	.217	220.0	.88	.86
3	.073	.80	.021	246.1	.99	3.30
4	.169	− 2.85	− .075	257.9	1.04	8.02
5	.269	− 4.45	− .117	263.0	1.05	13.05
6	.369	− 5.05	− .133	264.8	1.06	18.02
7	.469	− 5.65	− .149	266.6	1.07	23.06
8	.569	− 6.25	− .165	268.5	1.08	28.16
9	.669	− 4.20	− .110	262.2	1.05	32.36
10	.772	+ 1.15	+ .030	245.0	.98	34.85
11	.901	4.45	.117	262.9	1.05	43.62
12	1.029	0.75	.020	246.3	.99	46.70

TABLE XVI

LENGTHWISE VELOCITY DISTRIBUTION IN THE BOUNDARY LAYER AT 0.009 INCHES FROM SURFACE

January 15, 1964

Barometer 30.08 in. Hg.
Temperature 70° F.

BODY OF REVOLUTION L/D = 3

Dynamic Pressure q_o	3.80 lbs./sq. ft.	9.24 lbs./sq. ft.	22.9 lbs./sq. ft.
Station X/L	V/V_o	V/V_o	V/V_o
0.06	0.71	0.84	-
.15	.70	.86	-
.25	.60	.80	-
.35	.56	.66	-
.45	.48	.64	-
.55	.42	.58	-
.65	.42	.68	-
.75	.48	.74	-
.875	.37	.56	-

BODY OF REVOLUTION L/D = 4

X/L	V/V_o	V/V_o	V/V_o
0.06	0.71	0.88	0.90
.15	.60	.73	.93
.25	.55	.65	.80
.35	.40	.57	.75
.45	.41	.45	.66
.55	.38	.43	.64
.65	.35	.46	.89
.75	.44	.51	.86
.875	.39	.47	.66

TABLE XVI
(Continued)

BODY OF REVOLUTION L/D = 5

Dynamic Pressure q_o	3.80 lbs./sq. ft.	9.24 lbs./sq. ft.	22.9 lbs./sq. ft.
Station X/L	V/V_o	V/V_o	V/V_o
0.06	0.60	0.69	0.83
.15	.56	.58	.74
.25	.40	.51	.62
.35	.39	.48	.54
.45	.36	.36	.48
.55	.29	.35	.49
.65	.26	.41	.70
.75	.37	.46	.53
.875	.32	.34	.38

BODY OF REVOLUTION L/D = 6

X/L	V/V_o	V/V_o	V/V_o
0.06	0.39	0.48	0.67
.15	.36	.42	.58
.25	.34	.40	.59
.35	.30	.35	.51
.45	.26	.29	.49
.55	.24	.34	.69
.65	.30	.40	.62
.75	.31	.35	.51
.875	.27	.33	.37

TABLE XVII

EXPERIMENTALLY ESTIMATED LOCAL SKIN FRICTION INTENSITY STREAMLINED BODY OF REVOLUTION L/D = 3

q_0 = 3.8 lb./sq. ft. $R_L = 5.4 \times 10^5$

STATION s/L	$\left(\frac{\partial v}{\partial y}\right)_0$ $\frac{\text{ft/sec.}}{\text{ft.}}$	τ_0 lb/sq. ft.	τ_0/q_0
.036	65,800	.0247	.00650
.101	61,300	.0247	.00650
.204	54,700	.0205	.00538
.308	47,700	.0179	.00470
.408	41,600	.0156	.00410
.506	36,000	.0135	.00355
.607	32,000	.0120	.00315
.709	32,000	.0120	.00315
.816	35,400	.0130	.00350
.954	30,400	.0114	.00300

C_{D_f} = .0039

q_0 = 9.24 lb./sq. ft. $R_L = 8.58 \times 10^5$

STATION s/L	$\left(\frac{\partial v}{\partial y}\right)_0$ $\frac{\text{ft/sec.}}{\text{ft.}}$	τ_0 lb/sq. ft.	τ_0/q_0
.036	129,000	.0485	.00525
.101	120,000	.0450	.00490
.204	108,000	.0407	.00440
.308	96,000	.0360	.00390
.408	86,000	.0323	.00350
.506	75,000	.0282	.00305
.607	67,000	.0254	.00275
.709	77,000	.0291	.00315
.816	79,000	.0300	.00325
.954	68,000	.0258	.00280

C_{D_f} = .0036

TABLE XVII
L/D = 3 (Continued)

q_o lb/ft^2	22.9	47.6	72.6
STATION s/L	τ_o/q_o	τ_o/q_o	τ_o/q_o
0.036	0.00445	0.00420	0.00400
.101	.00422	.00395	.00375
.204	.00385	.00360	.00345
.308	.00350	.00331	.00320
.408	.00318	.00305	.00305
.506	.00290	.00295	.00405
.607	.00270	.00385	.00400
.709	.00330	.00370	.00355
.816	.00315	.00340	.00310
.954	.00265	.00285	.00250
	$C_{D_f} = .0032$	$C_{D_f} = .0034$	$C_{D_f} = .0036$

TABLE XVIII

EXPERIMENTALLY ESTIMATED LOCAL SKIN FRICTION INTENSITY STREAMLINED BODY OF REVOLUTION
$L/D \cong 4$

$q_o \cong 3.80$ lb./ft^2 $R_L \cong 7.18 \times 10^5$

STATION s/L	$\left(\frac{\partial v}{\partial y}\right)_0$ $\frac{ft/sec}{ft}$	τ_0 lb/sq ft	τ_0/q_o
0.028	56,900	0.0213	0.00561
.083	54,100	.0203	.00535
.183	48,600	.0182	.00480
.286	41,600	.0156	.00418
.386	37,100	.0139	.00365
.486	32,000	.0120	.00316
.586	29,400	.0110	.00290
.688	29,100	.0109	.00287
.794	33,400	.0125	.00330
.927	29,100	.0109	.00288

$C_{D_f} \cong .0035$

$q_o \cong 9.24$ lb./ft^2 $R_L \cong 7.18 \times 10^5$

STATION s/L	$\left(\frac{\partial v}{\partial y}\right)_0$ $\frac{ft/sec}{ft}$	τ_0 lb/sq ft	τ_0/q_o
0.028	112,000	0.0421	0.00455
.083	106,000	.0396	.00428
.183	89,000	.0344	.00373
.286	74,000	.0296	.00320
.386	68,500	.0257	.00278
.486	59,400	.0222	.00240
.586	53,100	.0199	.00215
.688	57,400	.0215	.00233
.794	61,400	.0249	.00270
.927	58,200	.0218	.00218

$C_{D_f} \cong .0029$

TABLE XVIII
L/D = 4 (Continued)

$q_o = 22.9$ lb./ft^2 $R_L = 1.76 \times 10^6$

STATION s/L	$\left(\frac{\partial V}{\partial y}\right)_0$ $\frac{\text{ft/sec}}{\text{ft}}$	τ_0 lb/sq ft	τ_0/q_o
0.028	230,000	0.0862	0.00377
.083	212,000	.0796	.00348
.183	184,000	.0691	.00302
.286	160,000	.0600	.00262
.386	142,000	.0531	.00232
.486	124,000	.0466	.00204
.586	119,000	.0446	.00195
.688	169,000	.0631	.00276
.794	163,000	.0606	.00265
.927	125,000	.0470	.00205

$C_{D_f} = .00257$

q_o lb/ft^2	47.6	72.6
STATION s/L	τ_0/q_o	τ_0/q_o
0.028	0.00340	0.00310
.083	.00313	.00285
.183	.00277	.00253
.286	.00245	.00230
.386	.00225	.00264
.486	.00263	.00395
.586	.00350	.00378
.688	.00319	.00320
.794	.00257	.00255
.927	.00188	.00180
	$C_{D_f} = .00285$	$C_{D_f} = .00308$

TABLE XIX

EXPERIMENTALLY ESTIMATED LOCAL SKIN FRICTION INTENSITY STREAMLINED BODY OF REVOLUTION $L/D = 5$

$q_o = 3.80$ lb./sq. ft. $R_L = 8.935 \times 10^5$

STATION s/L	$\left(\frac{\partial v}{\partial y}\right)_o$ $\frac{\text{ft/sec}}{\text{ft}}$	τ_o lb/sq ft	τ_o/q_o
0.023	49,600	0.0186	0.00490
.079	46,700	.0175	.00460
.173	40,500	.0152	.00400
.276	34,900	.0131	.00345
.376	29,800	.0112	.00295
.476	25,300	.0095	.00250
.576	21,800	.0082	.00215
.677	19,800	.0074	.00195
.778	28,300	.0106	.00280
.909	24,300	.0091	.00240

$C_{D_f} = .00286$

$q_o = 9.24$ lb./sq.ft. $R_L = 1.41 \times 10^6$

STATION s/L	$\left(\frac{\partial v}{\partial y}\right)_o$ $\frac{\text{ft/sec}}{\text{ft}}$	τ_o lb/sq ft	τ_o/q_o
0.023	89,900	0.0337	0.00365
.079	83,000	.0311	.00337
.173	71,700	.0269	.00292
.276	61,600	.0231	.00250
.376	52,800	.0198	.00215
.476	42,900	.0161	.00175
.576	41,800	.0157	.00170
.677	49,100	.0184	.00200
.778	54,200	.0203	.00220
.909	40,500	.0152	.00165

$C_{D_f} = .00218$

TABLE XIX
L/D = 5 (Continued)

q_o = 22.9 lb./sq. ft. R_L = 2.188×10^6

STATION s/L	$\left(\frac{\partial V}{\partial y}\right)_o$ $\frac{\text{ft/sec}}{\text{ft}}$	τ_o lb/sq ft	τ_o/q_o
0.023	171,000	0.0641	0.00280
.079	155,000	.0582	.00255
.173	134,000	.0504	.00220
.276	116,000	.0434	.00190
.376	101,000	.0378	.00165
.476	90,000	.0333	.00148
.576	92,000	.0344	.00150
.677	131,000	.0492	.00215
.778	101,000	.0378	.00165
.909	70,000	.0263	.00115

C_{D_f} = .0018

q_o = lb/ft^2	47.6	72.6
STATION s/L	τ_o/q_o	τ_o/q_o
0.023	0.00233	0.00206
.079	.00210	.00190
.173	.00180	.00165
.276	.00155	.00150
.376	.00145	.00220
.476	.00238	.00325
.576	.00253	.00303
.677	.00217	.00255
.778	.00162	.00190
.909	.00105	.00100
	C_{D_f} = .00194	C_{D_f} = .0022

TABLE XX

EXPERIMENTALLY ESTIMATED LOCAL
SKIN FRICTION INTENSITY
STREAMLINED BODY OF REVOLUTION
L/D = 6

q_o = 3.80 lb./sq. ft. R_L = 1.05 X 10^6

STATION s/L	$\left(\frac{\partial v}{\partial y}\right)_o$ $\frac{\text{ft/sec}}{\text{ft}}$	τ_o lb/sq ft	τ_o/q_o
0.021	30,100	0.0113	0.00297
.072	29,200	.0109	.00287
.169	27,400	.0103	.00271
.269	25,600	.0096	.00253
.369	23,200	.0087	.00228
.469	20,000	.0075	.00198
.569	18,100	.0068	.00180
.669	22,900	.0086	.00227
.772	23,200	.0087	.00230
.901	20,800	.0078	.00205

C_{D_f} = .00212

q_o = 9.24 lb./sq. ft. R_L = 1.66 X 10^6

STATION s/L	$\left(\frac{\partial v}{\partial y}\right)_o$ $\frac{\text{ft/sec}}{\text{ft}}$	τ_o lb/sq ft	τ_o/q_o
0.021	60,300	0.0226	0.00245
.072	57,800	.0217	.00235
.169	53,300	.0200	.00216
.269	48,000	.0180	.00195
.369	41,800	.0157	.00170
.469	37,600	.0141	.00153
.569	40,500	.0152	.00164
.669	48,000	.0180	.00194
.772	44,500	.0167	.00181
.901	39,200	.0147	.00159

C_{D_f} = .00170

TABLE XX
L/D ≅ 6 (Continued)

q_o ≅ 22.9 lb./sq. ft. R_L ≅ 2.57×10^6

STATION s/L	$\left(\frac{\partial v}{\partial y}\right)_o$ $\frac{\text{ft/sec}}{\text{ft}}$	τ_o lb/sq ft	τ_o/q_o
0.021	136,000	0.0510	0.00223
.072	131,000	.0492	.00215
.169	122,000	.0458	.00200
.269	110,000	.0414	.00181
.369	96,000	.0361	.00158
.469	92,000	.0343	.00150
.569	129,000	.0485	.00212
.669	116,000	.0435	.00190
.772	95,000	.0355	.00155
.901	68,000	.0254	.00111

C_{D_f} ≅ .00165

q_o lb/ft^2	47.6	72.6
STATION s/L	τ_o/q_o	τ_o/q_o
0.021	0.00215	0.00207
.072	.00207	.00200
.169	.00190	.00184
.269	.00170	.00167
.369	.00150	.00255
.469	.00230	.00265
.569	.00220	.00236
.669	.00190	.00200
.772	.00148	.00147
.901	.00105	.00088
	C_{D_f} ≅ .00172	C_{D_f} ≅ .00192

Fig. 1

THE STREAMLINED BODIES TESTED

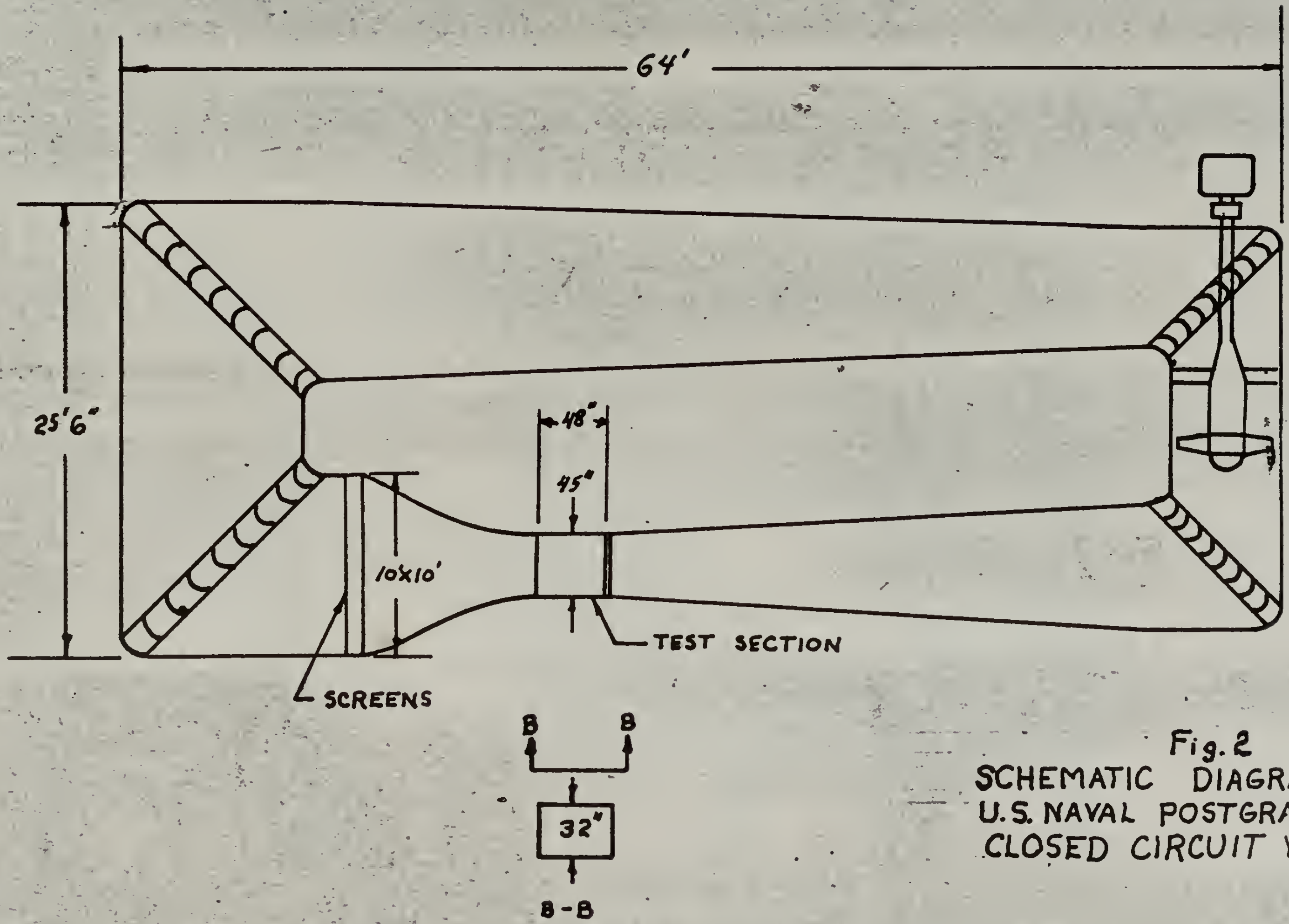

Fig. 2
SCHEMATIC DIAGRAM OF THE
U.S. NAVAL POSTGRADUATE SCHOOL
CLOSED CIRCUIT WIND TUNNEL

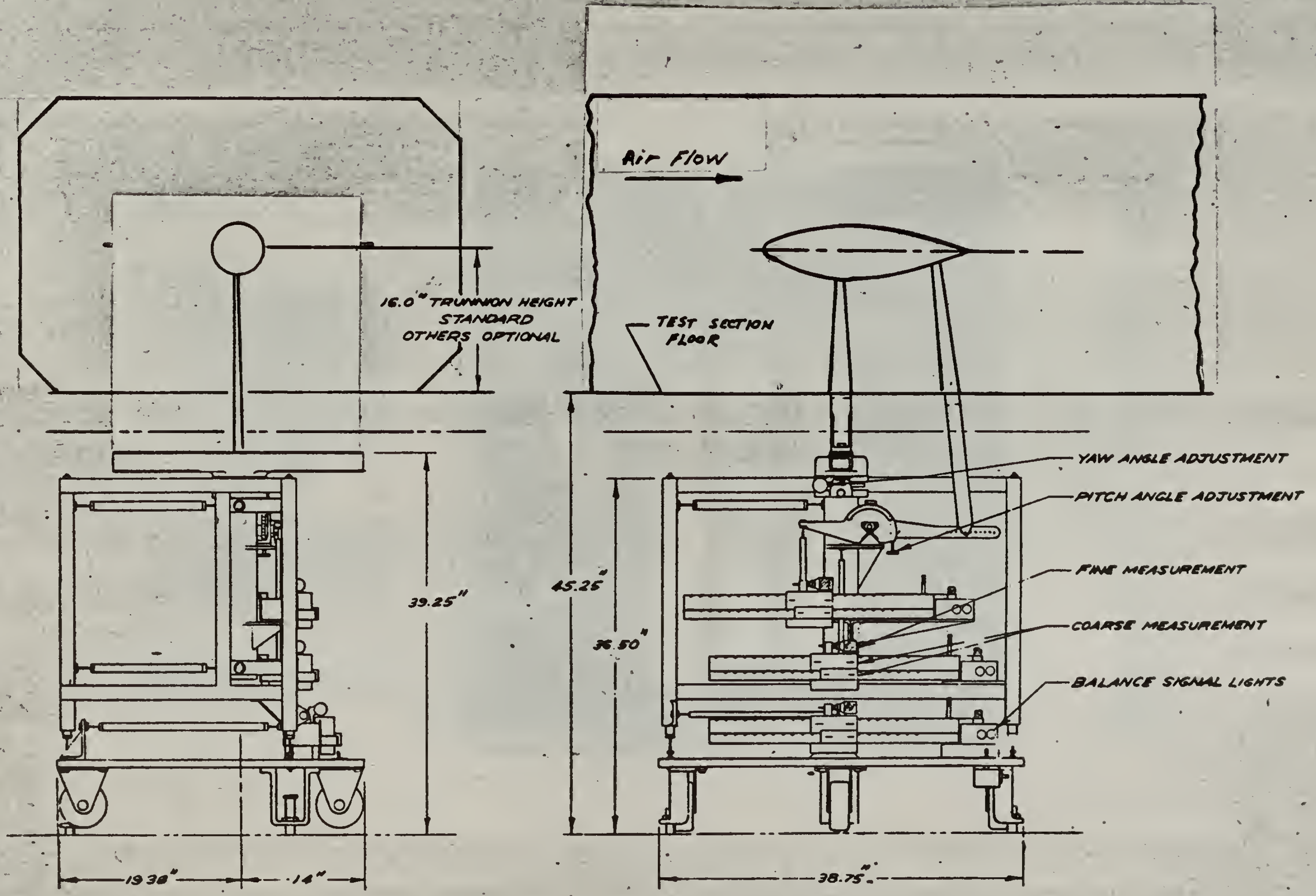

Fig. 3
AEROLAB 3 COMPONENT BEAM BALANCE

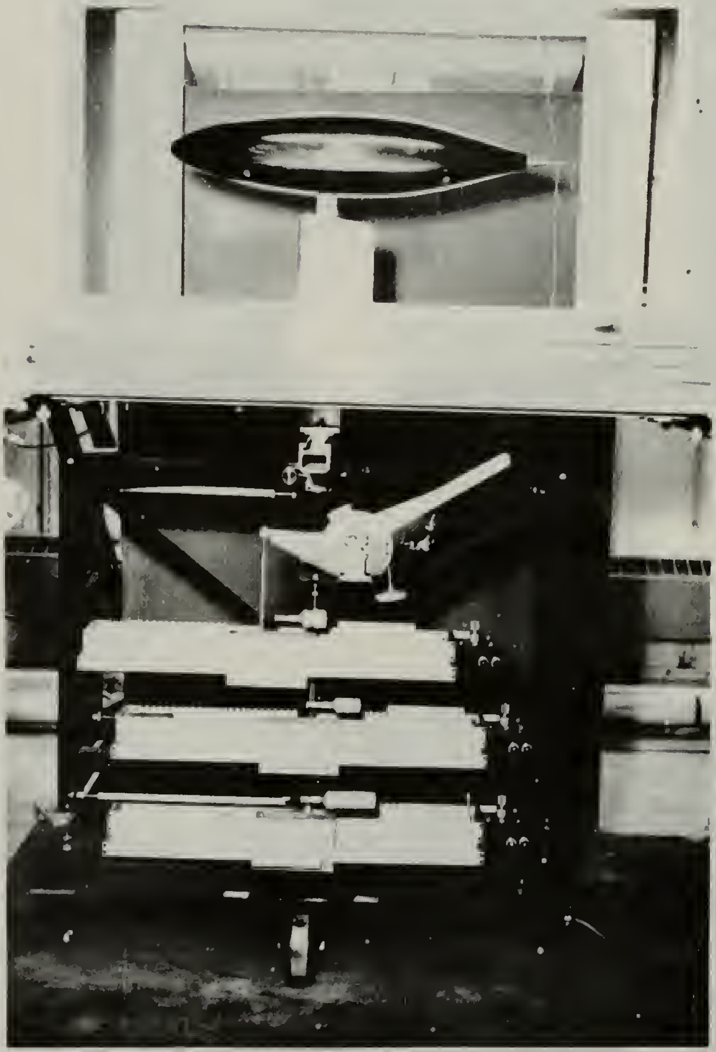

Fig. 4a

EQUIPMENT SETUP FOR TOTAL DRAG MEASUREMENT

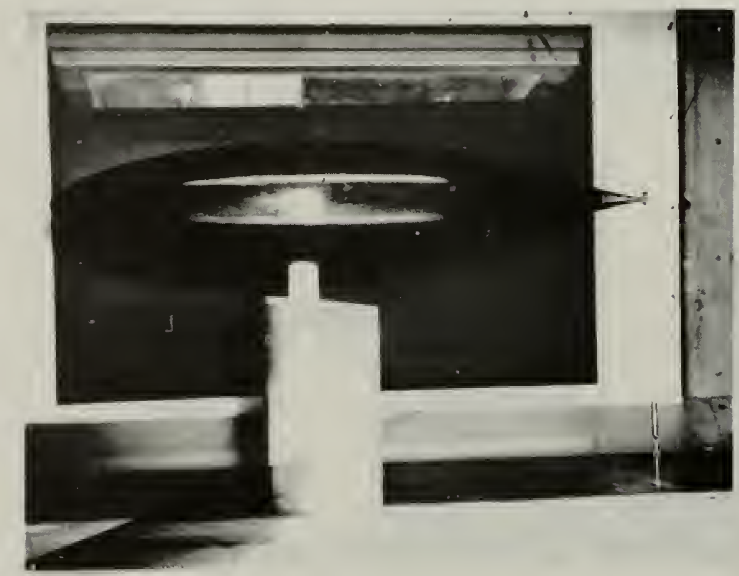

Fig. 4b
SIDEVIEW OF MODEL AND TEST SECTION

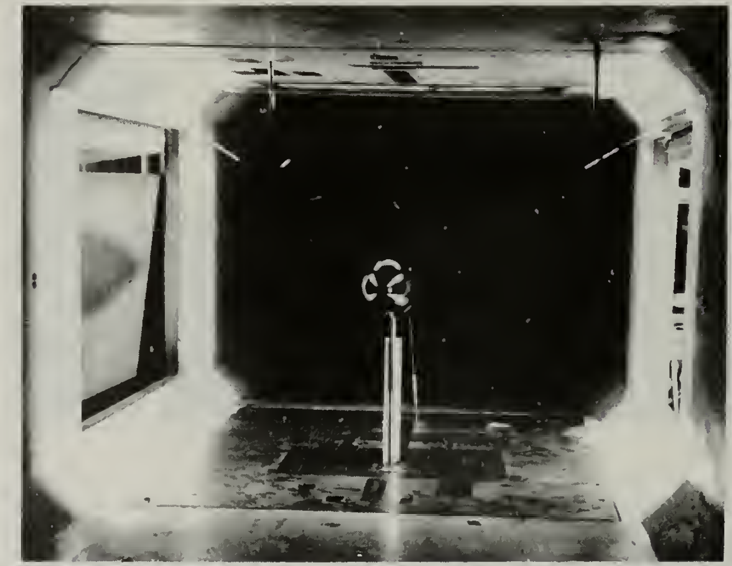

Fig. 4c
FRONTVIEW OF MODEL AND TEST SECTION

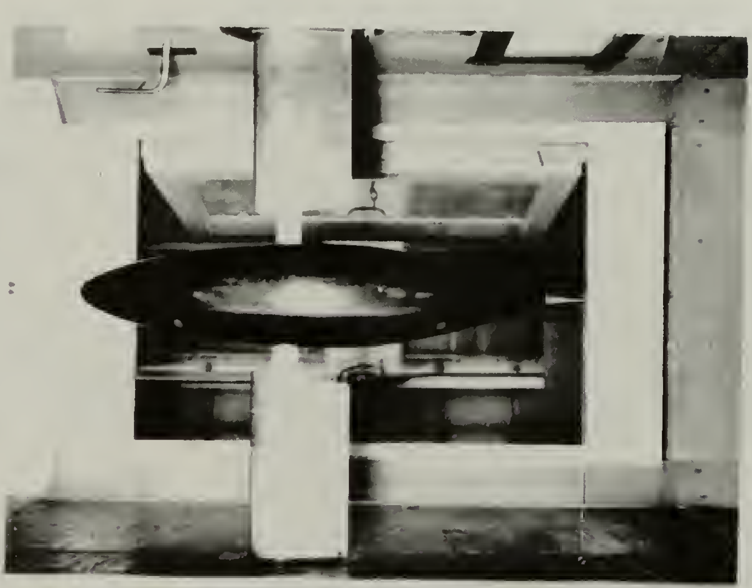

Fig. 5

MODEL WITH DUMMY SUPPORT

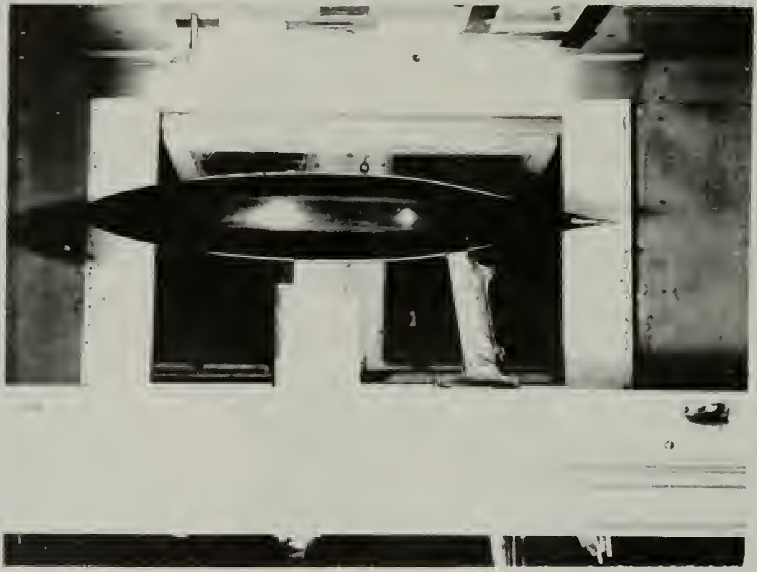

Fig. 6

EQUIPMENT SETUP FOR
PRESSURE MEASUREMENTS

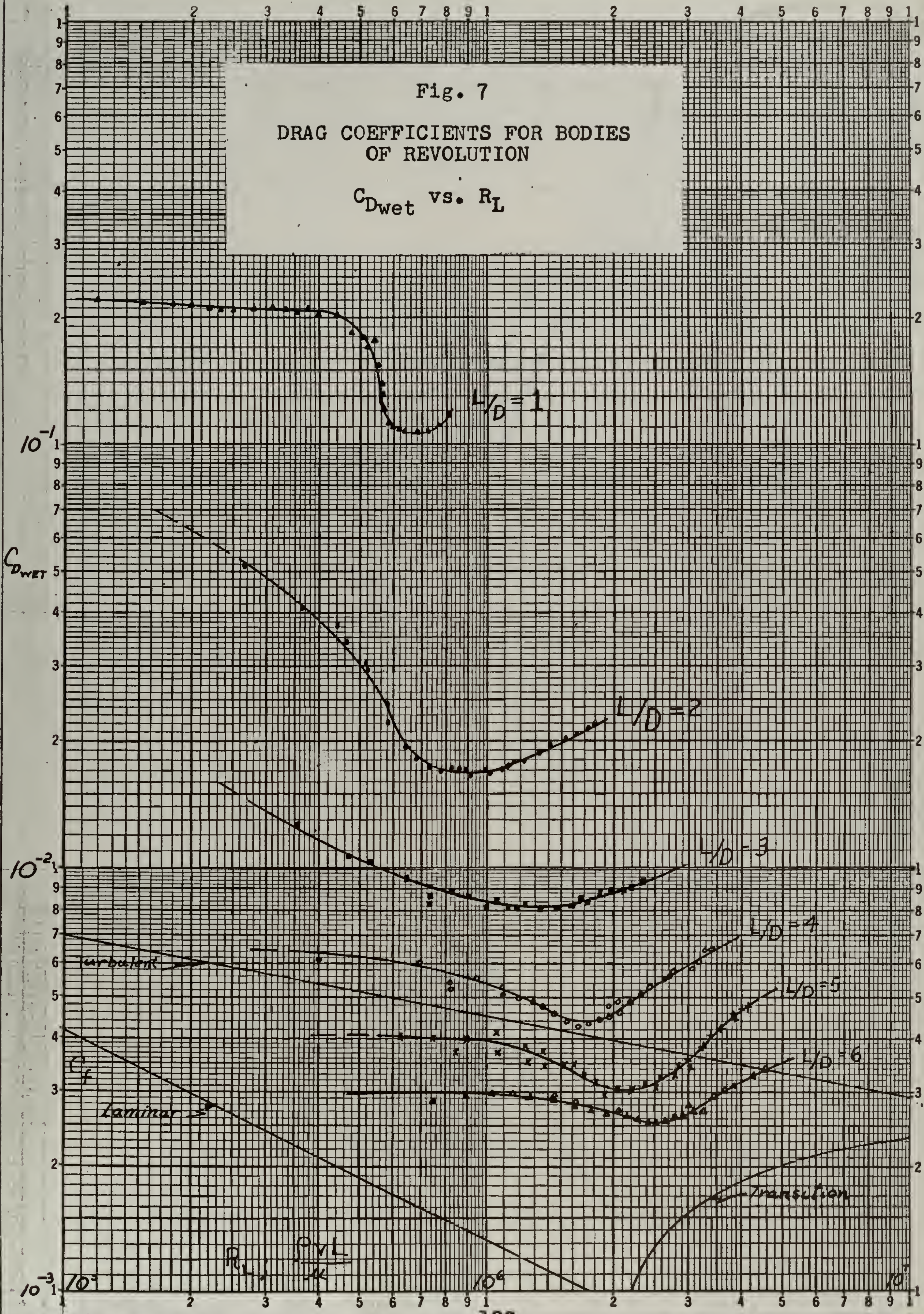

Fig. 7

DRAG COEFFICIENTS FOR BODIES OF REVOLUTION

$C_{D_{wet}}$ vs. R_L

Fig.
ORIENTATION OF MUTUALLY PERPENDICULAR PRESSURE AND FRICTIONAL FORCES

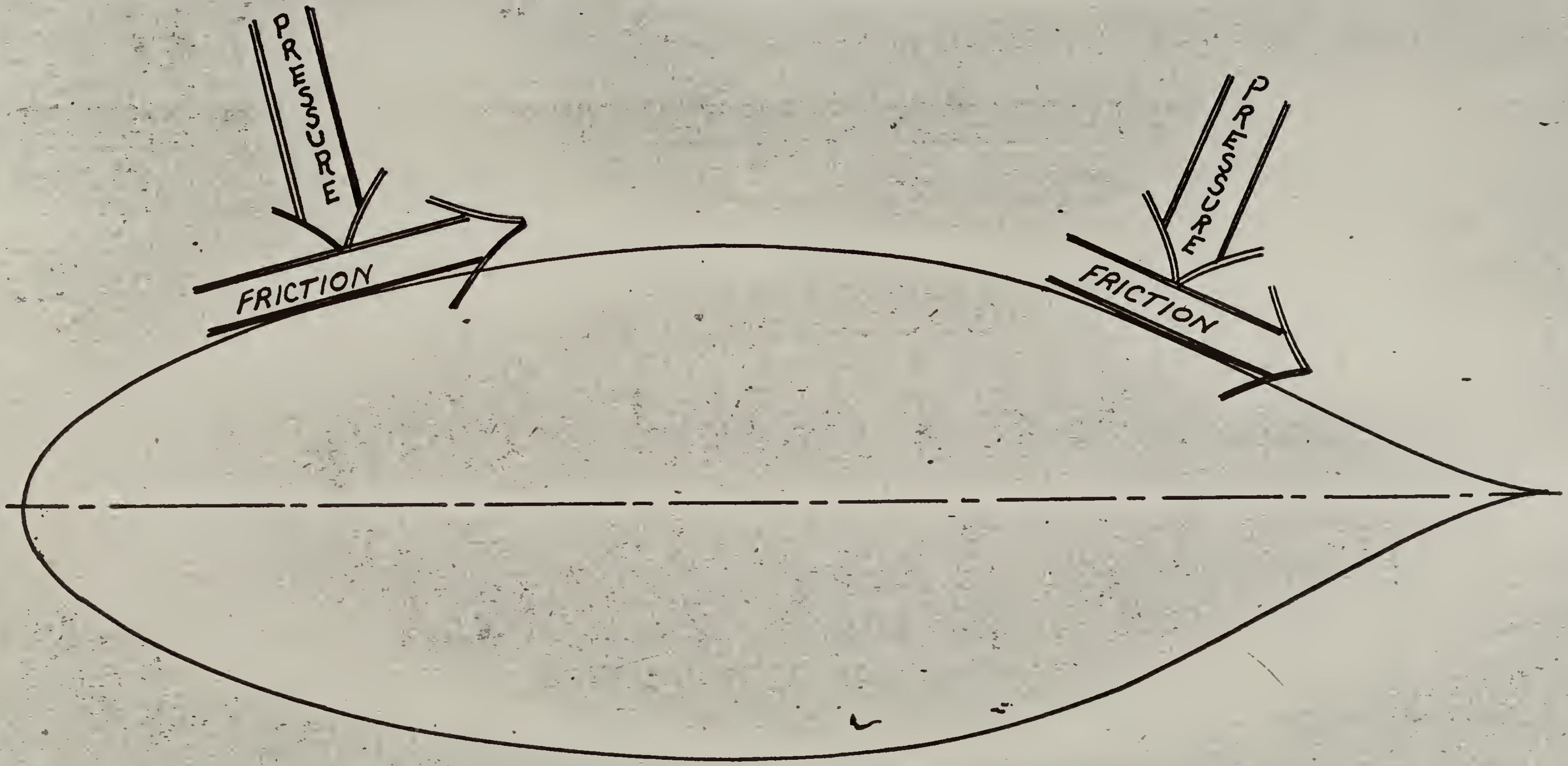

Fig. 9 a
DISTRIBUTION OF NORMAL PRESSURES AND INTEGRATION OF PRESSURE DRAG ON A BODY OF REVOLUTION
L/D = 1
Scale = 1/2 X

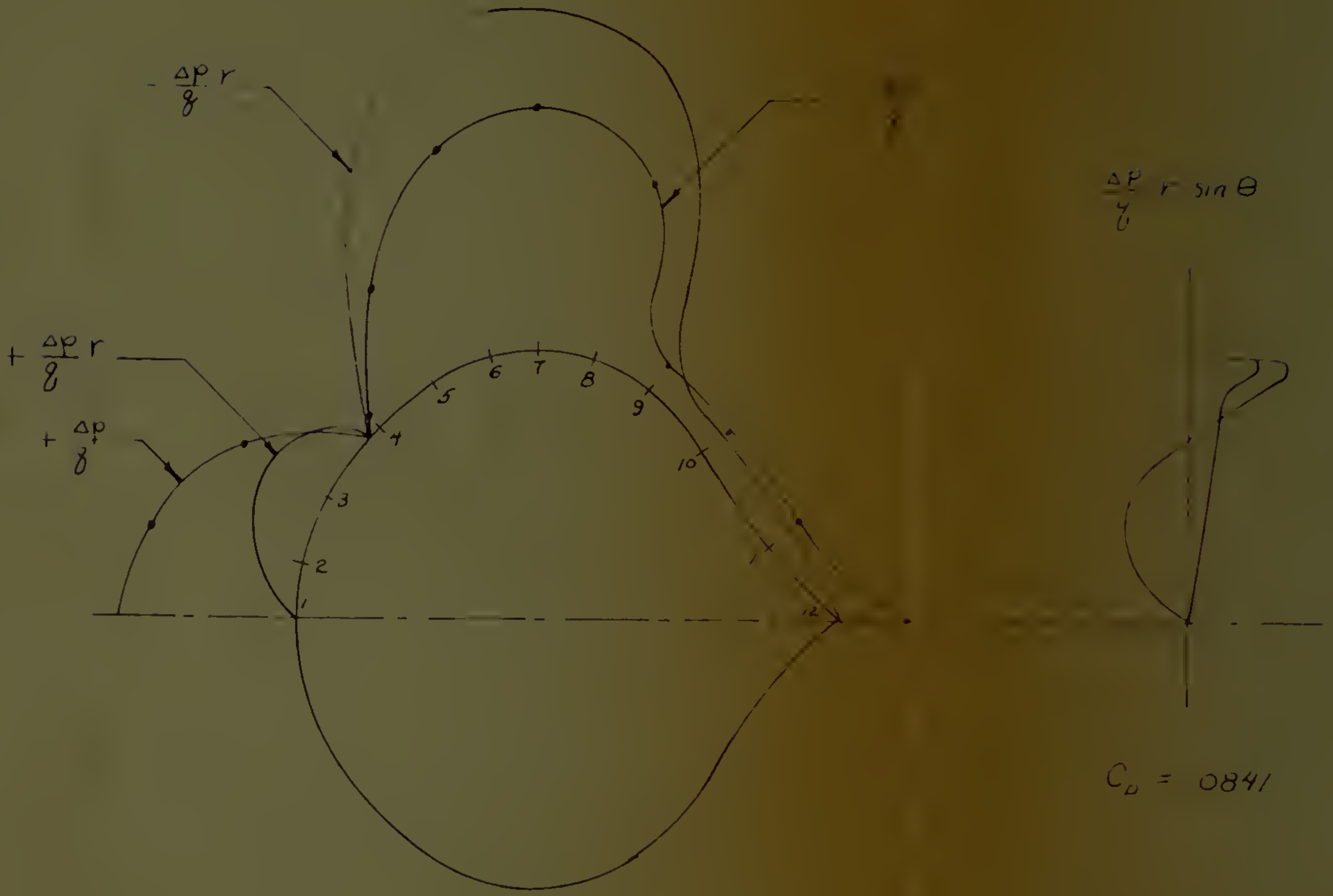

Fig. 96

DISTRIBUTION OF NORMAL
PRESSURE AND
INTEGRATION OF PRESSURE
DRAG ON A BODY OF
REVOLUTION
[illegible]
Scale = 1/2 X
12 cm of [illegible]

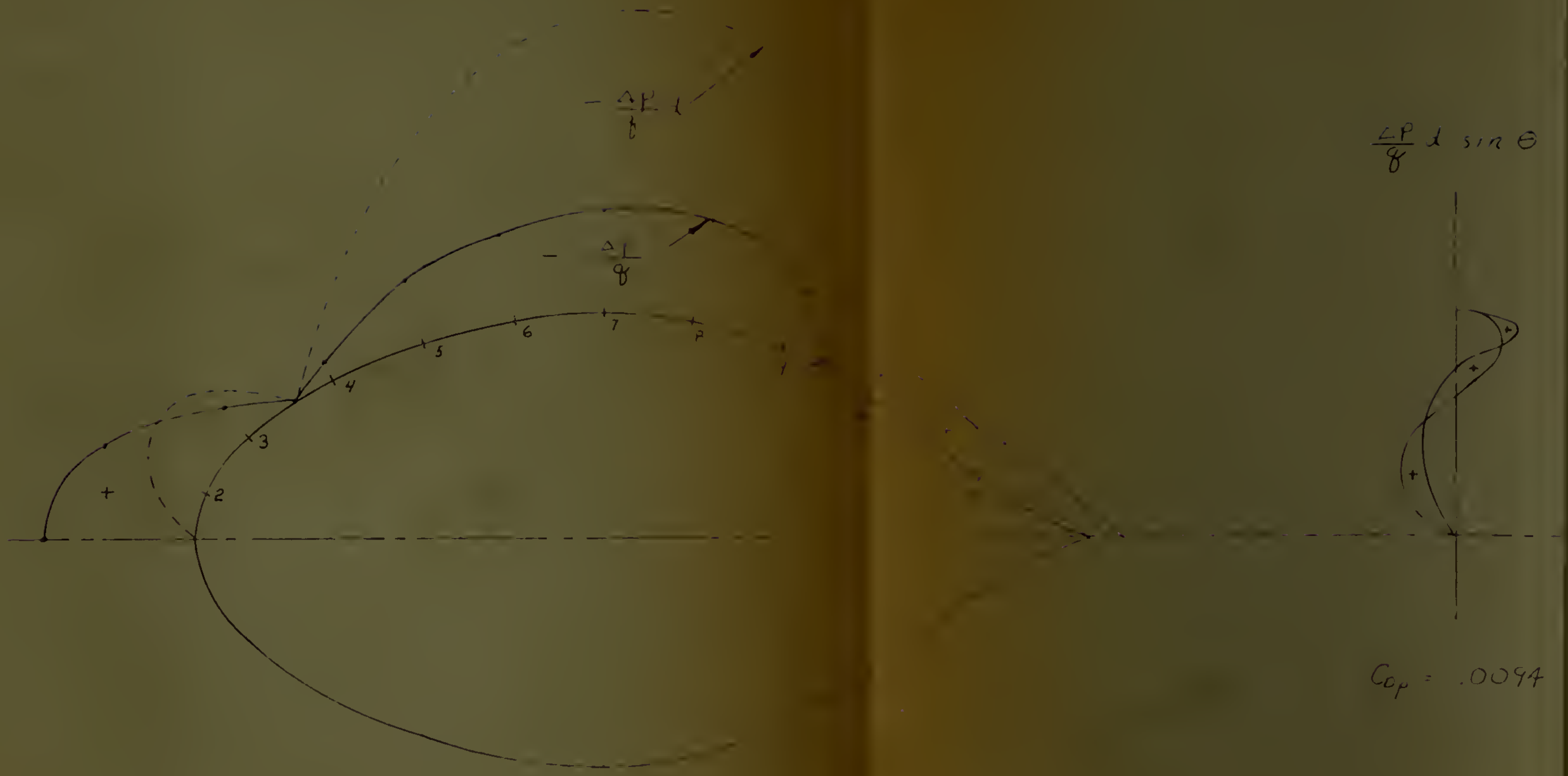

Fig. 96

DISTRIBUTION OF NORMAL
PRESSURE ON A
BODY OF REVOLUTION
[illegible]
Scale [illegible]
25 cm [illegible]

Fig 9d
DISTRIBUTION OF NORMAL
PRESSURES ON A
BODY OF REVOLUTION
L/D = 4
Scale 1/2 X
25 cm of silicone

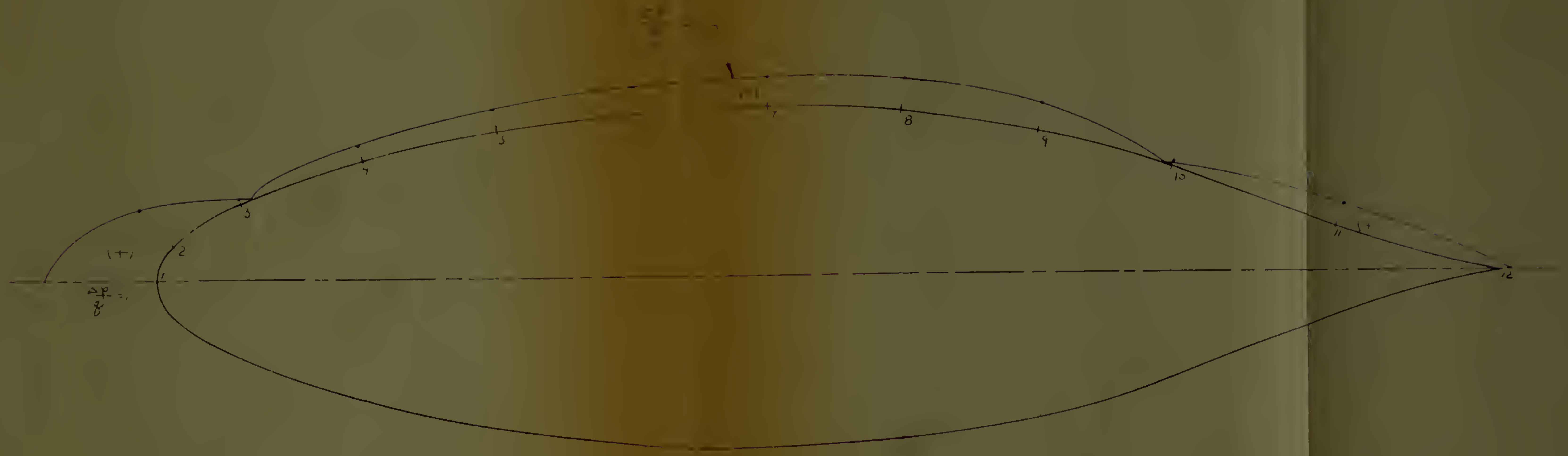

Fig. 9e
DISTRIBUTION OF NORMAL
PRESSURES ON A
BODY OF REVOLUTION
L/D = 5
Scale = 1/2 X
25cm of silicone

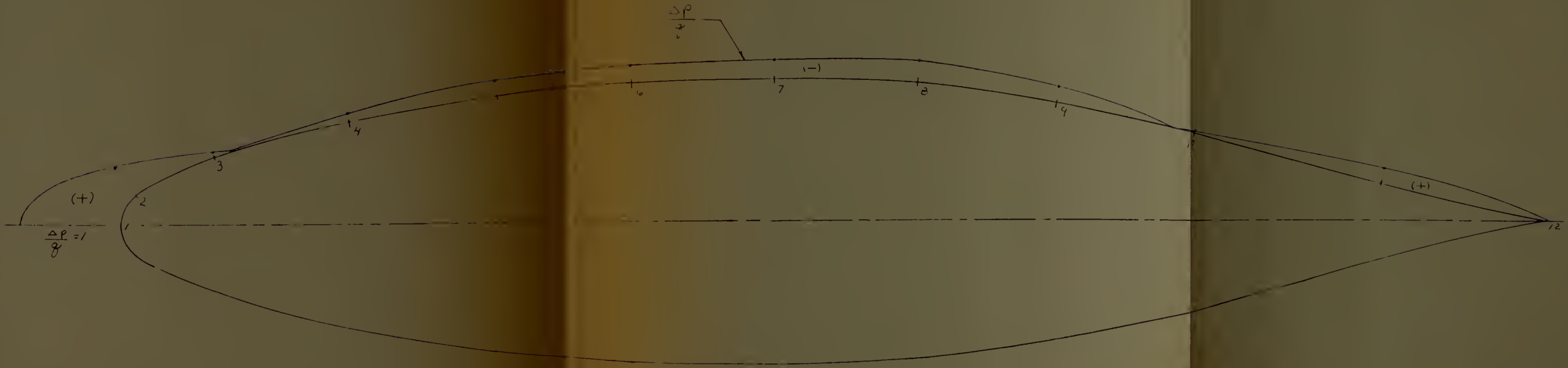

Fig. 9f
DISTRIBUTION OF NORMAL
PRESSURES ON A
BODY OF REVOLUTION
L/D = 6
Scale = 1/2 X
25cm of silicone

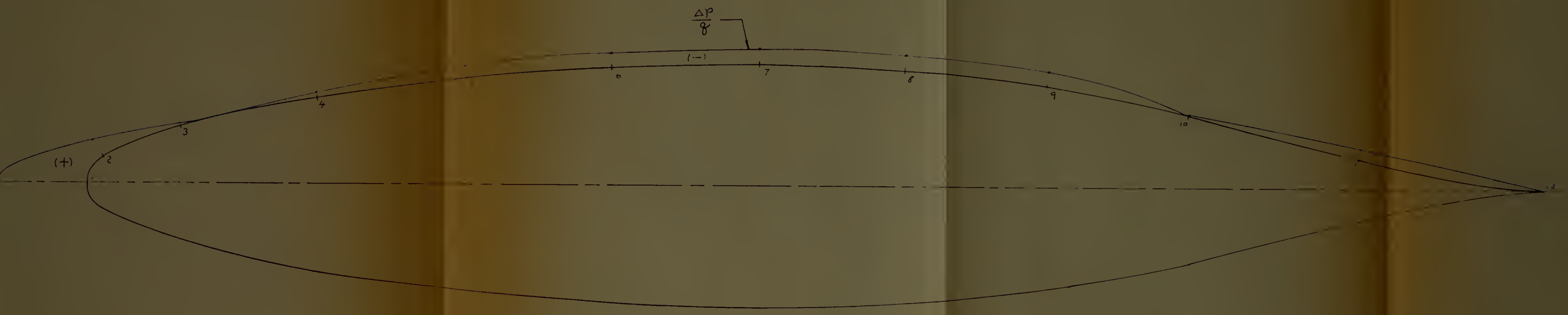

Fig. 10

PRESSURE DRAG COEFFICIENTS FOR BODIES OF REVOLUTION C_{D_P} vs. R_L

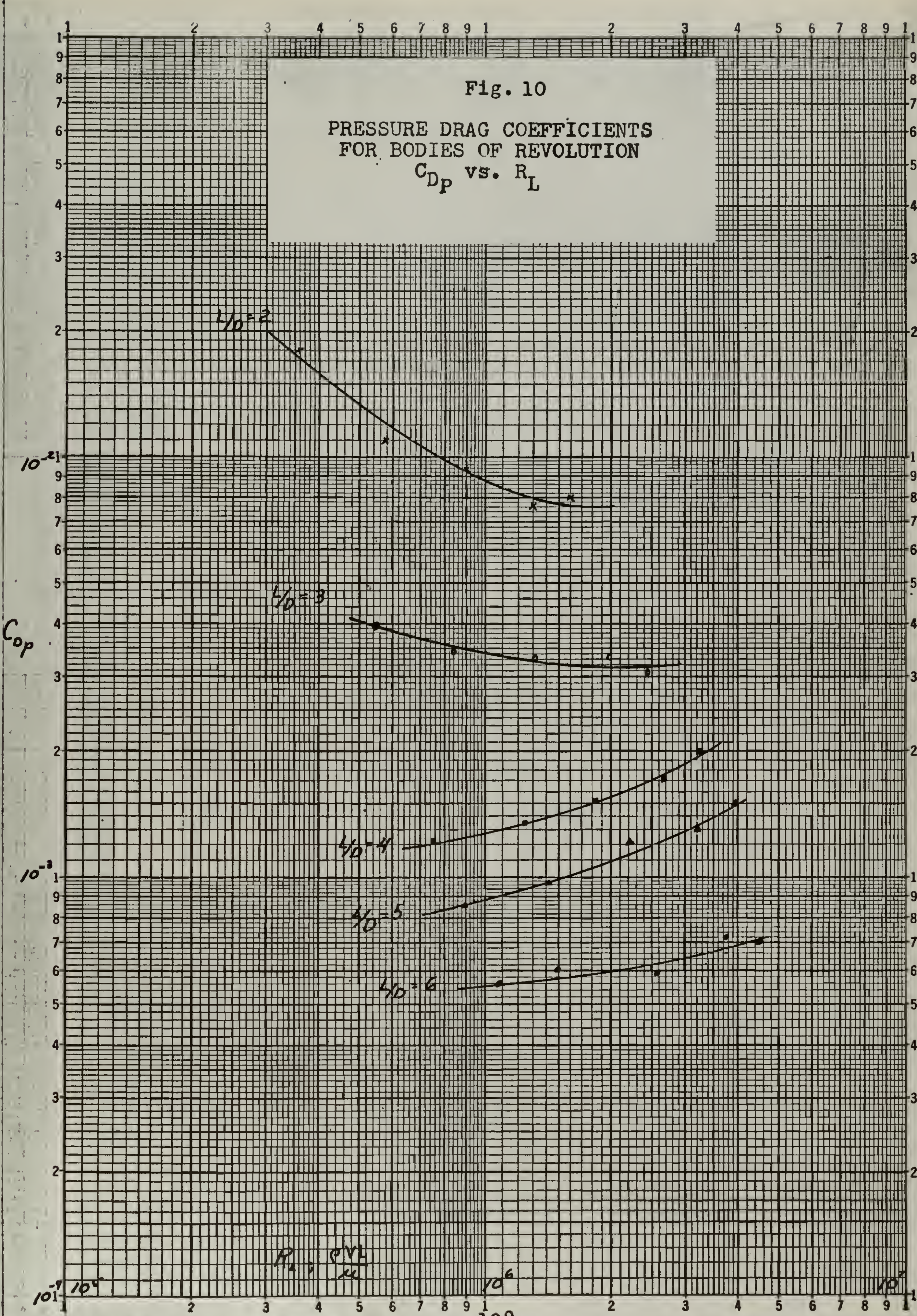

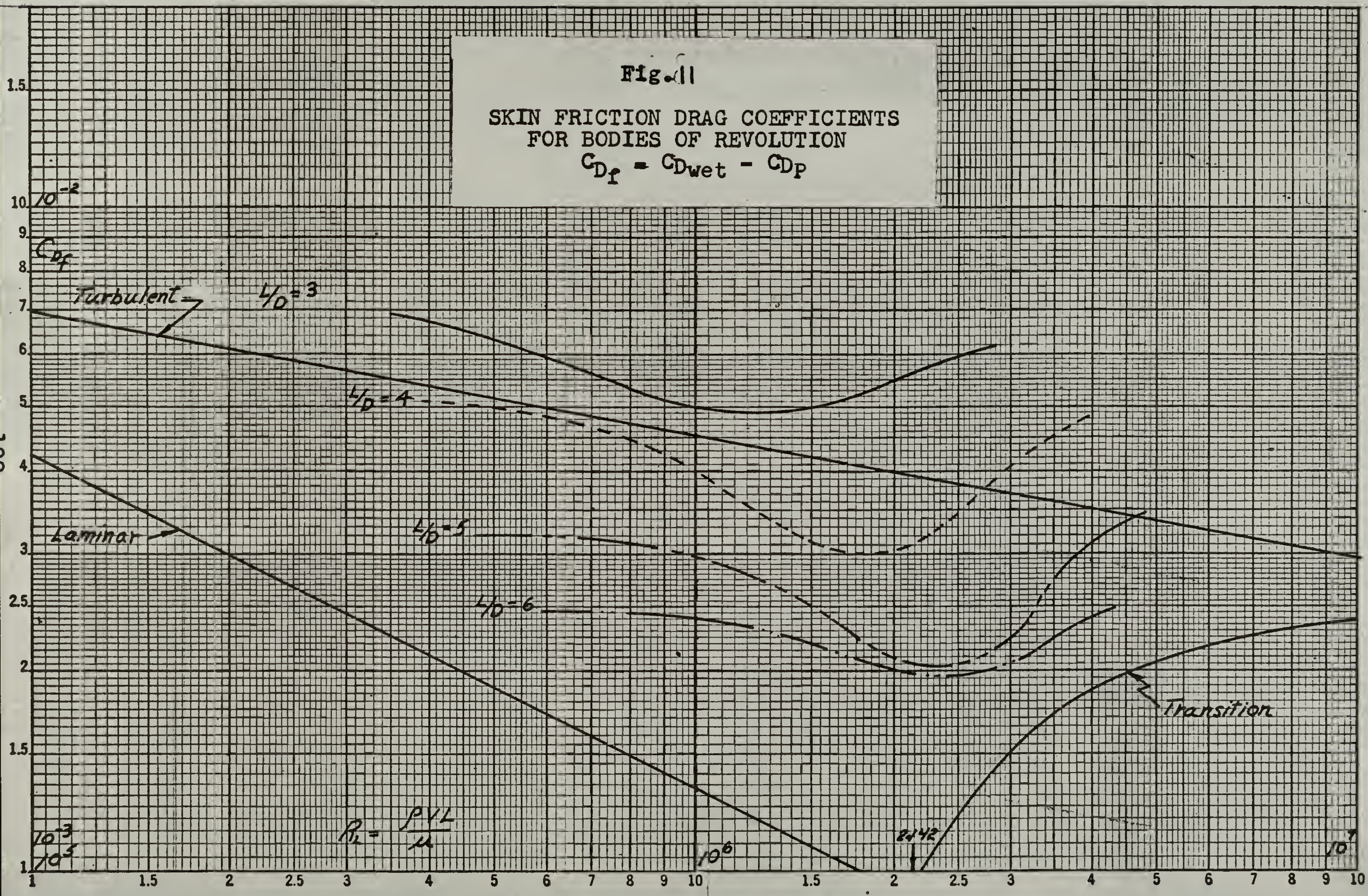

Fig. 11

SKIN FRICTION DRAG COEFFICIENTS FOR BODIES OF REVOLUTION

$C_{D_f} = C_{D_{wet}} - C_{D_P}$

Fig. 12

PERCENTAGE OF FRICTIONAL DRAG COMPARED TO TOTAL DRAG VERSUS THE RATIO OF DIAMETER OVER LENGTH

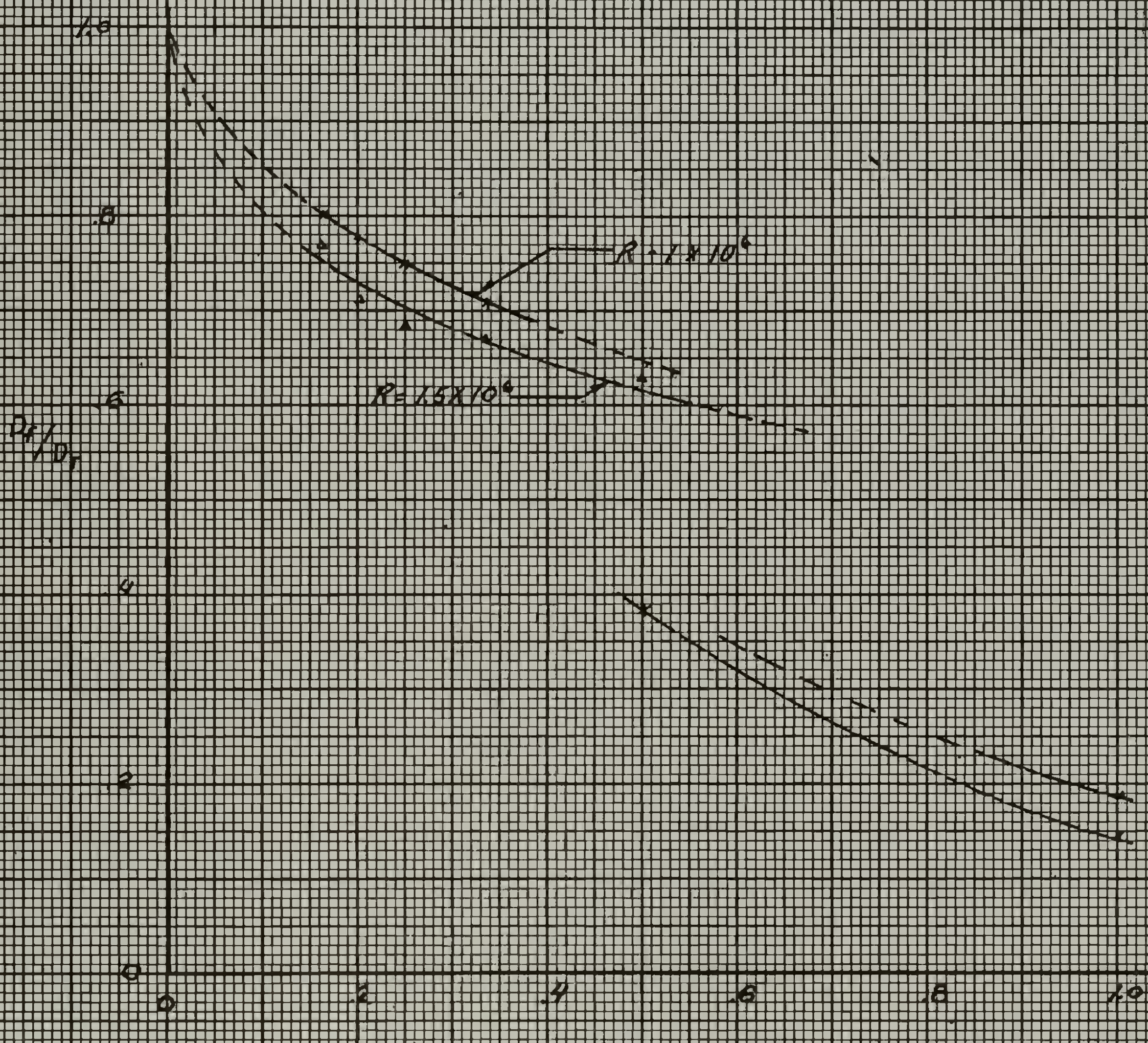

Fig. 13

COMPARISON OF LAMINAR BOUNDARY LAYER PROFILE SLOPES ON BODIES OF REVOLUTION WITH A FLAT PLATE

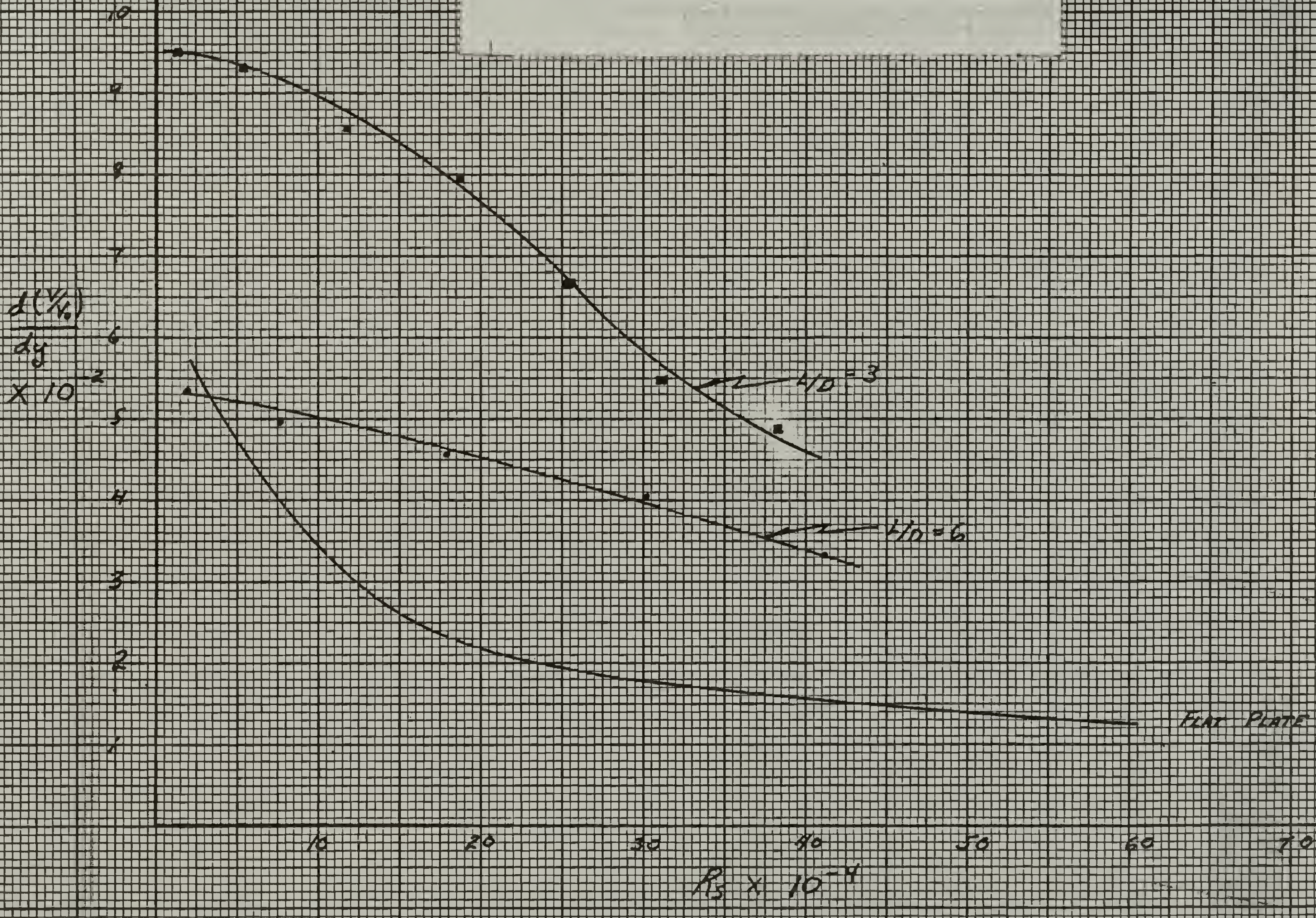

Fig. 14a

PRESSURE DISTRIBUTION OVER A BODY OF REVOLUTION

L/D = 1

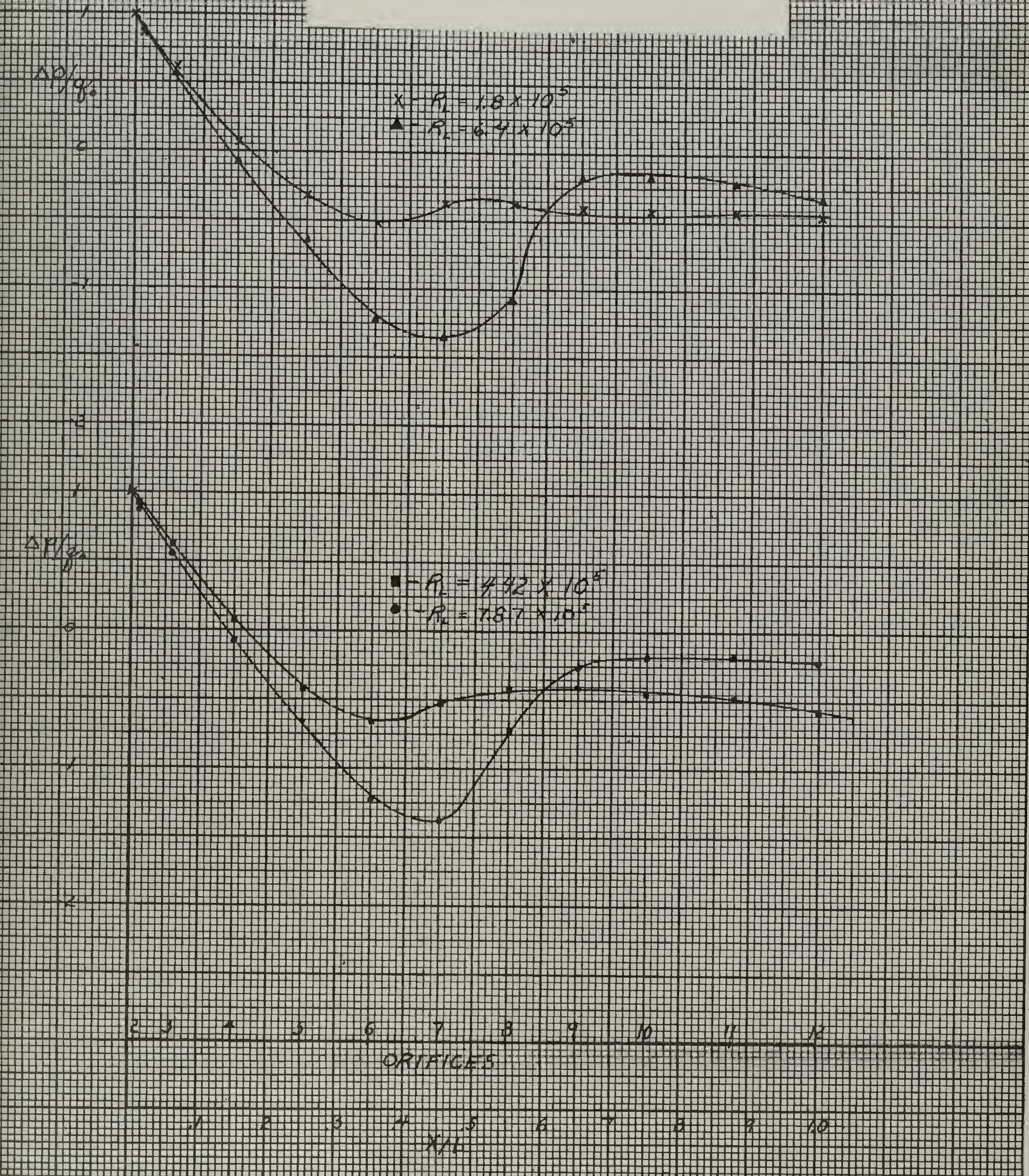

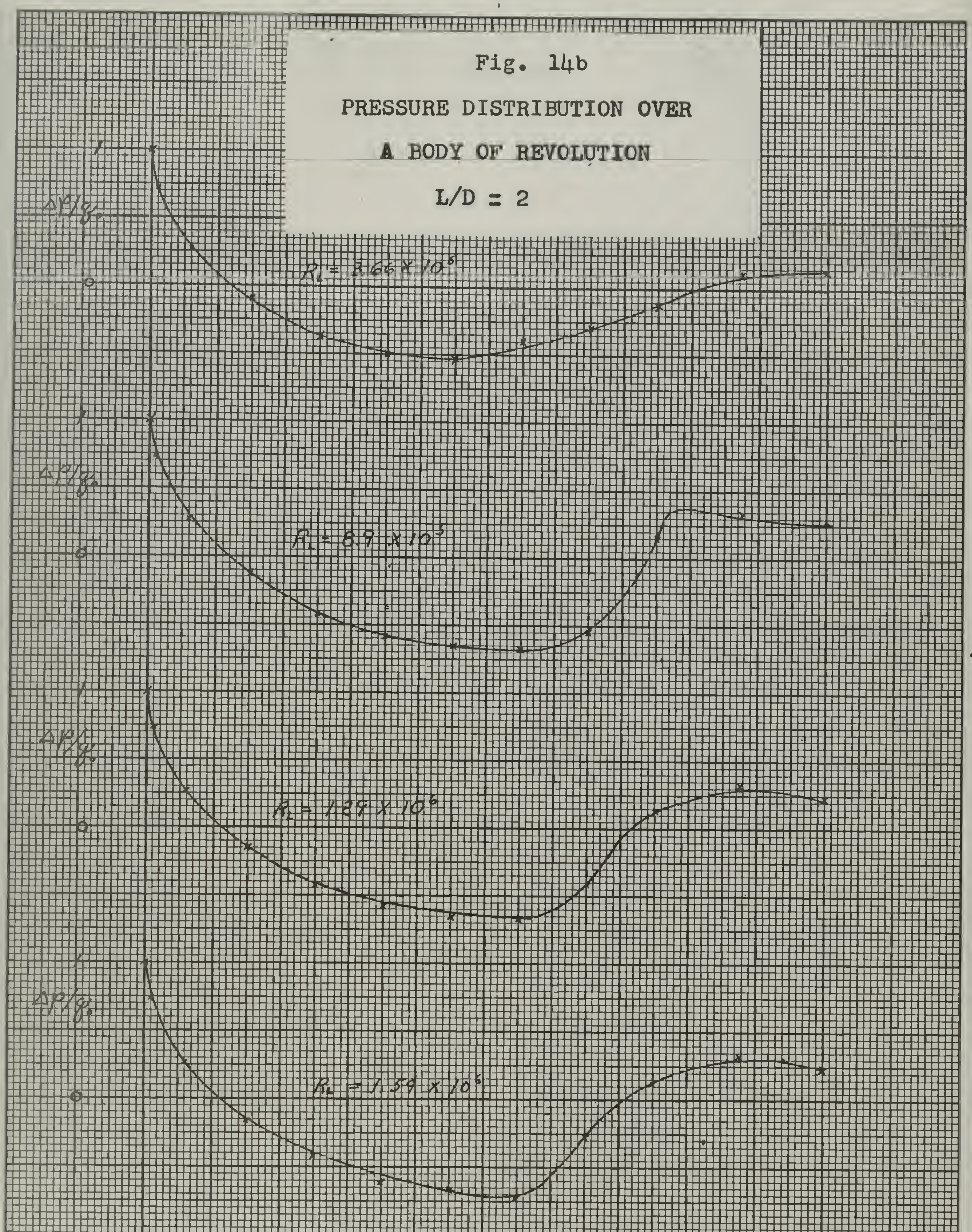

Fig. 14b

PRESSURE DISTRIBUTION OVER

A BODY OF REVOLUTION

L/D = 2

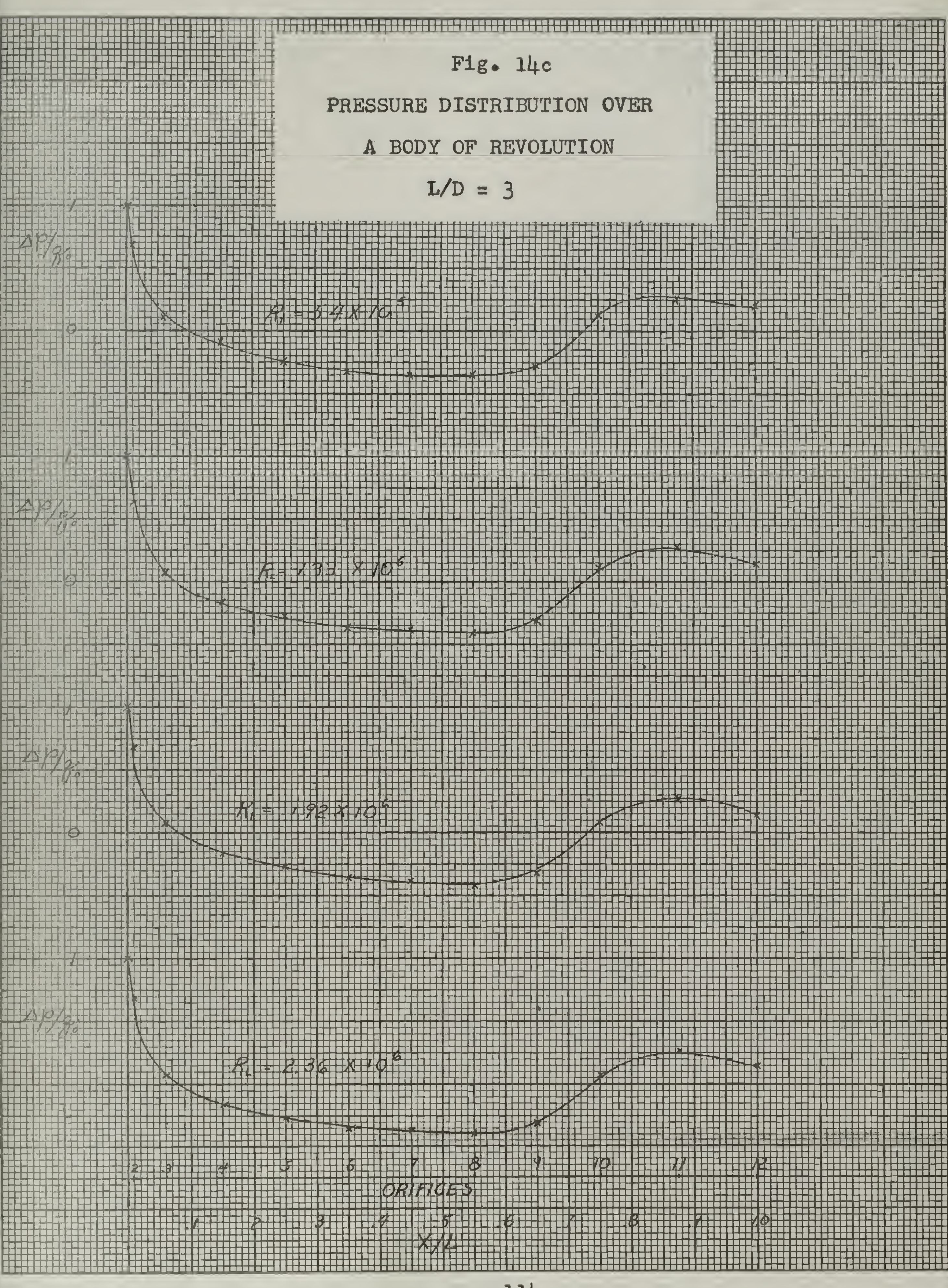

Fig. 14c

PRESSURE DISTRIBUTION OVER

A BODY OF REVOLUTION

L/D = 3

Fig. 14d

PRESSURE DISTRIBUTION OVER

A BODY OF REVOLUTION

L/D = 4

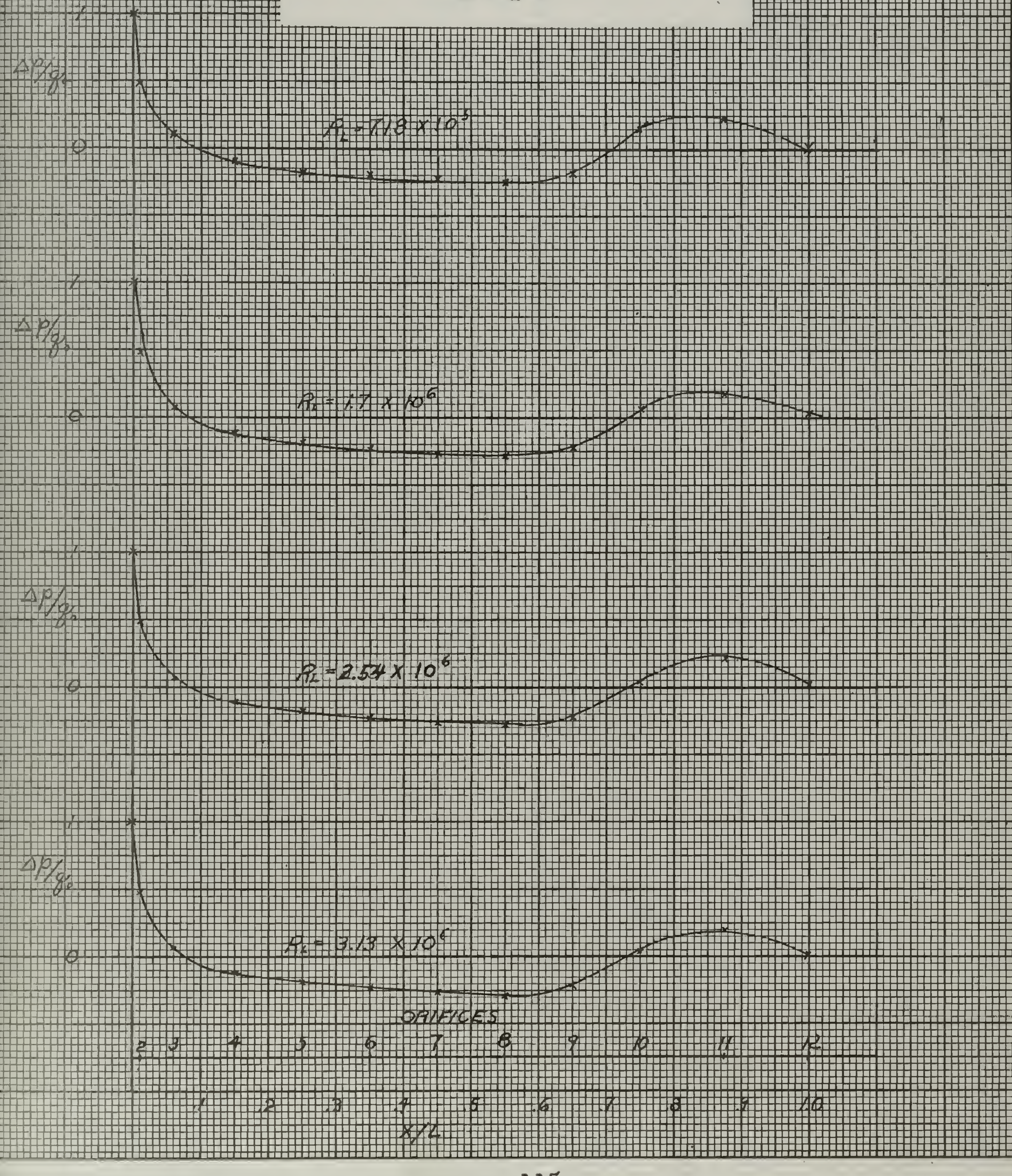

Fig. 14e

PRESSURE DISTRIBUTION OVER

A BODY OF REVOLUTION

L/D = 5

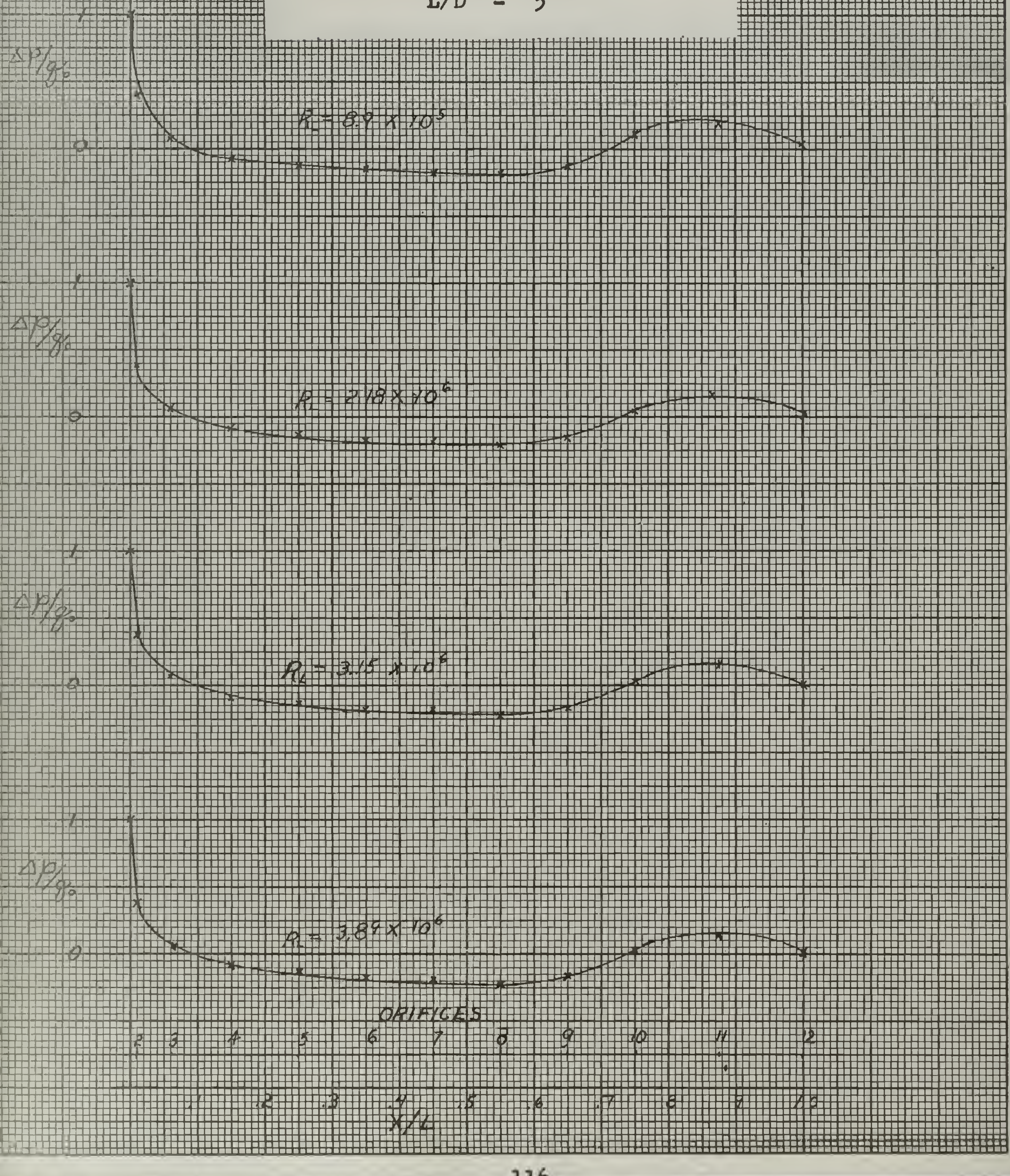

Fig. 14f

PRESSURE DISTRIBUTION OVER

A BODY OF REVOLUTION

L/D = 6

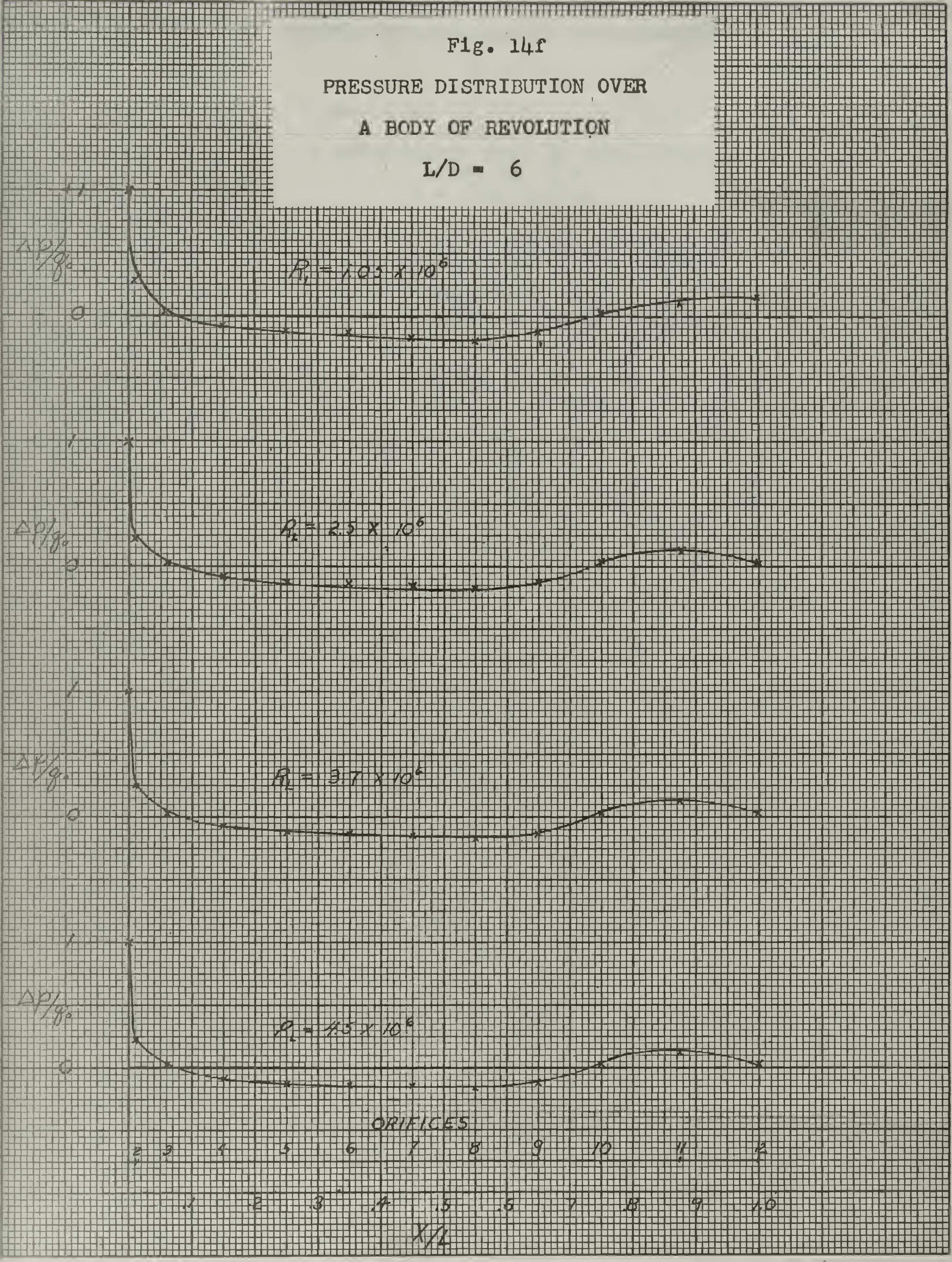

Fig. 15

LENGTHWISE VELOCITY DISTRIBUTION
IN THE BOUNDARY LAYER OF
A STREAMLINED BODY OF REVOLUTION
V/V_o vs. X/L
Y = .009 inches

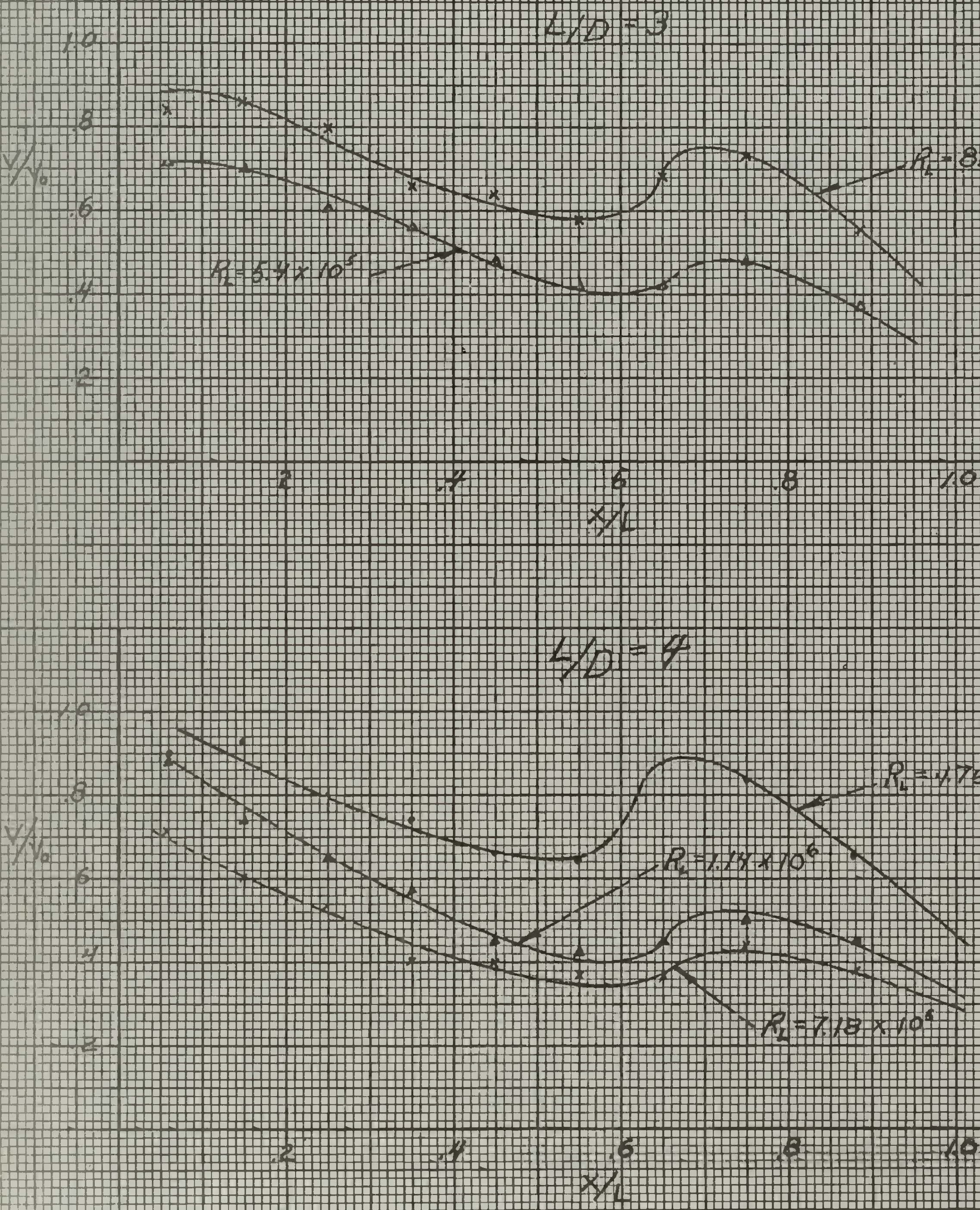

Fig. 16

LENGTHWISE VELOCITY DISTRIBUTION IN THE BOUNDARY LAYER OF A STREAMLINED BODY OF REVOLUTION
V/V_o vs. X/L
Y = .009 inches

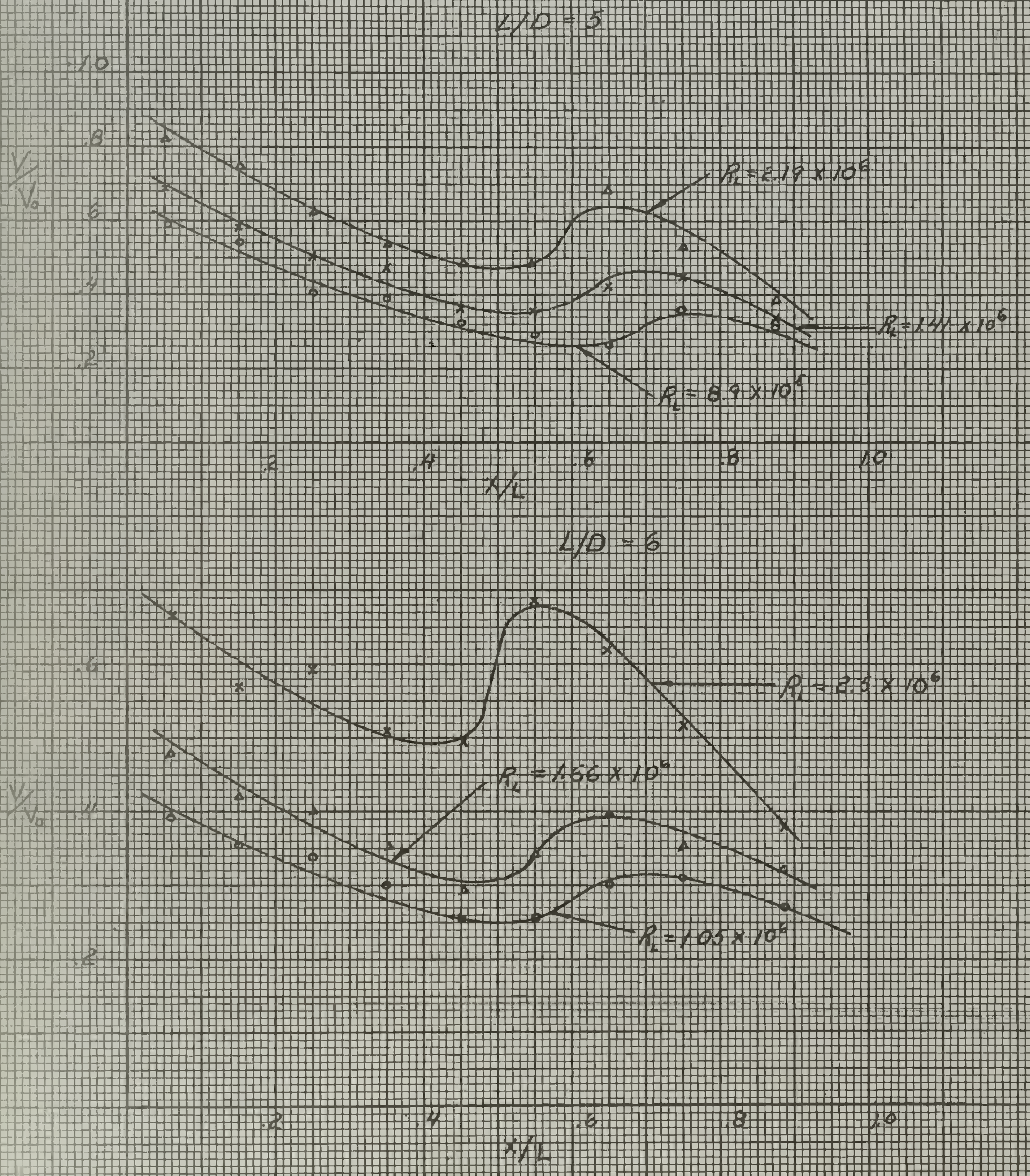

Fig. 17

ESTIMATED LENGTHWISE VARIATION OF
NONDIMENSIONAL SHEAR STRESS
ON A BODY OF REVOLUTION

L/D = 3

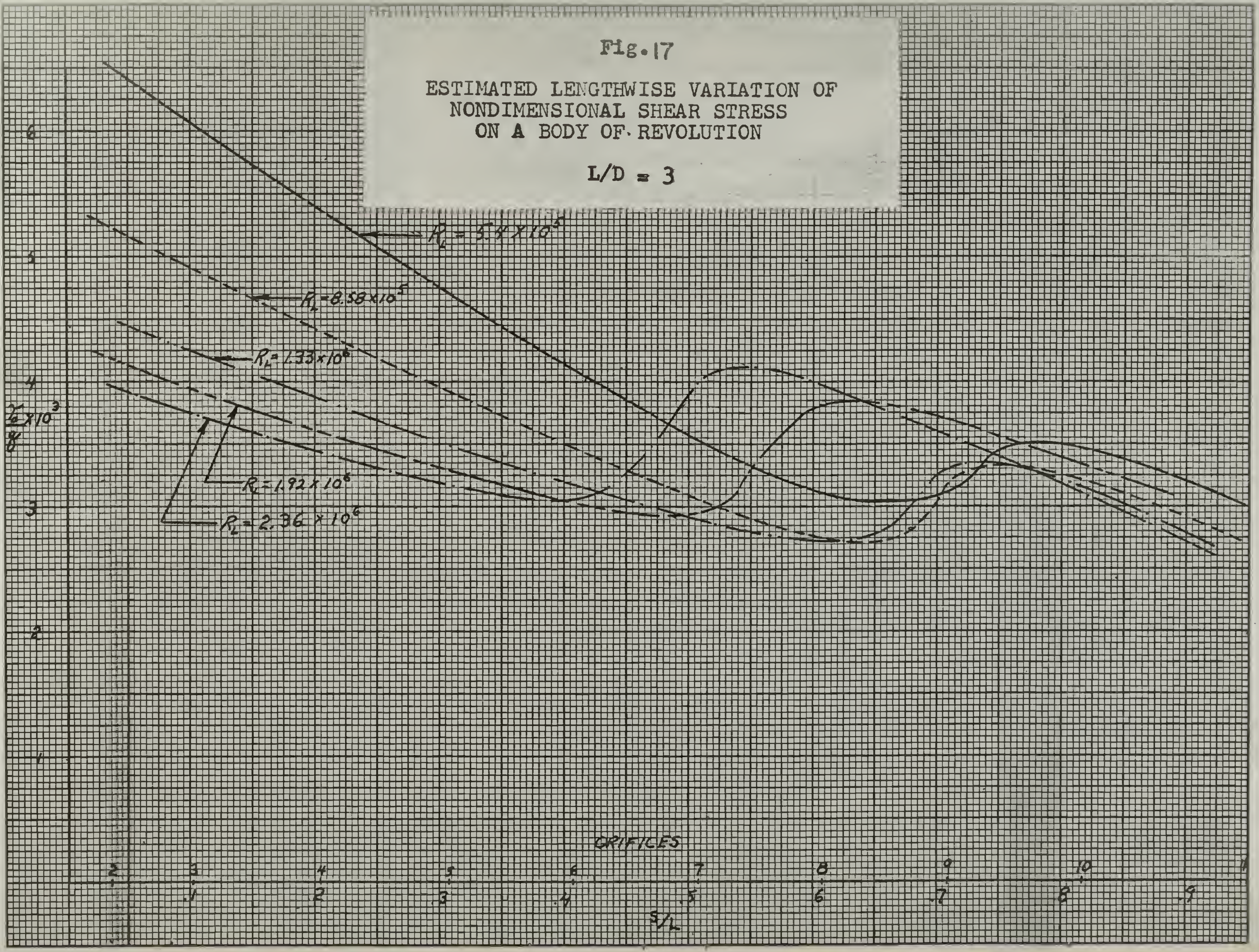

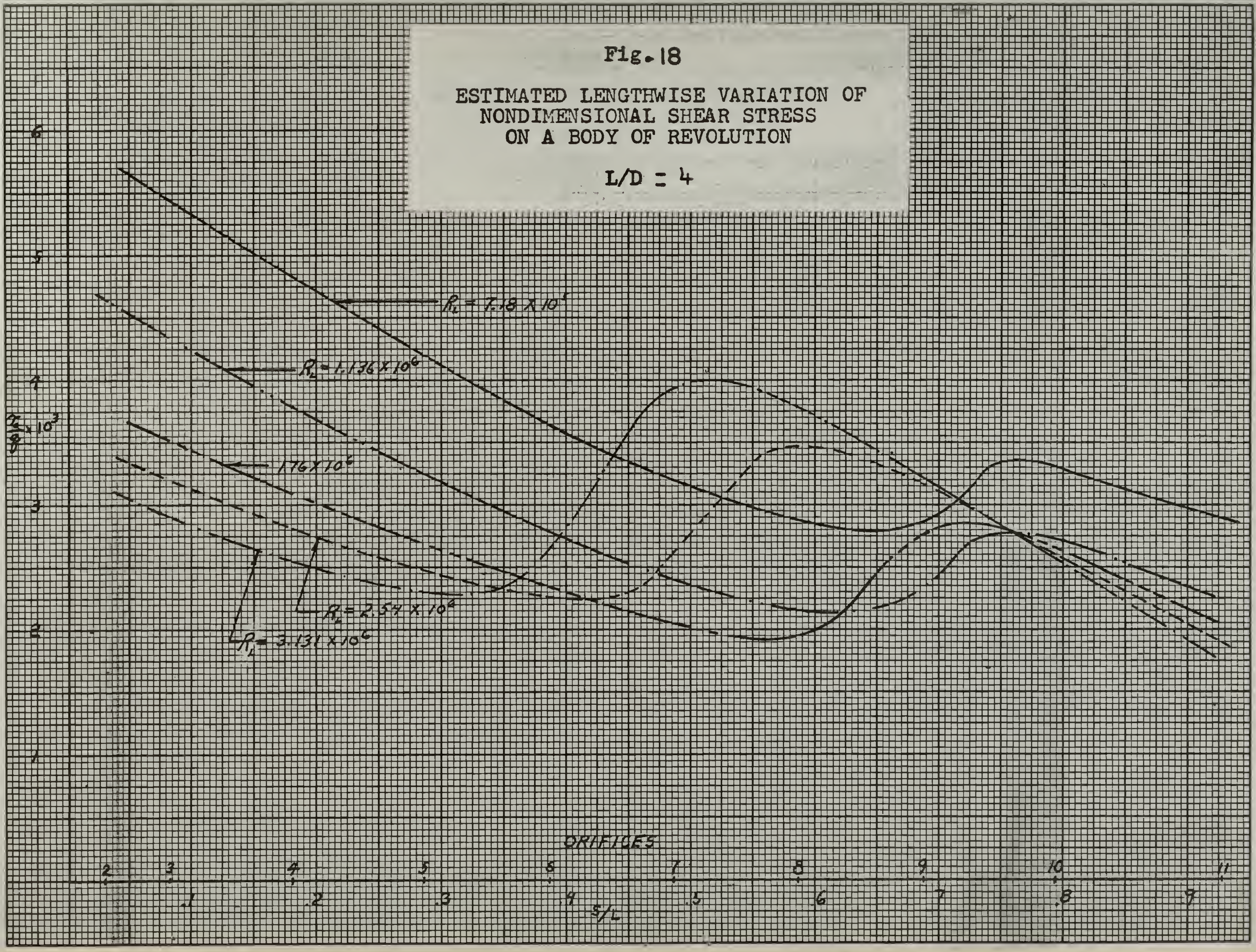

Fig. 18

ESTIMATED LENGTHWISE VARIATION OF
NONDIMENSIONAL SHEAR STRESS
ON A BODY OF REVOLUTION

L/D = 4

Fig. 19

ESTIMATED LENGTHWISE VARIATION OF NONDIMENSIONAL SHEAR STRESS ON A BODY OF REVOLUTION

L/D = 5

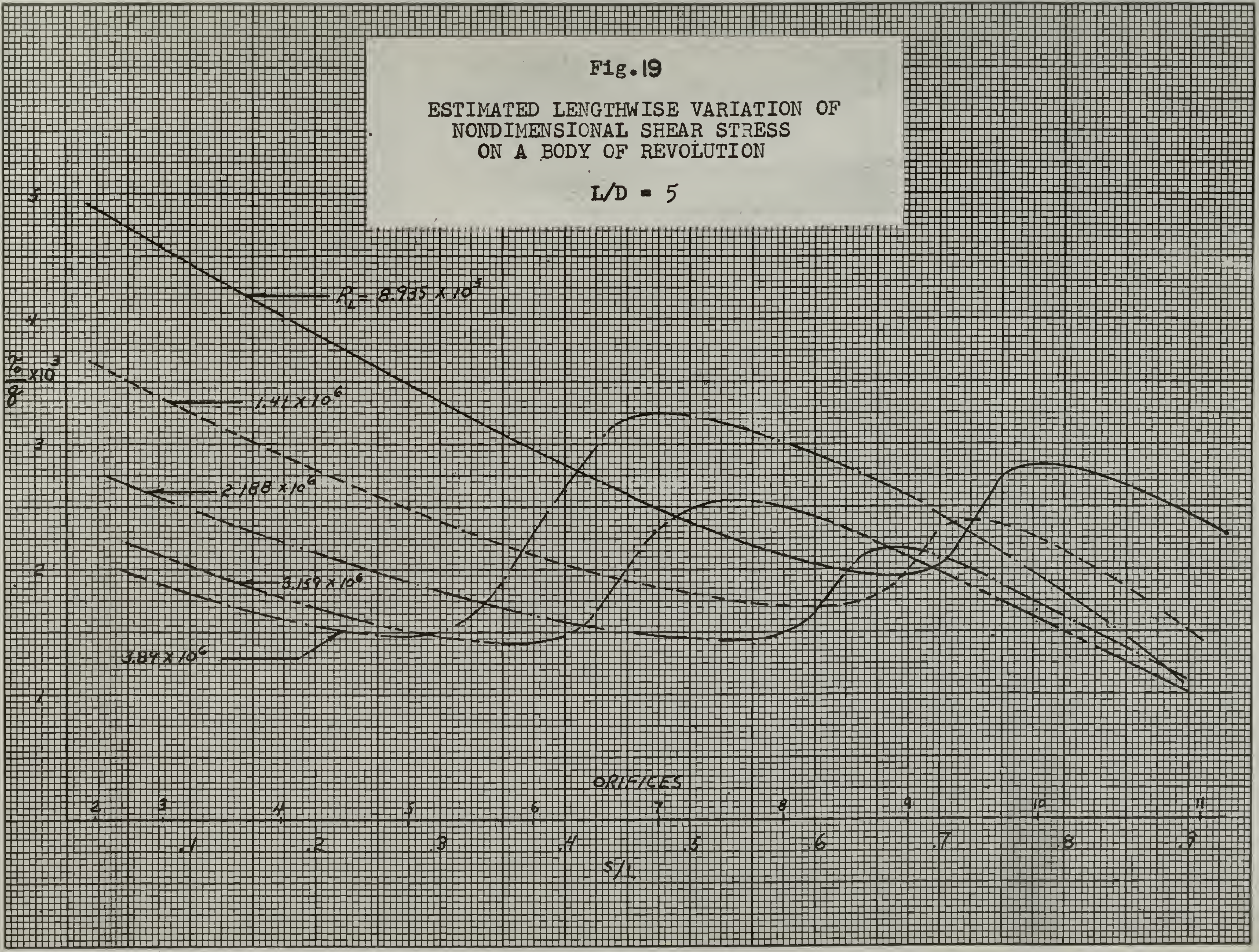

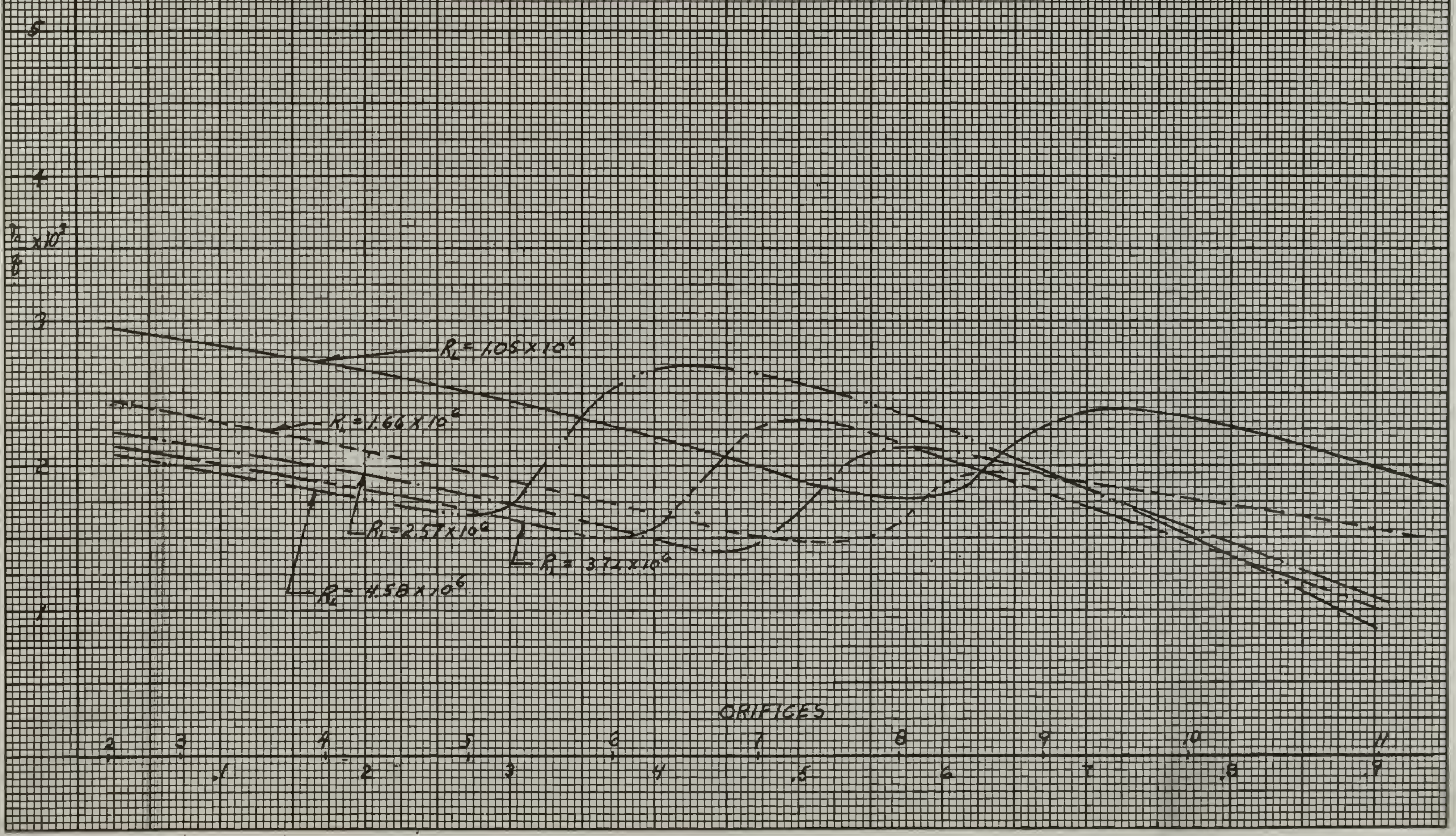

Fig. 20

ESTIMATED LENGTHWISE VARIATION OF
NONDIMENSIONAL SHEAR STRESS
ON A BODY OF REVOLUTION

L/D = 6

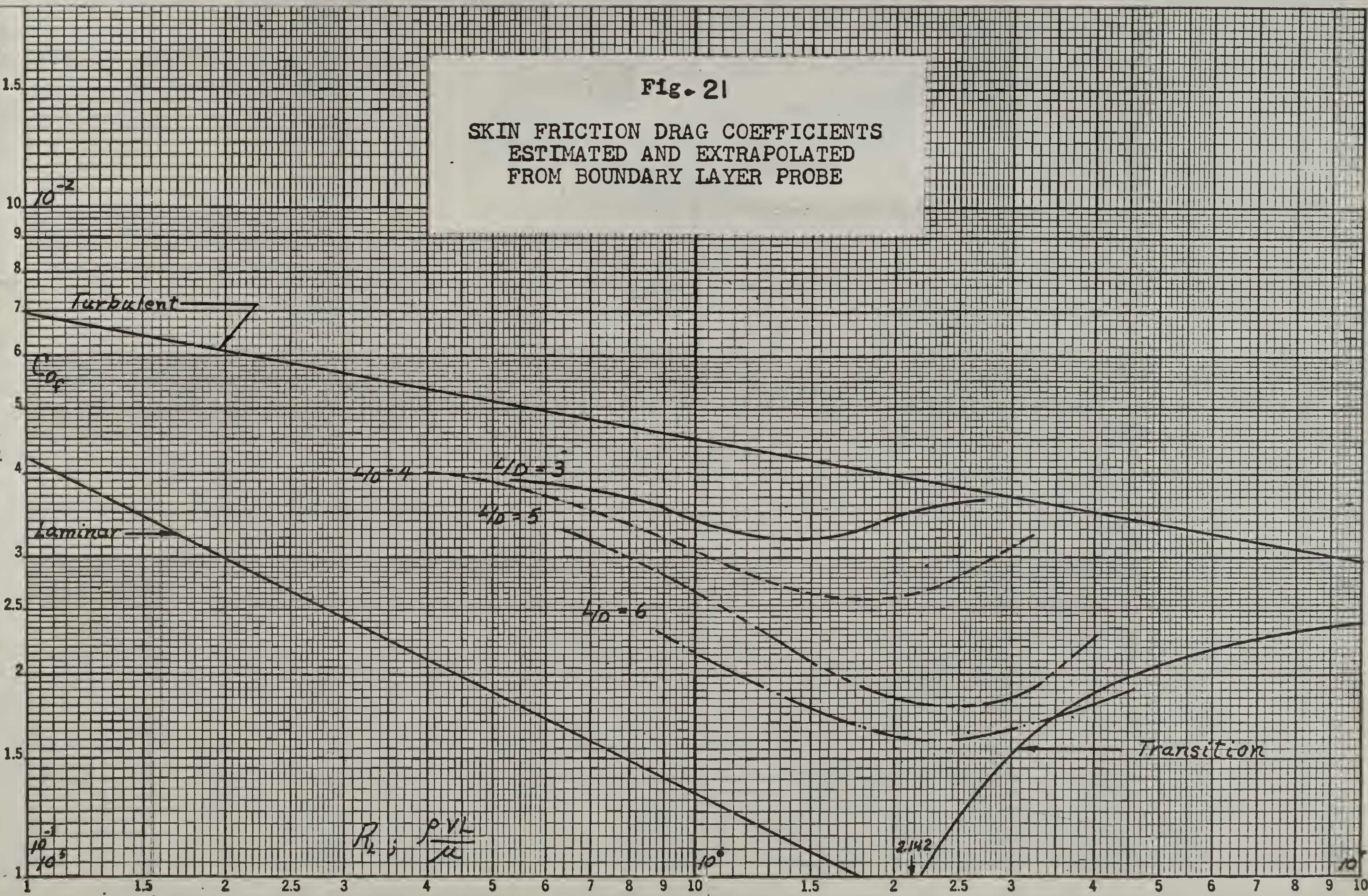

Fig. 21

SKIN FRICTION DRAG COEFFICIENTS ESTIMATED AND EXTRAPOLATED FROM BOUNDARY LAYER PROBE

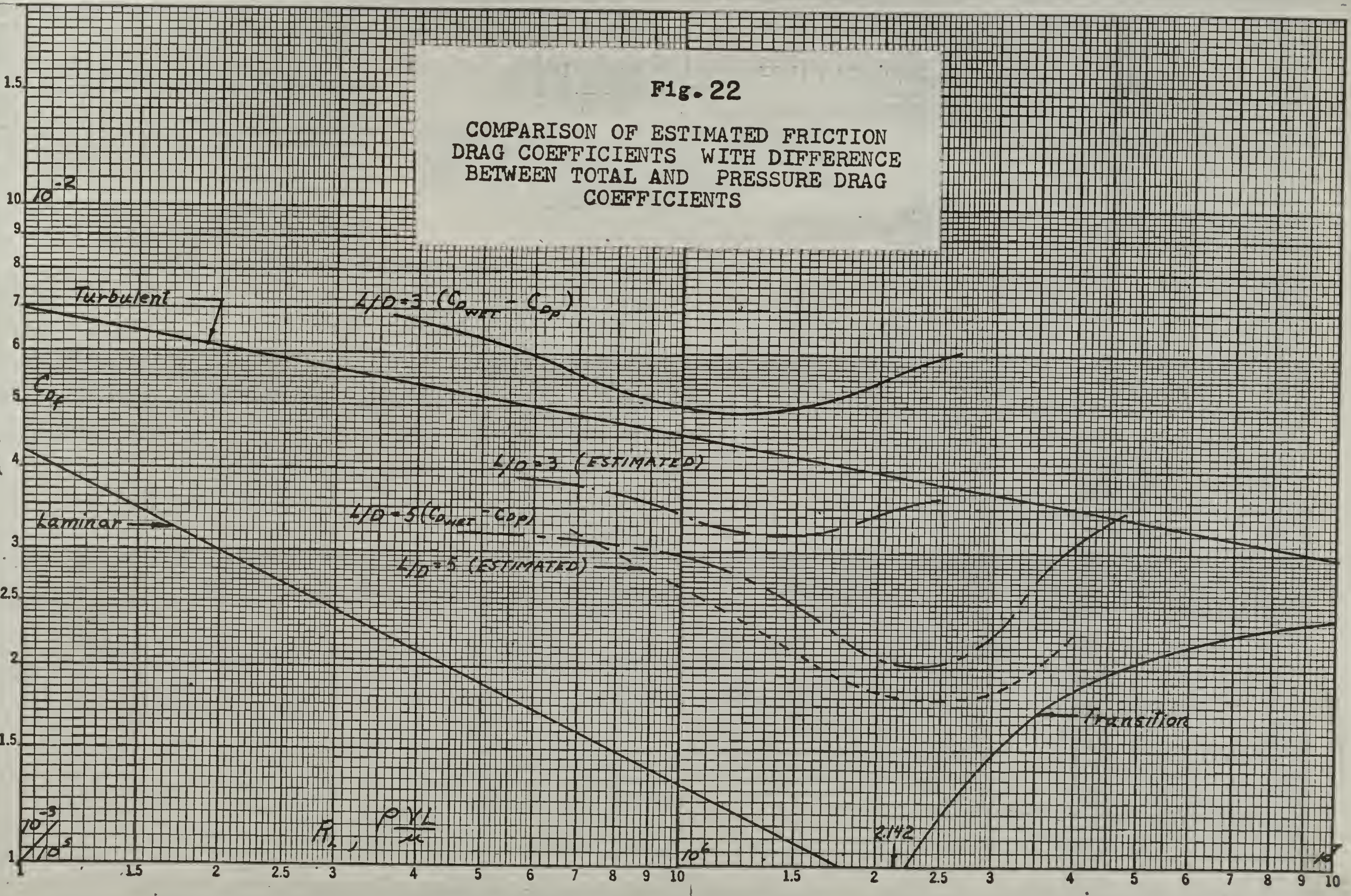

Fig. 22

COMPARISON OF ESTIMATED FRICTION DRAG COEFFICIENTS WITH DIFFERENCE BETWEEN TOTAL AND PRESSURE DRAG COEFFICIENTS

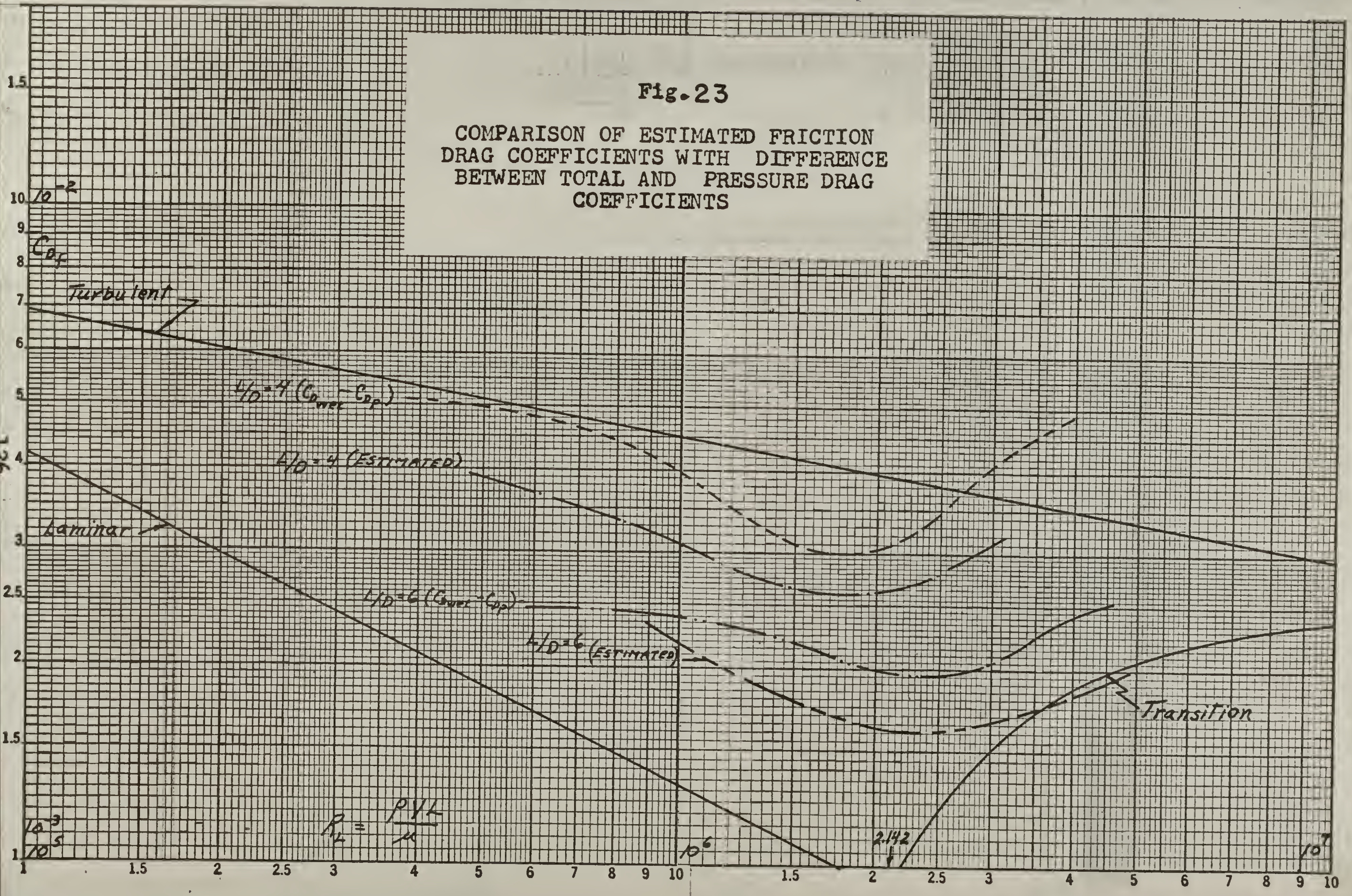

Fig. 23

COMPARISON OF ESTIMATED FRICTION DRAG COEFFICIENTS WITH DIFFERENCE BETWEEN TOTAL AND PRESSURE DRAG COEFFICIENTS

[redacted]